You are cordially invited to attend

MinWien2023

17 to 21 September 2023

A joint meeting of the three Mineralogical Societies

DMG Deutsche Mineralogische Gesellschaft

ÖMG Österreichische Mineralogische Gesellschaft

Slovenská mineralogická spoločnosť

Topics: Mineralogical, Petrological, Geochemical Sciences, deposits & related disciplines (basic, applied & industrial topics)

Pre-confe

Male Ka

16-17 S

Guides: P. Bačik I. Bro

Conference dinner

Wednesday 20 September 2023
Festival Hall, Vienna's City Hall

Half-day tours

18-21 September, 2023

Programme

Sunday, 17 September 2023
Mineralogy for the public
Young Scientists meet each other
Opening Ceremony
ether Party

Thursday,
eptember 2023
Scientific sessions
Poster presentations
Industrial exhibition

Poster Prizes for young scientists
DMG - General Assembly
Public lecture

Abstracts, H - N

Conference Site: Alma Mater Rudolfina - University of Vienna
Geozentrum - UZAII, Josef-Holaubek-Platz 2, 1090 Vienna
Organisation: Institut für Mineralogie und Kristallographie
Further information: https://minwien2023.univie.ac.at
e-mail: minwien2023.mineralogie@univie.ac.at

Photo on courtesy of Stephan Wolfsried

DOI: https://doi.org/10.23689/fidgeo-6024

"Nothing is more important than health" Eduard Suess (1831-1914) Eduard Suess was a leading contributor to the city of Vienna's projects of the century: the 1st Vienna spring-water pipeline and the regulation of the Danube

M. Hamilton[1]

[1]Geological Archive, Department of Geology, University of Vienna
e-mail: margarete.hamilton@univie.ac.at

E. Suess not only played an important role as a professor of paleontology and geology at the University of Vienna, but as a member of the Vienna City Council he also submitted his expertise on the two century projects of the city of Vienna.

In the Archive of the Geological Institute at the University of Vienna exist handwritten notes by E. Suess between 1861 and 1869 dealing with the meetings of the Vienna City Council with regard to the quality of the water for the city and, as a result, the health of the population.

In his memoirs, which were published posthumously in 1916, Suess points out in an essential conversation with the then mayor Cajetan Felder (1814-1894) that "nothing is more important than the health" of the population of Vienna. The rapid population increase, the infections with dysentery, typhus and cholera in 1855 were a significant problem, also poor water quality and a lack of sewerage.

Between 1869 and 1873 a 90 km long canal was built from the springs in the foothills of the Eastern Alps via tunnels and aqueducts to the water tanks of the city of Vienna. This first Vienna high spring water pipeline was officially opened on October 24, 1873 with the commissioning of the high jet fountain on Schwarzenbergplatz in the presence of Emperor Franz Josef I. There also exist a copy of the piano piece "Die Hochquelle" composed by Eduard Strauss (1835-1916) in 1911. The piece is dedicated to the initiator of the first Vienna spring-water pipeline Eduard Suess.

The second major project to improve water quality and thus improve the health of Vienna's population was the regulation of the Danube bed. With the Danube Regulation Commission created in 1868, not only should the devastating floods of the Danube river be prevented, but also new facilities for the creation of shipping and trade should be made possible. Work began on May 14, 1870 in the presence of Emperor Franz Josef I, and just 5 years later, on April 15 and 16, 1875, the two breakthroughs were made on the north and east of the Danube.

In the geological archive exist three soil maps of Vienna from the years 1873-1875 showing the course of the Danube in the old and new beds. A copy of a letter from the Emperor to E. Suess from 1911 has also survived, in which the Emperor praised E. Suess for his achievements for the benefit of the people of Vienna.

Figure 1. Stadler R Lithographie: Der neue Springbrunnen vor dem Schwarzenberg-Palais (1873)

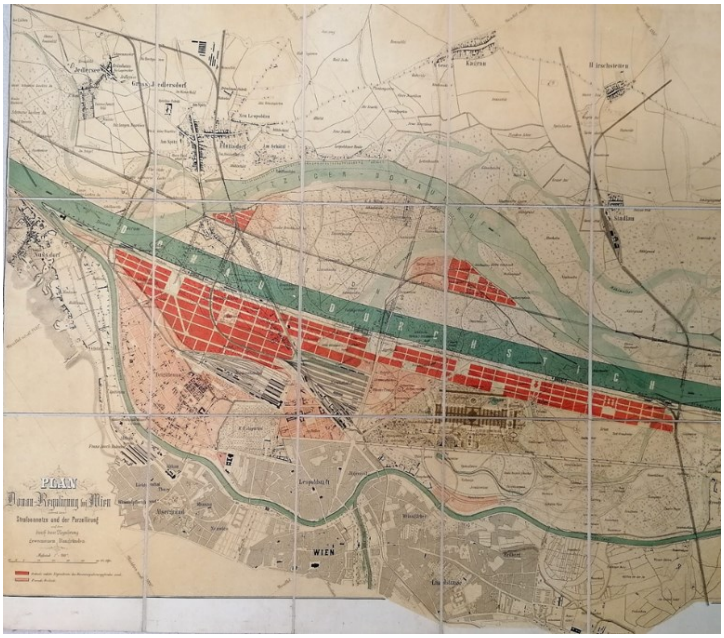

Figure 2. Plan der Donauregulierung in Wien. Donauregulierungskommission (1875). Geological Archive, KS ¼

Drenning A (1973): Die 1. Wiener Hochquellenleitung. - Festschrift aus Anlaß der 100-Jahr-Feier am 24.Oktober 1973

NN (1875): „Die Donau-Regulierung bei Wien“. - Herausgegeben aus Anlaß der feierlichen Eröffnung der Schiffahrt im neuen Strombette am 30. Mai 1875 von der Donau-Regulierungs-Commission in Wien

Stadler R (1873): Die Wasserversorgung der Stadt Wien in ihrer Vergangenheit und Gegenwart. Denkschrift zur Eröffnung der Hochquellenwasserleitung im Jahr 1873. 296 pp

Suess E (1916): Erinnerungen. 154 p

Geochemical patterns in karst bauxite of the Unterlaussa mining district (Upper Austria)

F.J. Hampl[1], F. Melcher[1], I. Dunkl[2], B. Schmidt[3], V. Bertrandsson Erlandsson[1]

[1]Chair of Geology and Economic Geology, Montanuniversität Leoben, Peter-Tunner-Straße 5, 8700 Leoben, Austria
[2]Department of Sedimentology & Environmental Geology, Geoscience Center, Georg-August-Universität Göttingen, Goldschmidtstraße 3, 37077 Göttingen, Germany
[3]Department of Mineralogy, Geoscience Center, Georg-August-Universität Göttingen, Goldschmidtstraße 1, 37077 Göttingen, Germany
e-mail: ferdinand.j.hampl@gmx.at

Numerous studies demonstrated the great potential of karst bauxites as sources of critical metals. The European karst bauxites may thus help to gain more independence from questionable non-European metal suppliers. Yet several European karst bauxites are untouched by modern scientific methods and the processes that are responsible for their element enrichment and depletion patterns are not fully understood. However, understanding the geochemical patterns in karst bauxites is not only fundamental for a prudent economic usage but can also facilitate reconstructions of paleo-environments and redox processes during weathering and diagenesis. To better understand the geochemical patterns, we investigated three profiles of Upper Cretaceous karst bauxite in the Unterlaussa mining district (Upper Austria) and used geochemical and mineralogical methods such as (micro-) X-ray fluorescence, (laser ablation-) inductively coupled plasma mass spectrometry, scanning electron microscopy, electron microprobe mapping and X-ray diffraction.

According to our results, the boehmitic karst bauxite was formed by intense weathering of a polygenetic sediment (parent material) that was deposited on karstified dolostone (Hampl & Melcher, 2023). The presence of detrital chromite in the karst bauxite suggests that sediments formed by weathering of ophiolitic material in the hinterland of the depositional site were also part of the parent material. (Sub)tropical weathering of the composite parent material caused the dissolution of aluminosilicates and the enrichment of weathering-resistant minerals. These weathering processes not only led to chemical depletion and enrichment patterns that are typical for karst bauxites (e.g., pronounced Al_2O_3, Fe_2O_3 and TiO_2 enrichment, and SiO_2, alkali and alkaline earth metal depletion) but also resulted in substantial enrichment of several critical metals compared to the upper continental crust: e.g., rare earth elements (REEs; La-Lu + Sc, Y) up to 2277 ppm, Li up to 900 ppm, or V up to 916 ppm. Most of the REEs and Li are enriched in the lowermost part of the bauxite and clay minerals are the most likely hosts. Moreover, the element distribution patterns also indicate reducing conditions in the lower part and redeposition in the upper part of the bauxite. Even though Cr- and U-mobility normally only plays a subordinate role in karst bauxites, we found a macroscopic, authigenic chromium oxyhydroxide mineralization and discrete U-minerals in reduction spheroids. Aside from U, some of these reduction spheroids are extremely rich in redox-sensitive elements such as V, Cr, or Mn. We discuss possible formation models for this unique U-mineralization.

Our results highlight the economic potential and the ample information content of karst bauxites and call for more European initiative to investigate them.

Hampl FJ, Melcher F (2023): The formation of the Unterlaussa karst bauxite (Austria) – A re-evaluation of the established model. - J Geochem Explor 245, 107141. https://doi.org/10.1016/j.gexplo.2022.107141

The inner beauty of Roman Egyptian blue: micro-CT and mineralogy

J. Heinemann[1], P. Tropper[1], G. Degenhart[2], B. Zerobin[3], G. Goldenberg[3], A. Rodler[4,5]

[1]University of Innsbruck, Institute of Mineralogy and Petrography, 6020 Innsbruck, Austria
[2]Medical University of Innsbruck, Institute of Radiology, 6020 Innsbruck, Austria
[3]University of Innsbruck, Institute of Archaeologies, 6020 Innsbruck, Austria
[4]Austrian Archaeological Institute of the Austrian Academy of Sciences, Franz-Klein Gasse 1, 1190 Vienna
[5]Department of Lithospheric Research, University of Vienna, Josef-Holaubek-Platz 2, 1090 Vienna
e-mail: peter.tropper@uibk.ac.at

Egyptian blue was the first synthetic pigment made by humankind. It mostly consists of the mineral cuprorivaite, which is a calcium-copper-silicate ($CaCuSi_4O_{10}$). This study reports the results of a mineralogical and computer tomographic study of Egyptian blue finds from the Roman sites of Aguntum in East Tyrol, as well as from Retznei and Wagna (formerly Flavia Solva) in southern Styria, Austria. The aim is to expand our understanding of the material processing and production technology of the artificial pigment Egyptian blue. Samples of Egyptian blue pellets were investigated with respect to their elemental composition and spatial distribution of the calcium-copper-silicate cuprorivaite $CaCuSi_4O_{10}$.

A thin section (with three cut layers) of an Egyptian blue pellet from Aguntum was examined using optical microscopy (OP), micro-X-ray fluorescence analysis (μ-XRF) and scanning electron microscopy coupled with energy dispersive X-ray spectroscopy (SEM-EDX). The pigment's initial composition as well as the manufacturing process seem to be the decisive factors for the quality of the final product. A relationship between the presence of trace iron (Fe), titanium (Ti), and sulfur (S) with the quartz and copper source of the initial raw material mixture is discussed.

In addition, micro-computed tomography (μ-CT) of three Egyptian blue finds (Aguntum, Retznei, Wagna-Flavia Solva) was performed, revealing several concise differences between the samples. The pellets from Aguntum and Retznei contained a significantly higher content of cuprorivaite and smaller crystals than the sample from Wagna-Flavia Solva. The spatial distribution of individual mineral phases was analysed with μ-CT-3D images. Here, the connective density, average particle size as well as spacing between individual particles of specific phases can be visualised. This confirms the semi-quantitative measurement of a phase's proportion to the total volume of a sample.

Concerning clues about the initial raw material mixture of the pellets, the results show that chalcosine and possibly quartz from beach sand were used as source for the Egyptian blue pellet from Aguntum. In addition, μ-CT data indicate that the pellet from Retznei contains the highest amount of cuprorivaite, followed by the sample from Aguntum, while that from Wagna-Flavia Solva contains the least amount of cuprorivaite.

Compressibility of pearceite-polybasite group minerals

C. Hejny[1]

[1]*University of Innsbruck, Innrain52, 6020 Innsbruck, Austria*
e-mail: Clivia.hejny@unibk.ac.at

Pearceite-polybasite group minerals (PPGM), $[(Ag,Cu)_6(As,Sb)_2S_7][Ag_9CuS_4]$, display Ag^+ fast ion conduction character. The crystal structure is described as being composed of two different layers: layer A with general composition $[(Ag,Cu)_6(As,Sb)_2S_7]^{2-}$ and layer B with general composition $[Ag_9CuS_4]^{2+}$. Ionic conductivity is observed in layer B (Bindi et al. 2007). The root-name *pearceite* is given to minerals where As is dominant over Sb and the root-name *polybasite* for Sb-dominant phases. A suffix attached to the root-name stands for the superstructure variant, the three most common ones are (1) trigonal with lattice parameters $a \approx 7.5$, $c \approx 12.0$ Å , PPG-*Tac*, trigonal with lattice parameters $a \approx 15.0$, $c \approx 12.0$ Å, PPG-*T2ac* and monoclinic with $a \approx 26.0$, $b \approx 15.0$ $c \approx 24.0$ Å, $\beta \approx 90°$, PPG-*M2a2b2c,* although a number of different crystal structures and their temperature-induced phase transitions are known (e.g., Bindi et al. 2006).

In-situ single-crystal diffraction experiments of PPGMs in a diamond anvil cell were performed to test the possibility of using pressure as a switch for the ionic conductivity. Initial experiments have indeed shown that it is possible to induce phase transitions from the ionic conduction form with the aristotype crystal structure PPG-*Tac* to an ordered or partially ordered superstructure form with Ag ions "frozen-up" into fixed atomic positions. In this way a crystal of pearceite-*Tac* transformed to the -*T2ac* crystal structure at a pressure of 0.5(1) GPa and a crystal of polybasite-*T2ac* showed a phase transition to the -*M2a2b2c* superstructure variant at 4.5(2) GPa. In both cases the compressibility is significantly larger along the *c*-direction, i.e. perpendicular to the layered structure, which is in accordance with a reduction of the size for the ionic conductivity pathways. The limited number of datapoints within the small pressure range from AP to 5.4GPa and without considering phase transitions only allows for an estimation of the bulk modulus, which, with a value of K = 48(1) GPa, is well in accordance of other sulphosalt materials.

Bindi L, Evain M, Pradel A, Albert S, Ribbs M, Menchetti S (2006): Fast ion conduction character and ionic phase-transitions in disordered crystals: the complex case of the minerals of the pearceite–polybasite group. - Phys Chem Miner 33, 677-690

Bindi L, Evain M, Spry PG, Menchetti S (2007): The pearceite-polybasite group of minerals: Crystal chemistry and new nomenclature rules. - Amer Miner 92, 918-925

Research insights based on documents from the Geological Archive of the University of Vienna

M. Heninger[1], B. Holly[2], P. Nagl[3], R. Wohlschlägl[1], M. Hamilton[4]

[1]Institut für Geologie, Universität Wien
[2]Institut für Mineralogie und Kristallographie, Universität Wien
[3]Department für Lithosphärenforschung, Universität Wien
[4]Geologisches Archiv, Universität Wien
e-mail: margarete.hamilton@univie.ac.at

The main task of the Geological Archive is the acquisition, evaluation, order, description, preservation, and utilization of written material, audiovisual material, and collections that are created in the institute and above all by the academic people working there. Of course, archiving is always linked to librarianship; nevertheless, in the present case, it is a special archive that deals with the preservation not of specialized library literature, but of documents and objects of geological research, whose historical significance is undisputed, but goes beyond literature.

In today's age of digitization and the new technical possibilities, an important aspect is making the holdings accessible via electronic media (Hamilton 2021). Furthermore, in accordance with the educational mandate of archiving, interested students are offered the opportunity to get to know the history of geosciences in detail in a special course and also to establish a connection to current research and to present it in seminars.The works presented here give an insight into specially selected documents from the Geological Archive and show their diversity.

Otto Ampferer (1875-1947) - The theory of the undercurrent: Plate tectonics and the name "Alfred Wegener" (1880-1930) are almost inextricably linked. Ships, research centers and asteroids have been named after the German explorer. Otto Ampferer and his undercurrent theory, which he presented as early as 1906, are less well known. He developed this theory in the course of his alpine research and mapping work. Remarkably, it comes very close to today's concept of "seafloor spreading".

Perhaps because his contributions were difficult for laypeople to read, the Austrian geologist is far less known as the godfather of institutions and sites than his German colleague. However, the interested reader soon notices his pictorial and skilful use of language as well as the high scientific quality of his contributions - reason enough to take a closer look at the researcher.

Historical personnel files of assistants and demonstrators: The present personnel files include documents from the period 1873 to 1945, which were first written in current, later in cursive handwriting and typewritten. In addition to letters that deal directly with the employment and salary of people, there are also ministerial decrees and documents that are directly or indirectly related to the military service of employees in the First and Second World Wars. The existing documents not only reflect the drastic change in correspondence, but also the special challenges for the University of Vienna in this very special time.

Historical geological maps - their origin and preservation: One of the oldest surviving maps in the Geological Archive of the Institute for Geology at the University of Vienna is the "Geognostic Map of the Areas of Krems and Manhardsberge" (1848). Based on this geological map, the author deals with the life and work of the map author Johann Baptist Čžjžek (1806-1855) and gives an overview of the creation and preservation of historical geological maps. Furthermore, the creation of geological maps in the past and present is examined.

Walter Medwenitsch - Expedition to East Africa in 1971: Walter Medwenitsch (1927-1992), whose numerous study trips took him halfway around the world, undertook a 15-day expedition to East Africa in February 1971. Driven by a broad interest in all natural sciences - but especially in geology (doctorate 1949 at the University of Vienna) - during these two weeks he visited cyanite and carbonatite deposits in Kenya, studied the young volcanism of the East African Rift Valley and dealt with the glaciology of the Kilimanjaro massif. His curiosity also led him to the extinct volcano Mount Kenya and its glaciers and to the Pleistocene fossils of Tanzania's Olduvai Gorge, considered part of the 'Cradle of Mankind'.

In the geological archive of the University of Vienna there is a comprehensive geological report by W. Medwenitsch ("Notes on the geological excursion to East Africa") on this wide-ranging expedition, as well as numerous maps and excerpts from reports that contain additional information on the areas visited.

Figure 1: Insights into the newly organized Geological Archive of the University of Vienna. Left: History of the Geological Institute, Box 1; Center top: geological maps, map box 1; Right: Walter Medwenitsch, box 5; center bottom: Otto Ampferer, Box 3 (Photos: M Hamilton)

Hamilton M (2021): The collections of the Archive of the History of Geology at the University of Vienna. - In: 15th International ERBE-Symposium, Eggenburg 2021. Proceedings, 58-74.

Glass transition temperatures and crystallization kinetics of a synthetic, anhydrous, amorphous calcium-magnesium carbonate

K.-U. Hess[1], J. Schawe[2], M. Wilding[3], K.E. Goetschl[4], S. Sturm[5], K. Müller-Caspary[5], E. Sturm[1], W. Schmahl[1], E. Griesshaber[1], T. Bissbort[1], D. Weidendorfer[1], M. Dietzel[4], D.B. Dingwell[1]

[1] Earth and Environmental Sciences, Ludwig-Maximilians-Universität München, Theresienstraße 41/III, 80333 Munich, Germany
[2] Mettler-Toledo GmbH, Analytical, Heuwinkelstrasse 3, 8603, Nänikon, Switzerland
[3] School of Earth Sciences, Wills Memorial Building, Queens Road, Bristol, BS8 1RJ, United Kingdom
[4] Institute of Applied Geosciences, Graz University of Technology, Rechbauerstraße 12, 8010 Graz, Austria
[5] Fakultät für Chemie und Pharmazie, Physikalische Chemie, Ludwig-Maximilians-Universität München, Butenandtstraße 5-13, 81377, Munich, Germany
e-mail: hess@lmu.de

We report the first calorimetric observations of glass transition temperatures and crystallization rates of anhydrous, amorphous calcium-magnesium carbonate using fast scanning differential scanning calorimetry (FDSC). The hydrous amorphous $Ca_{0.95}Mg_{0.05}CO_3 \cdot 0.5H_2O$ (ACMC05) solid was precipitated from a $MgCl_2$–$NaHCO_3$ buffered solution, separated from the supernatant, and freeze-dried. Part of the freeze-dried samples were additionally dried at 250 °C for up to 6 hours in a furnace in a high purity nitrogen atmosphere to produce anhydrous ACMC. The limiting fictive temperature of the anhydrous $Ca_{0.95}Mg_{0.05}CO_3$ was determined (by applying different heating rates (2000-6000 K/s, see Fig. 1) and correcting for thermal lag) to be 376 °C and the intensity of the glass transition or relaxational heat capacity is $\Delta Cp = 0.16$ J/(g K). Additionally, the heating rate dependence of the peak temperature of the corrected crystallization peaks is used to determine the activation energy of crystallization to be 275 kJ/mol. A high-resolution transmission electron microscopy study has been performed on the hydrous and anhydrous samples to provide further characterization of their compositional and structural states.

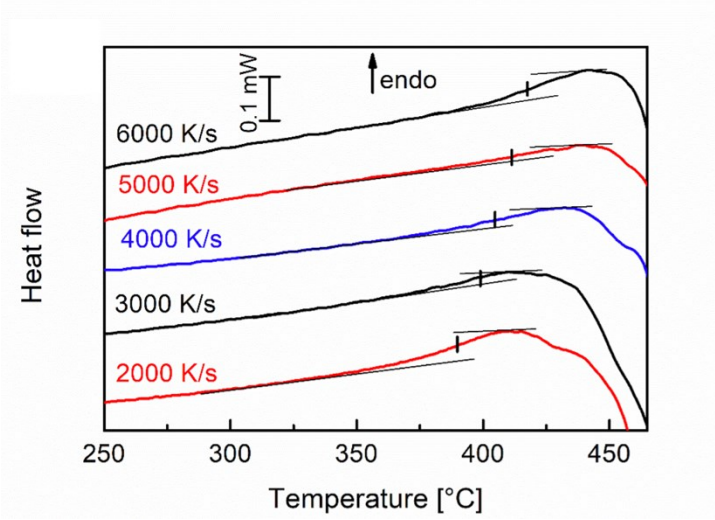

Figure 1. Heat flow curves of ACMC05.

The compositions of coherent exsolution lamellae in alkali feldspar measured with atom probe tomography

D. Heuser[1], R. Dubosq[2], G. Bian[1], G. Habler[1], E. Petrishcheva[1], B. Gault[2], C. Lengauer[3], C. Rentenberger[4], R. Abart[1]

[1]Department of Lithospheric Research, University of Vienna
[2]Department Microstructure Physics and Alloy Design, Max Plank Institut für Eisenforschung GmbH, Düsseldorf
[3]Department of Mineralogy and Crystallography, University of Vienna
[4]Physics of Nanostructured Materials, University of Vienna
e-mail: david.heuser@univie.ac.at

In the past, the compositions of experimentally produced coherent exsolution lamellae in alkali feldspars had to be determined indirectly from the "distorted" lattice parameters, because their small size prevented direct in-situ composition measurements. This indirect approach is based on strain models hinging on elastic constants, which are, however, subject to considerable uncertainties, especially for alkali feldspars with intermediate compositions (Robin 1974; Sipling & Yund 1976). In this study, we directly measured the compositions of experimentally produced exsolution lamellae using atom probe tomography (APT), a technique with near-atomic resolution which became available for non-conductive materials in the last decade.

At first, two K-rich gem quality alkali feldspars (Madagascar orthoclase and Volkesfeld sanidine) were shifted to intermediate Na-K-compositions by cation exchange with NaCl-KCl salt melt at 900 °C and subsequently annealed at ambient pressure and temperatures between 440 and 560 °C. Annealing conditions were within the miscibility gap of disordered alkali feldspar solid-solution and the initial compositionally homogeneous feldspars exsolved into a coherent lamellar intergrowth. Transmission electron microscopy (TEM) investigation of the exsolved feldspars revealed fully coherent exsolution lamellae subparallel to (-801) with lamellar widths of 5-30 nm. As the cell parameters of alkali feldspar exhibit considerable compositional dependence, the lattices of the more Na-rich and the more K-rich lamellae must be distorted in order to maintain coherency across the lamellar interfaces. In electron diffraction patterns this lattice distortion is evident from a splitting of the reflections corresponding to lattice planes sub-parallel to the lamellar interfaces.

APT revealed compositionally distinct domains corresponding to the expected Na-rich und K-rich lamellae. Time series experiments with different annealing durations were done at a given temperature to check when the lamellar compositions become stable, i.e. when thermodynamic equilibrium between the Na-rich and the K-rich lamella is reached. Even at the lowest applied temperatures equilibrium was reached within a few days, and lamellar compositions may be regarded as binodal points. The binodal points obtained at different temperatures delineate the coherent binodal curves. The results were compared to previously determined coherent solvi from the literature. Interestingly, Volkesfeld sanidine and Madagascar orthoclase show similar Na-K element partitioning and thus similar thermodynamic non-ideality of the alkali feldspar solid-solution in feldspar-salt melt cation exchange experiments at ambient pressure and temperatures between 800 and 1000 °C, but the coherent solvus of Volkesfeld sanidine lies well below the one of Madagascar orthoclase.

This apparent discrepancy may either be due to different degrees of thermodynamic non-ideality of the alkali feldspar solid-solution at the comparatively low temperatures of exsolution. Alternatively, this may be explained by different elastic properties of Volkesfeld sanidine and Madagascar orthoclase, which feed into the Gibbs energy of the soldi-solution via the elastic energy associated with coherent lamellar intergrowth.

Robin PYF (1974): Stress and strain in cryptoperthite lamellae and coherent solvus of alkali feldspars. - Amer Mineral 59, 1299-1318

Sipling PJ, Yund RA (1976). Experimental determination of the coherent solvus for sanidine-high albite. - Amer Mineral 61, 897-906

On the existence of a new $MgWO_4$ polymorph

E. Hildebrandt[1], V. Kahlenberg[1], H. Krüger[1], S.Wagner[1]

[1]*University of Innsbruck, Institute of Mineralogy and Petrography, Innrain 52, 6020 Innsbruck, Austria*
e-mail: volker.kahlenberg@uibk.ac.at

Single-crystals of a quenchable high-temperature polymorph of magnesium tungstate ($MgWO_4$-II) have been grown using the flux method. Polycrystalline material of the same compound could be obtained from solid-state reactions performed at 1200 °C. Basic crystallographic data of the previously unknown modification are as follows: triclinic symmetry, space group $P\bar{1}$, $a = 6.5525(6)$ Å, $b = 7.5883(7)$ Å, $c = 7.6976(6)$ Å, $\alpha = 119.064(9)°$, $\beta = 95.545(7)°$, $\gamma = 107.645(8)°$, $V = 304.84(5)$ Å^3 and $Z = 4$. The crystal structure was solved from single-crystal diffraction data using direct methods and subsequently refined including fractional atomic coordinates and anisotropic displacement factors for all atoms to a residual value of $R1 = 2.16$ % for 1517 independent observed reflections ($I > 2\sigma(I)$) and 110 parameters.

Both the divalent and hexavalent cations exhibit an octahedral oxygen coordination environment. The coordination spheres of the two symmetrically independent tungsten cations involve one very long W–O distance each and, therefore, one could also denote them as (5+1) coordinated. By sharing common edges and corners, the octahedra form a three-dimensional network, which can be built up from infinite rod-like elements running along [010] having a 2 × 2 octahedra wide cross section. Actually, a single rod can be imagined to be cut from the ReO_3-structure type and contains a total of four corner-sharing single-chains of octahedra. Within each single chain, strictly alternating cation sequences corresponding to …Mg–W–Mg–W… can be observed. The [WO_6]-groups show a pronounced distortion due to second-order Jahn-Teller effects.

$MgWO_4$-II is topologically equivalent to the monoclinic so-called VO_2(HT) structure-type. A detailed analysis of the relationships with other ABO_4-compounds is presented based on concepts of group theory. Solid-state characterization has been supplemented by micro-Raman spectroscopy. Finally, the thermal expansion tensor of $MgWO_4$-II between ambient temperature and about 700 °C has been determined. The calculations indicate that the thermal expansion in $MgWO_4$-II is highly anisotropic and quasi two-dimensional with a very low value α_2 along the direction of the above-mentioned octahedral chains of the network.

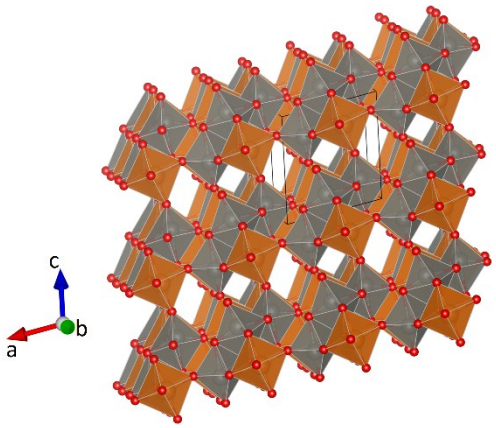

Figure 1. Side view of the crystal structure of $MgWO_4$-II. The MgO_6- and WO_6-octahahedra are colored orange and grey, respectively. Small red spheres represent oxygen atoms. The outline of a single unit-cell is shown as well.

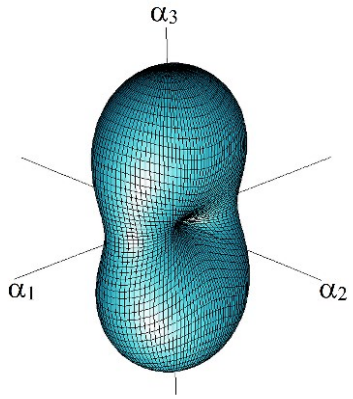

Figure 2. Three-dimensional representation surface of the thermal expansion tensor α_{ij} of $MgWO_4$-II at 500 °C.

Using combined C, Cd, Ba, and Ni isotopes as novel biomarkers to decipher Archean microbial metal cycling

S.V. Hohl[1], Y. Lv[2], S. Viehmann[3], Yi-bo Lin[4], Y. Zhang[5], Y. Jiang[1]

[1]State Key Laboratory of Marine Geology, Tongji University, Shanghai; P.R. China
[2]State Key Laboratory of Geological Processes and Mineral Resources, China University of Geosciences, Beijing, P.R. China
[3]Department of Mineralogy, University of Hannover, Germany
[4]State Key Laboratory of Minerals Resources Research, Nanjing University, Nanjing, PR China
[5]Key State Laboratory of Palaeobiology and Stratigraphy (LBS)
Nanjing Institute of Geology and Palaeontology (NIGPAS)
e-mail: sv_hohl@tongji.edu.cn

Stromatolitic carbonates are geochemical archives that allow studying the long-term interplay of the biosphere, atmosphere, and hydrosphere through deep-time, with the unique potential to also investigate early life environments and the evolution of the metallome. Recently non-traditional stable isotopes of bioactive metals emerged as novel proxies to reconstruct the micronutrient cycling in stromatolitic microbial habitats.

In this study, we use stromatolites from the ~2.95 billion-year-old Pongola Supergroup (South Africa) as field laboratory for combined in-situ trace metal mapping and layer-specific novel stable metal isotope compositions to determine biogeochemical metal cycling in early Earth microbial habitats. LA ICP-MS maps reveal intrinsic bio-sedimentary enrichments of Ni and Cd in laminae; in contrast, Ba shows a more heterogeneous distribution throughout the stromatolite. Intra-laminae δ^{60}Ni and δ^{112}Cd follow typical kinetic isotopic fractionation, i.e., the isotopic composition of Cd and Ni evolves to heavier values with decreasing respective element concentrations arguing for carbonate precipitation from a fractionated Ni and Cd pool heavier than ambient silicate rocks. Further correlations with δ^{13}C and macronutrient P argue for co-existing methanogenetic, and photogenetic metal uptake responsible for pronounced isotopic fractionation. In contrast, δ^{138}Ba records isotope fractionation related to variable aragonite precipitation rates in the stromatolite, i.e., Ba evolves to isotopically heavier values with increasing concentrations under variable alkalinity in microbial habitats.

We show that the combination of Cd and Ni isotopes has a unique potential as novel isotope biomarker for early Earths bio-chemical sediment record of where traditional biomarkers are not applicable due to fragmentary preservation of organic material.

Deformation induced dissolution-precipitation of zircon in greenschist facies metasediments

M. S. Hollinetz[1], B. Grasemann[1], C. McFarlane[2], B. Huet[3], D. Schneider[4]

[1)] Department of Geology, University of Vienna
[2)] Department of Earth Sciences, University of New Brunswick
[3)] Department of Hard Rock Geology, GeoSphere Austria
[4)] Department of Earth and Environmental Sciences, University of Ottawa
e-mail: marianne.sophie.hollinetz@univie.ac.at

Dissolution-precipitation coupled to mass transfer via an intergranular fluid is an essential mechanism to allow growth of metamorphic minerals and continuous equilibration during prograde metamorphism at greenschist facies conditions where the temperature is too low for allowing significant solid-state diffusion. As the prevailing stress field may control sites of preferred dissolution and precipitation, and mass transfer in the fluid may be highly anisotropic depending on the orientation and abundance of grain boundaries, all processes involved are inevitably linked with deformation. Although dissolution-precipitation and fluid-mediated mass transfer is well established for major components and growth metamorphic index minerals, little is known about the effects of these processes on accessory minerals that are considered nonreactive during metamorphism, consisting of elements that are considered as chemically immobile (e.g. Zr, Ti, Th). In this contribution, we present two case studies from the Staufen-Höllengebirge Nappe (Austroalpine Unit, Eastern Alps) which allow us to investigate the behaviour of Zr during greenschist facies prograde metamorphism in metasediments. At each locality we characterized detrital and metamorphic zircon populations with high-resolution SEM imaging and use a novel laser-ablation based strategy termed 'bulk inclusion dating' (Hollinetz et al. 2022) as a proxy for quantifying the extent of metamorphic zircon formation.

The first case study focuses on a chloritoid-bearing schist sampled at the base of the Staufen-Höllengebirge Nappe. Thermodynamic modelling predicts chloritoid growth in a P-T field between 450–490 °C and 0.5–0.7 GPa, indicating upper greenschist facies conditions. A conspicuous feature of this rock are numerous minute (0.1–3 μm), euhedral zircon crystals found both in chloritoid porphyroblasts and as matrix phases. From the zircon morphology, crystal size distribution, orientation and spatial distribution of different micro-zircon populations in the chloritoid core, its rim and the matrix, we interpret syntectonic zircon precipitation and progressive coarsening from a Zr-bearing fluid migrating along grain boundaries. Since no detrital zircon grains are observed in this sample, the Zr source is most likely a detrital Ti-phase that broke down during prograde metamorphism (e.g., titanite). Bulk inclusion dating of the chloritoid rim and its zircon inclusions yields a U-Pb age of 116.7 ± 9.1 Ma (MSWD: 1.5, n: 79), consistent with the Early Cretaceous timing of nappe stacking (Ortner et al. 2008). Systematic imaging of the targeted chloritoid domain combined with trace element data clarifies the abundance and size of different U-Pb bearing inclusions and unambiguously link the U-Pb age to micro-zircon inclusions. Our data therefore implies total mobilization of Zr during late prograde metamorphism.

The second case study focuses on metaconglomerates and -sandstones sampled in the Permian cover of the Staufen-Höllengebirge Nappe. In these lower greenschist facies samples, sedimentary features are preserved, but overgrown by a metamorphic mineral assemblage

consisting of chloritoid + pyrophyllite + muscovite + hematite + rutile + quartz that is consistent with P-T conditions of c. 350 °C and 0.2-0.6 GPa. Although all samples contain the same metamorphic mineral assemblage, they preserve significant differences regarding their primary sedimentological features (i.e., size of detrital clasts, layering) as well as secondary structural features (i.e. pressure solution cleavages). We investigated low-strain samples that exhibit a weakly developed fabric and high-strain samples with a pronounced spaced cleavage. Large, rounded detrital zircon grains that are occasionally fractured and/or porous are abundant in all samples. However, only in high-strain samples we find tiny zircon outgrowths on detrital grains and sparse submicron zircon (0.1–1 μm) in chloritoid. U-Pb ages of detrital zircon dominantly are between 700–400 Ma with the youngest concordant ages at c. 290 Ma. Bulk inclusion micro-zircon data in low-strain samples yield pre-Cretaceous dates younger than the detrital population, which indicates limited metamorphic zircon growth. In the "high-strain" samples, the bulk inclusion dates suggest significant micro-zircon crystallization in the Early Cretaceous. Combining microstructural observations and bulk-inclusion zircon data strongly suggests that Zr mobility and metamorphic zircon growth may be linked to intensity of deformation assisted by dissolution-precipitation.

We document deformation assisted Zr mobility in greenschist-facies metasediments and show that dissolution-precipitation coupled to mass transfer via an intergranular fluid is a process that is also relevant for elements reputed as immobile. As ongoing technological advances continuously shrink the limits imposed by instrumentation, the bulk-inclusion strategy can fill the gap in our understanding of the geological process leading to the precipitation of micro-zircon. This approach allows integration between metamorphic conditions, deformation and age constraints and opens up new applications in the investigation of low-grade metamorphic rocks, potentially including dating of deformation.

Hollinetz MS, Schneider DA, McFarlane CRM, Huet B, Rantitsch G, Grasemann B (2022): Bulk inclusion micro-zircon U–Pb geochronology: A new tool to date low- grade metamorphism. - J Metamorphic Geol 40, 207-227

Ortner H, Ustaszewski M, Rittner M (2008): Late Jurassic tectonics and sedimentation: breccias in the Unken syncline, central Northern Calcareous Alps. - Swiss J Geosci 101, 55-71

From allanite to monazite and back: a complex polymetamorphic REE-phase evolution

M. S. Hollinetz[1], B. Huet[2], C. McFarlane[3], D. Schneider[4], B. Grasemann[1]

[1)] Department of Geology, University of Vienna
[2)] Department of Hard Rock Geology, GeoSphere Austria
[3)] Department of Earth and Environmental Sciences, University of Ottawa
[4)] Department of Earth Sciences, University of New Brunswick
e-mail: marianne.sophie.hollinetz@univie.ac.at

REE-bearing minerals (e.g. allanite / epidote, monazite, xenotime) are suitable targets for in-situ U-Th-Pb geochronology, thus it is essential to understand their stabilities during metamorphism for bringing the age data into any tectonic framework. At lower greenschist facies conditions, allanite / REE-rich epidote forms from the breakdown of detrital or low-grade metamorphic REE-bearing phosphates (e.g., monazite, xenotime). Depending on the bulk rock chemistry, the reverse reaction can occur at the greenschist – amphibolite facies transition or allanite remains stable at amphibolite facies conditions (e.g., Janots et al. 2008).

In this contribution, we present complex allanite – monazite – xenotime phase relations in chloritoid- and staurolite-bearing micaschist sampled at the base of the Schöckel Nappe (Austroalpine Unit, Eastern Alps). The samples contain large chloritoid, staurolite and retrogressed plagioclase porphyroblasts in a matrix of white mica, ilmenite, rutile and quartz. We distinguish two rock types that exhibit different REE-bearing minerals assemblages. Type 1 samples exhibit a simple REE-mineralogy that consist of a LREE-rich allanite core, which is overgrown by chemically zoned REE-rich epidote rim. U-Th-Pb dating using laser-ablation ICPMS yields an age of 275.2 ± 6.2 Ma (MSWD: 2.2, n: 45). In type 2 samples, the REE-phase relationships are much more complex. Few mm-scale LREE-rich allanite porphyroblasts possessing relicts of HREE-rich epidote rims are observed. Another generation of chemically zoned REE-epidote formed in fractures crosscutting both zones. Small (20–50 μm) REE-rich epidote blasts with a similar chemical composition occur in the vicinity of the large porphyroblasts. Additionally, up to 1 mm long aggregates consisting of small (10–20 μm) highly zoned, REE-rich epidote crystals intergrown with apatite are abundant. BSE imaging reveals highly irregular, micron-scale chemical zoning within the REE-epidote aggregate, resulting in a patchy appearance. In these aggregates small (<10 μm) monazite inclusions are typical. Small (<10 μm) xenotime crystals surrounding both the LREE-rich allanite and the REE-epidote aggregate also occur. U-Th-Pb dating that targeted the LREE-rich allanite was unsuccessful due to its high common Pb concentration. The zoned REE-rich epidote (overgrowth, blasts and aggregates) yield an age of 108.8 ± 6.2 Ma (MSWD: 3.1, n: 13).

Combining petrography, chemical composition and geochronological data from both sample types, we interpret LREE-rich allanite growth followed by formation of REE-rich epidote during prograde metamorphism in the Permian. Due to different bulk rock compositions, this assemblage remained stable at peak metamorphic conditions in type 1 samples, but was replaced by clusters of small monazite and xenotime crystals. During the Early Cretaceous metamorphic overprint in the allanite stability field, Permian monazite was destabilized and replaced by REE-rich epidote and apatite.

Janots, E, Engi, M, Berger, A, Allaz, J, Schwarz, JO, Spandler, C (2008): Prograde metamorphic sequence of REE minerals in pelitic rocks of the Central Alps: implications for allanite–monazite–xenotime phase relations from 250 to 610 °C. - J Metam Geol 26, 509-526

Raman spectroscopy of calcium oxalate hydrates from plant leaves

N. Horáková[1], J. Cempírek[1]

[1]Department of Geological Sciences, Masaryk University, Brno, Czech Republic
e-mail: nice.horak@gmail.com

There are several types of biominerals in plants; the most common are crystals and aggregates of calcium oxalate (CaOx), calcium carbonate (amorphous $CaCO_3$ or calcite) and amorphous silica. Ca-oxalates are represented by three hydrated forms of CaC_2O_4: whewellite (monohydrate; COM), weddellite (dihydrate; COD), and caoxite (trihydrate; COT). The most common mineral is COM whereas COD and COT are considered to be metastable phases; on the other hand, they are assumed to be precursor phases during COM or COD formation (Conti et al. 2015). Plant crystals are formed from endogenously synthesized oxalic acid which combines with calcium from the environment (Franceschi & Nakata, 2005).

We used synthetic analogues of CaOx hydrates to acquire high-resolution reference Raman spectra (Fig. 1). Consequently, we identified different CaOx hydrates in leaves of five different species of the *Araceae* family.

In the studied plants, the most common phase is COM in the form of needles (raphids), or crystalline sand; COD more commonly forms druses, dipyramids or crystal twins, and COT is usually in the form of prisms or rounded aggregates. All three CaOx hydrates were found in 3 plant species, only COD in 4 plants and COM as the most common form in all five plants. COM is widespread, it is contained in all parts of the plant, mostly in the form of long needles stored in idioblasts, whereas the COD is in most cases in petiole in the form of druses. COT as the least stable phase is present only in rare cases in the leaves, its crystals were found in a large amount especially in Alocasia macrorrhiza Stingray.

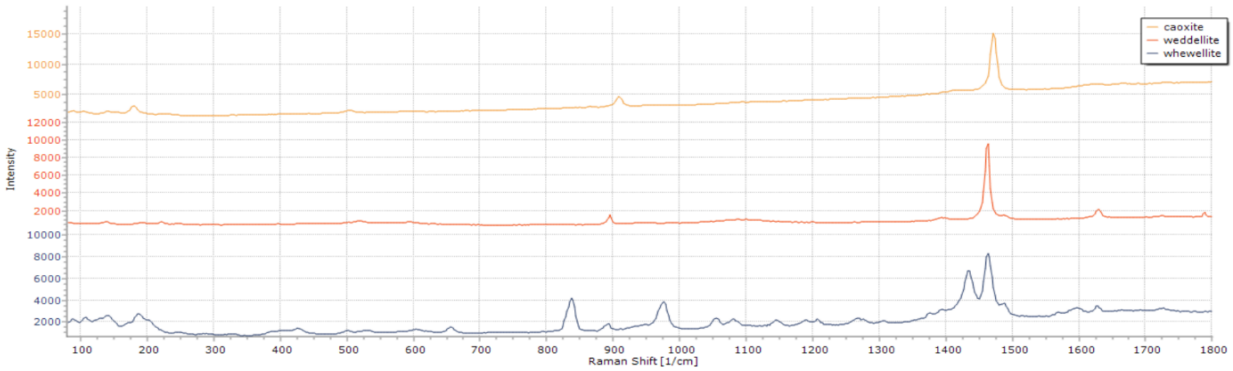

Figure 1 Raman spectra of COM, COD, and COT. - Foto: N. Horáková

Conti C, Casati M, Colombo C, Possenti E, Realini M, Gatta GD, Zerbi G (2015): Synthesis of calcium oxalate trihydrate: New data by vibrational spectroscopy and synchrotron X-ray diffraction. - Spectrochima Acta A, Molecular and Biomolecular Spectroscopy 150, 721-730

Franceschi VR, Nakata PA (2005): Calcium oxalate in plants: formation and function. - Annu Rev Plant Biol 56, 41-71

Fluid "self-purification" – Insight from the particle attachment processes during the growth of three-dimensional mineral dendrites

Z. Hou[1], D. Woś[2], A. Rogowitz[1,3], C. Tschegg[4], A.H.N. Rice[1], L. Nasdala[1], F. Fusseis[5], P. Szymczak[2], B. Grasemann[1]

[1]University of Vienna
[2]University of Warsaw
[3]University of Graz
[4]Glock Health, Science and Research GmbH, Deutsch-Wagram, Austria
[5]The University of Edinburgh
e-mail: zhaoliang.hou@univie.ac.at

Manganese (Mn) dendrites are a common type of mineral dendrites which can typically be found as two-dimensional branch-like patterns on rock surfaces, such as bedding planes and joints suggesting a fluid-rock interaction. Their three-dimensional (3D) counterpart has so far been massively overlooked, and thus little is known about 3D mineral dendrite growth processes and potential implications for fluid-rock interaction. Here, we combined high-resolution X-ray, electron-based micro-analyses with numerical modelling to show that the formation of natural 3D dendrites is an aggregation process of Mn-oxide nanoparticles in an aqueous environment. The dendrites form a < 15 mm high "forest" (Figure 1) in clinoptilolite-tuffs (zeolites), with trunks and branches, both having a core-rim structure and in the upper part of the forest, an alternating concentric core-rim layering. Secondary electron microscope (SEM) observations indicate dendrite growth reduced the rock's original porosity from ~17% in the matrix to ~1% - 4% in the internal rims and 0% in the cores. High-resolution SEM shows dendrite-forming Mn oxides are built by sub-angular to rounded, several-nanometer- to 1-µm-sized particles that have been aggregated forming larger clusters. Using the lattice Boltzmann method we modelled the formation and evolutionary processes of the 3D Mn dendrites. This allowed us to track the diffusing population of Mn ions and oxygen molecules as well as the reaction between them that led to the formation of Mn-oxide nanoparticles. The mobility and aggregation of nanoparticle populations were then tracked.

Our numerical models suggest sensitive feedback between dendrite morphology and the volume of infiltrating fluids, as well as the concentrations of Mn ions. Our work provides three important findings. First, 3D mineral dendrites can offer a simple system to investigate the affecting physical parameters of particle attachment processes in nature, such as the interplay of diffusion and surface energy effects between particles on dendrite growth dynamics. Second, the growth of the 3D dendrites, aggregating the particles in the surrounding fluids, can be seen as a fluid "self-purification" process. Third, the formation of the banding structures of the 3D dendrites, as well as the sensitive growth of dendrites in relation to the volume of infiltrating fluid and concentrations of Mn ion, strongly suggest the dendrites encode the hydrogeochemical history of the hosting rocks.

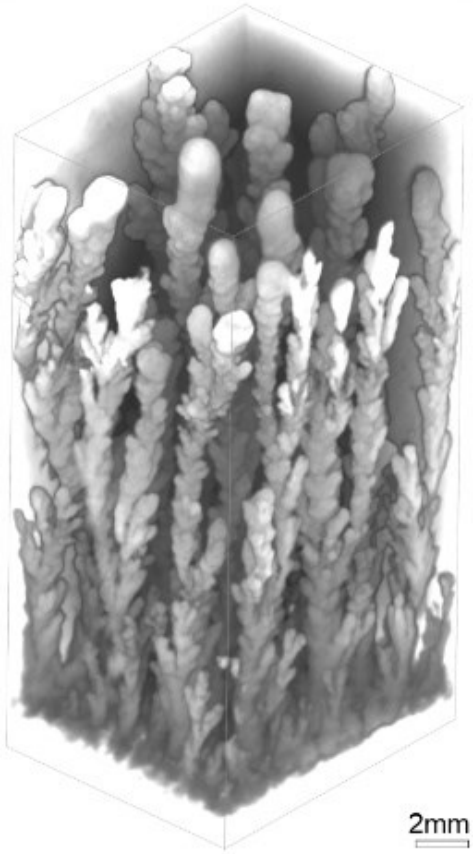

Figure 1. X-ray microtomography data show a 3D mineral dendrite forest.

Creep, fail, and creep again at eclogite facies: interactions between metamorphism and deformation at the Hohl eclogite body (Koralpe, Eastern Alps, Austria)

B. Huet[1], A. Rogowitz[2], S. Schorn[2]

[1]GeoSphere Austria
[2]Institute of Earth Sciences, University of Graz
e-mail: benjamin.huet@geosphere.at

We present (micro)structural, petrographical, and chemical data from a series of low Mg – high Ti eclogite samples collected at the Hohl eclogite body (Koralpe, Eastern Alps, Austria). The eclogite mass is characterized by a pronounced foliation defined by the shape preferred orientation of the major minerals (average: 030/40) and mineral lineation defined by the shape preferred orientation of prismatic minerals (average: 324/18). In addition to omphacite, garnet, amphibole, epidote and rutile, minor euhedral quartz grains are present. Overall, grains show rather straight grain boundaries and uniform extinction. Thermodynamic forward modelling indicates that eclogitization occurred under fluid saturated conditions at about 1.8 GPa and 640 °C, which is slightly below the peak conditions.

The eclogite fabric is crosscut by a complex network of mineral veins characterized by coarse elongated crystals. These veins have a thickness comprised between a few millimeters and a few centimeters and contain the same assemblage as the host eclogite. In comparison to the host, they are enriched in quartz and epidote and depleted in garnet. Minerals composition is similar to the composition of the host eclogite indicating that veining occurred at eclogite facies conditions. One vein set is subperpendicular to the main foliation (average: 234/27) and the other is subparallel to it (average: 055/51). In both sets, the long axis of crystals is subparallel to the vein boundary and strikes NW-SE, which is compatible with crystal growth in the same tectonic regime as the eclogite fabric. Wing cracks indicate that the veins formed as shear fractures. Deflection of the eclogite fabric adjacent to the veins implies ductile reactivation of the veins as flanking structures and strain localization under top-to-the-W shearing. In consequence, the reactivated veins are characterized by undulatory extinction, twinning and subgrain formation in quartz, all being indicative of dislocation creep.

Our investigations document strong interactions between chemical (i.e., metamorphism) and mechanical (i.e., deformation) processes operating at eclogite facies and illustrate how metamorphic reactions dictate the deformation style of an eclogite. The microstructures of the eclogite host are interpreted as evidence of fluid-triggered syn-tectonic prograde eclogitization accommodated by diffusion and dissolution-precipitation processes. Ongoing prograde metamorphism resulted in progressive dehydration and minor melting of the already equilibrated eclogite. Subsequent increase in the pore-fluid pressure induced brittle failure and allowed precipitation of an eclogite facies assemblage in the vein. Finally, the quartz enriched veins localized ductile strain and deformed by dislocation creep. Hence, within the same tectonic event and without remarkable change of boundary conditions, eclogite can creep, fail and creep again.

Thermodynamic forward modelling of main and REE-bearing phases linking in situ U-Th-Pb REE-epidote ages and pressure-temperature conditions

B. Huet[1], D.A. Schneider[2], G. Rantitsch[3]

[1]GeoSphere Austria, Vienna
[2]Department of Earth and Environmental Sciences, University of Ottawa
[3]Department of Applied Geosciences and Geophysics, Montanuniversität Leoben
e-mail: benjamin.huet@geosphere.at

REE-epidote is a solid solution of epidote-group minerals with rare earth elements plus yttrium that is a common phase of greenschist facies metapelites and a popular target for geochronology. Linking the time information to metamorphic conditions is however complicated by the diversity of reactions leading to the formation of REE-epidote as these involve REE- and/or Ca-bearing phases (e.g., monazite, apatite, calcite and plagioclase). We compiled a thermodynamic dataset for the system NaKCaFeMgAlSiTiHCOCeYPF from several sources (Berman, 1988; Connolly, 1995; Franzolin et al., 2011; Gaboreau et al., 2005; Hoschek, 2016; Pourteau et al., 2014; Spear, 2010; Spear & Pyle, 2010) in order to model equilibrium assemblages and phase chemistry for both main and REE-bearing phases in metapelites, especially in the greenschist facies.

We tested the dataset on a graphitic micaschist of the Schwarzkopf Formation collected at the foot of the Hochgamsburg (Fusch valley, Tauern Window). The sample shows relatively simple phase relationships and exhibits evidence for only one metamorphic event. The metamorphic assemblage consists of porphyroblasts of chloritoid, kyanite, REE-epidote and apatite in a matrix of muscovite, paragonite, margarite and quartz. Small rutile, graphite, xenotime and zircon are present as inclusions or in matrix. REE-epidote occurs as euhedral to subhedral, 250-1000 μm long grains and displays a microstructural and chemical core-mantle-rim zonation. The core has a patchy or oscillatory BSE pattern and is rich in inclusions of amoeboid quartz and minute graphite, as well as subordinate muscovite, chloritoid, rutile, xenotime and thorite. The mantle is discontinuous (< 60 μm thick), inclusion-free and shows a bright smoother BSE pattern. The rim corresponds to dark and thin discontinuous overgrowths (< 20 μm thick). Core, mantle and rim contain decreasing contents of REE+Th+U in the range 0.5–0.6, 0.4–0.6 and 0.1–0.3 a.p.f.u., respectively. The core and mantle are LREE-rich whereas the rim is HREE+Y-rich. LA-ICPMS analyses of REE-epidote mantle were carried out using a 20 μm laser spot diameter. All thirty-one analyses define a 27.5 ± 1.3 Ma U-Th-Pb isochron date (MSWD: 0.69) that is consistent with the conventional Tera-Wasserburg U-Pb date of 27.0 ± 2.3 Ma (MSWD: 0.36).

Thermodynamic forward modelling indicates that the observed assemblage chloritoid+kyanite+REE-epidote+muscovite+paragonite+margarite+apatite+rutile+xenotime+quartz is stable together with a graphite buffered COH-fluid in a narrow field centred at 12 kbar – 500 °C, in agreement with results of Raman spectroscopy on carbonaceous material (511 ± 26 °C). This field corresponds to the innermost part of the REE-epidote stability domain, in which the Ce-concentration progressively decreases from the margin to the centre. Modelling helps with interpreting the zonation of REE-epidote. The core grew from U-Th-rich monazite and most likely lawsonite once REE-epidote became stable. Xenotime inclusions represent products of this reaction. The mantle formed during continued growth further inside the REE-

epidote stability domain under increasing temperature. The HREE+Y-rich rim finally grew in an environment depleted in LREE, where xenotime was the main REE-source. Additionally the modelled compositions of chloritoid, white micas and apatite is compatible with the measured ones. Tests on the effect of unknown inputs (e.g., the bulk rock concertation of F) or poorly constrained thermodynamic data (e.g., the standard enthalpy of endmember allanite) indicate that these parameters have little impact on the results.

We could therefore acquire estimates for pressure and temperature and timing as well as coupling them tightly through thermodynamic modelling. The U-Th-Pb isochron date 27.5 ± 1.3 Ma represents the timing of the REE-epidote mantle growth and therefore corresponds to conditions close to peak metamorphism at 12 kbar – 500 °C. These P-T-t constraints are entirely consistent with the Barrovian metamorphic event that is widespread in the Tauern Window ("Tauernkristallisation").

Berman RG (1988): Internally-consistent thermodynamic data for minerals in the system Na_2O-K_2O-CaO-MgO-FeO-Fe_2O_3-Al_2O_3-SiO_2-TiO_2-H_2O-CO_2. - J Petrol 29, 445-522

Connolly JAD (1995): Phase diagram methods for graphitic rocks and application to the system C-O-H-FeO-TiO_2-SiO_2. - Contr Miner Petrol 119, 94-116

Franzolin E, Schmidt MW, Poli S (2011): Ternary Ca-Fe-Mg carbonates: subsolidus phase relations at 3.5 GPa and a thermodynamic solid solution model including order/disorder. - Contr Miner Petrol 161, 213-227

Gaboreau S, Beaufort D, Vieillard P, Patrier P, Bruneton P (2005): Aluminum phosphate-sulfate minerals associated with Proterozoic unconformity-type uranium deposits in the East Alligator River Uranium Field, Northern Territories, Australia. - Canad Miner 43, 813-827

Hoschek G (2016): Phase relations of the REE minerals florencite, allanite and monazite in quartzitic garnet-kyanite schist of the Eclogite Zone, Tauern Window, Austria. – Eur J Miner 28, 735-750

Pourteau A, Bousquet R, Vidal O, Plunder A, Duesterhoeft E, Candan O, Oberhänsli R (2014): Multistage growth of Fe-Mg-carpholite and Fe-Mg-chloritoid, from field evidence to thermodynamic modelling. - Contr Miner Petrol 168, 25 pp

Spear FS (2010): Monazite–allanite phase relations in metapelites. - Chem Geol 279, 55-62

Spear FS, Pyle JM (2010): Theoretical modeling of monazite growth in a low-Ca metapelite. - Chem Geol 273, 111-119

Mineralogy and geochemistry of the Majala and Chacarilla Formations in Northern Chile (Atacama Desert): Implications for provenance, tectonic setting and paleoenvironmental conditions

N. Hurem[1], J. Méndez[2], V. Gesualdi[3], M. Yurac[4], M. Belvedere[3, 5], C. Salazar[2], C. A. Meyer[6], D. Hippler[1]

[1]Graz University of Technology, Institute of Applied Geosciences, 8010 Graz, Austria
[2]Universidad Mayor, Escuela de Geología, 7500000 Providencia, Santiago de Chile, Chile
[3]Università degli Studi di Firenze, Dipartimento di Scienza della Terra, 50121 Firenze, Italy
[4]Unidad de Patrimonio Paleontológico, Consejo de Monumentos Nationales7500000 Providencia, Santiago de Chile, Chile
[5]NBFC, National Biodiversity Future Center, Piazza Marina 61, Palermo 90133, Italy
[6]University of Basel, Department of Environmental Sciences, 4056 Basel, Switzerland
e-mail: nejla.hurem@student.tugraz.at

The Mesozoic sedimentary record of the northern Atacama and Tarapacá region in Chile is still to be fully explored. Mineralogical and geochemical studies as well as dating methods have never been carried out in this region, even though numerous and well-preserved Late Jurassic to Early Cretaceous dinosaur tracksites have been found recently. A pioneer field campaign was therefore carried out in 2022 in the Quebrada Huatacondo followed by a second campaign in 2023 in the Quebrada Arca. At both sites, Late Jurassic to Early Cretaceous sedimentary rocks of the Majala and Chacarilla Formations are well-exposed and constitute a promising geological archive. We sampled the sedimentary rocks, mainly fine-grained sandstones and siltstones, along the lithological sections in order to investigate the depositional and paleo-environmental conditions, provenance and tectonic setting as well as paleo-weathering and climate. In order to achieve our goals, we performed mineralogical and geochemical analysis using XRD and XRF in combination with high-resolution photogrammetry of the outcrops.

Preliminary results indicate that most of the fine-grained sandstones and siltstones can be classified as (sub-) litharenites mainly consisting of quartz and minor to accessory contributions of alkali feldspar, illite and chlorite. Finely-disseminated magnetite and pyrite produce the dark fresh-cut color and the reddish weathering color. Calcite and/or quartz constitute the main cementing phases. The geochemical composition of the sampled sedimentary rocks equals an almost upper crustal composition with distinct formation-specific differences between sand- and siltstones of the Majala and Chacarilla Formations: Rocks of the Majala Fm are slightly enriched in Cr, Ni and Cu, whereas rocks of the Chacarilla Fm show slight differences in elemental composition between the base and the top part. Summarizing the preliminary results, changes in the geochemistry between the two formations can already be clarified. With the complementary new data of the Quebrada Arca, the paleo-environmental conditions of the region can be reconstructed in a promising way. Additional U-Pb dating of the formations will provide desirable age constraints of deposition and provenance to set up an overall picture of the Late Jurassic to Early Cretaceous paleo-environment in Northern Chile.

The importance of volatiles in the formation of magmatic sulfide ore deposits: experimental constraints

G. Iacono-Marziano1[1], M. Le Vaillant[2], S.J. Barnes[2], B. Godel[2]

[1] Institut des Sciences de la Terre d'Orléans, CNRS-Université d'Orléans-BRGM, Orleans, France
[2] CSIRO Mineral Resources, Perth, Australia
e-mail: giada.iacono@cnrs-orleans.fr

Research studies provide growing evidence for the presence of fluids within magmatic mineral systems of mafic-ultramafic composition, although these ore-forming magmas are generally considered as volatile-poor. Here we summarize the results of two experimental studies that clarify the role of volatiles in the formation of magmatic sulfide ore deposits in mafic-ultramafic magmas: (i) interaction experiments simulating magmatic assimilation of sulfate and/or organic compounds (Iacono-Marziano et al. 2017); (ii) a more recent experimental study shedding light on previously unnoticed physical processes ensuing from the association between sulfide melt and fluid phase (Iacono-Marziano et al. 2022). The silicate melt composition used for both studies is similar to the parental melt of the Noril'sk-Talnakh ore bearing intrusions in Polar Siberia and all materials used in the experiments were sampled from the Noril'sk region. Moreover, the experiments were conducted at magmatic conditions relevant to the emplacement pressures and temperatures of the Noril'sk-Talnakh intrusions, so that experimental findings are directly applicable to these world-class ores.

The addition of external sulfur to the magma is one of the most common ore-forming processes invoked for magmatic sulfide deposits. Sulphur can be introduced into the magma by several process, our experiments at magmatic conditions (1200 °C, 80 MPa) show that anhydrite assimilation in the presence of a reducing agent, i.e. organic matter-rich rocks such as coal, is extremely efficient in producing high sulfide supersaturation in the magma.

The association between the sulfide melt and the fluid phase has been shown to allow the upward transfer of the sulfide melt (Mungall et al. 2015). Our recent experimental results illustrate another physical process that occurs when the proportion of fluid phase in the magma is low: the sulfide-fluid association favors the accumulation of sulfide liquid by facilitating the coalescence of the sulfide droplets that are attached to the same fluid bubble. This leads to the accumulation of the sulfide melt in the upper part of the experimental samples. Coalescence of sulfide droplets may be facilitated by the lowering of their interfacial tension induced by the bubble. However, the main driver for coalescence to occur is likely to be the fact that connection to the bubbles keeps the droplets in contact for long enough to allow drainage of the melt film between them, as opposed to the situation in a flowing magma where adjacent droplets are sheared apart before the melt film has time to drain (Robertson et al. 2015). This process may enable sulfide droplets coalescence and deposition in flowing magma, which otherwise have been shown to be unlikely processes (Robertson et al. 2015).

Experimental results indicate that sulfur degassing to the fluid phase increases with increasing proportion of fluid phase, concurrently reducing sulfide melt stability. Consequently, the sulfide melt is consumed and its metal content augments. Experimental samples with increasing fluid contents present increasingly Ni- and Cu-rich sulfide melts, illustrating how metal enrichment of sulfide melt can be attained by sulfur degassing. Magma degassing can therefore lead to sulfide upgrading.

Extensive sulfur degassing may completely consume the sulfide melt and form platinum-group minerals (PGMs) at relatively high temperatures (1150 °C in our experiments). Platinum-group mineral formation in the experimental samples occurs by desulfurisation of the

sulfide melt, while Ni and Cu are partitioned between the silicate melt and the fluid phase. This suggests an unconventional mechanism of PGM formation at temperatures higher than those typical of sulfide melt crystallization.

The experimental results presented above illustrate how the occurrence of a fluid phase in a mafic-ultramafic magma may represent a significant boost for magmatic sulfide ore forming processes: sulfide melt accumulation, tenor increase, and crystallization of PGMs are indeed key processes in the formation of magmatic Ni-Cu-Co-PGE ore deposits. We use the world-class Noril'sk-Talnakh ore deposits, in Polar Siberia as a case study.

Noril'sk-Talnakh ores are hosted in mafic-ultramafic subvolcanic ribbon-shaped intrusions. Extensive interaction of the ore-forming magmas with evaporitic and carbonaceous rocks has been proposed to be at the origin of the mineralization and the coexisting abundant fluid phase (e.g. Iacono-Marziano et al. 2017). The three main ore types are described in ore-bearing intrusions: (i) massive sulfides in the lower part of the intrusion and largely in the country rocks; (ii) disseminated sulfides (also called globular ores) inside picritic and taxitic rocks, also in the lower part of the intrusion; (iii) low-sulfide PGE ores in the upper part of the intrusion (e.g. Le Vaillant et al. 2017; Schoneveld et al. 2020). In the second and third ore-types subspherical structures within the crystalline framework have been interpreted as fluid bubbles filled with late magmatic phases (segregation vesicles) and/or hydrothermal minerals (e.g. Le Vaillant et al. 2017; Schoneveld et al. 2020). In the lower part of the intrusion, these structures are systematically associated with sulfide minerals suggesting they represent sulfide-fluid associations preserved in the olivine-rich magmatic rocks (Le Vaillant et al. 2017). In the upper part of the intrusion, these subspherical structures are even more common, typically associated with oxide mineral coatings, and generally containing lower amounts of sulfide minerals but abundant PGMs (Schoneveld et al. 2020), suggesting higher extents of sulfur degassing and sulfide dissolution. In contrast, massive sulfides are proposed to have experienced low extents of sulfur degassing, attested by the lower metal contents with respect to disseminated sulfides.

The distribution of ore types in Noril'sk-Talnakh intrusions therefore strongly suggests an increasing extent of degassing toward the top of the intrusions, implying increasing sulfide melt consumption and metal enrichment. Several other magmatic sulfide ores present evidence of the occurrence of a fluid phase during ore formation (relevant information can be found in Iacono-Marziano et al. 2022). Although a role for volatiles is less clear in other deposits, an increasing number of examples of sulfide-fluid associations is reported, suggesting that the mechanisms illustrated by the experiments may be more common than currently considered. We conclude that the role of volatiles in the formation of magmatic sulfide deposits should probably be re-evaluated.

Iacono-Marziano G, Ferraina C, Gaillard F, Di Carlo I, Arndt NT (2017): Assimilation of sulfate and carbonaceous rocks: experimental study, thermodynamic modeling and application to the Noril'sk-Talnakh region (Russia). - Ore Geol Rev 90, 399–413

Iacono-Marziano G, Le Vaillant M, Godel BM, Barnes SJ, Arbaret L (2022): The critical role of magma degassing in sulphide melt mobility and metal enrichment. - Nature Communications 13, 2359

Le Vaillant M, Barnes SJ, Mungall JE, Mungall EL (2017): Role of degassing of the Noril'sk nickel deposits in the Permian-Triassic mass extinction event. - Proceedings of the National Academy of Sciences 114, 2485–2490

Mungall JE, Brenan JM, Godel B, Barnes SJ, Gaillard F (2015): Transport of metals and sulphur in magmas by flotation of sulphide melt on vapor bubbles. - Nature Geoscience 8, 216–219

Robertson JC, Barnes SJ, Le Vaillant M (2015): Dynamics of magmatic sulphide droplets during transport in silicate melts and implications for magmatic sulphide ore formation. - J Petrol 56, 2445-2472

Schoneveld L, Barnes SJ, Godel B, Le Vaillant M, Yudovskaya MA, Kamenetsky V, Sluzhenikin SF (2020): Oxide-sulphide-melt-bubble interactions in spinel-rich taxitic rocks of the Norilsk-Talnakh intrusions, polar Siberia. - Econ Geol 115, 1305–1320

Melting experiments reproducing early differentiation in primitive achondrites

S. Iannini Lelarge[1], M. Masotta[1,2], L. Folco[1,2], T. Ubide[3], M.D. Suttle[1,4], W.N. Wegner[5], L. Pittarello[5]

[1]Università di Pisa, Italy
[2]Centro per l'Integrazione della Strumentazione Università di Pisa (CISUP), Pisa, Italy
[3]The University of Queensland, Brisbane, Australia
[4]The Open University, Milton Keynes, United Kingdom
[5]Naturhistorisches Museum, Vienna, Austria
e-mail: lidia.pittarello@nhm.at

Even small planetary bodies can have experienced internal differentiation, i.e., separation of the metal-sulphur components from the silicates forming a core and a mantle, respectively. In the meteorite record, primitive and anomalous achondrites represent a puzzle for scientists, as they seem to result from a differentiation process, but contain some primitive characteristics. Dedicated heating experiments in a piston-cylinder at 1 GPa and temperature steps from 1050 °C to 1400 °C, for 24h, have been performed to understand the uncomplete differentiation occurring on the parent body(ies) of such meteorites. As starting material, chondrites representative of specific early chemical settings were chosen: a) shocked L6 (DAV 01001), for intermediate redox state among the ordinary chondrites, b) carbonaceous chondrite (CM2, MCY12002), for oxidised parent bodies, and c) enstatite chondrite (EL6, MCY14005), for the reduced material in the Solar System. The resulting samples have been investigated with scanning electron microscope, electron microprobe analyser, laser ablation inductively coupled plasma mass spectrometry, Raman spectroscopy, and synchrotron radiation-micro computed tomography.

The experiments with the L6 chondrite resulted in non-eutectic melting of a small percent of the sample, with the metal and sulphide phases being mobilised first, already for the lowermost heating temperatures, and the silicates melting according to the sequence plagioclase-Ca-pyroxene-low Ca-pyroxene-olivine. This melting sequence affects the composition of the first melt produced, which evolves from trachyandesitic to more andesitic terms for increasing vol% of melting. Despite the fast quenching, crystallisation of olivine dendrites could not be avoided. The chemical composition of the produced melt shows similarities with that of some andesitic to trachyandesitic anomalous achondrites, such as NWA 11119, EC002, GRA 60128/9, Almahata Sitta clast ALM-A, NWA 6698, and NWA 11575. This suggests that these anomalous achondrites could have formed by incipient melting of chondritic material under fast heating conditions, like due to planetary collisions.

In the case of the CM2 carbonaceous chondrite as starting material, the obliteration of the initial texture is immediate. The melt produced has a composition ranging from picrobasaltic to basaltic-andesite, but already at the "low" temperature experiments several phases crystallises from the melt, such as Ca-rich olivine, pyroxene, spinel, kirschsteinite, and Ca-phosphates. The composition of the newly formed phases and the melt closely recall those found in angrites, some rare and peculiar basaltic achondrites, which likely have an impact origin (Rider-Stokes et al., 2023), where one of the bodies had a carbonaceous composition.

The analyses of the experiments with the enstatite chondrite are still ongoing. However, this work shows the importance of an experimental petrologic approach in constraining magmatic processes in the early Solar System.

Rider-Stokes BG, Greenwood RC, Anand M, White LF, Franchi IA, Debaille V, Goderis S, Pitarello L, Yamaguchi A, Mikouchi T, Claeys P (2023): Impact mixing among rocky planetesimals in the early Solar System from angrite oxygen isotopes. - Nat Astron, https://doi.org/10.1038/s41550-023-01968-0

Deformation and reaction of crustal rocks under high-pressure, high-temperature conditions

S. Incel[1,2], L. K. Mohrbach[1,3], J. Renner[1]

[1]Institute for Geology, Mineralogy and Geophysics, Ruhr Universität Bochum, 44801 Bochum, Germany
[2]Present address: Imperial College London, Department of Materials, South Kensington Campus, SW7 2AZ, London, United Kingdom
[3]Present address: WWU Münster, Institute for Mineralogy, 48149 Münster, Deutsches Elektronen Synchrotron, Beamline P02.2, 22607 Hamburg, Germany
e-mail: sincel@imperial.ac.uk

In the plagioclase-rich lower continental crust, hydrous epidote-group minerals will, among other phases, replace plagioclase once minor amounts of fluids are available (Goldsmith 1981). It has previously been shown that reacting plagioclase aggregates are significantly weaker than their unreacted counterparts at otherwise identical conditions (Stünitz & Tullis 2001). Yet, it still remains unclear if the observed weakening is due to the nucleation and growth of inherently weaker product phase, e.g., epidote-group minerals, or due to inhibited grain growth in a polyphase aggregate as a result of Zener pinning. Our working hypothesis was the former: Epidote-group minerals are inherently weaker than plagioclase under the same experimental conditions. To test this hypothesis, we experimentally investigated the relative strength of pure epidote and pure plagioclase aggregates at a confining pressure of 1 GPa, two different temperatures (550 and 650 °C) and two different strain rates ($5 \cdot 10^{-5}$ and $5 \cdot 10^{-6}$ s^{-1}) using a Griggs apparatus. Furthermore, epidote-group minerals will be initially much smaller than plagioclase, they are replacing. Hence, we also investigated potential strength differences due to differences in grain size by deforming aggregates with a grain-size range of either ≈90-135 μm or <25 μm. Under identical conditions, epidote aggregates are significantly stronger than their plagioclase counterparts even when partially reacted. Furthermore, we observe that reaction can induce a change in deformation behavior from distributed cracking to faulting in our epidote aggregates.

Goldsmith JR (1981): The join $CaAl_2Si_2O_8$–H_2O (anorthite-water) at elevated pressures and temperatures. - Amer Mineral 66, 1183–1188

Stünitz H, Tullis J (2001): Weakening and strain localization produced by syn-deformational reaction of plagioclase. - Internat J Earth Sci 90, 136–148. https://doi.org/10.1007/s005310000148

Calorimetric characterisation of the alkali feldspar binary

F. Ingegneri[1], E. Dachs[2], R. Abart[1]

[1] Department of Lithospheric Research, University of Vienna
[2]Department of Chemistry and Physics of Materials
Section Materials Science and Mineralogy, Salzburg University
e-mail: flora.ingegneri@univie.ac.at

The thermodynamic study of materials is vital as thermodynamic data such as Gibbs energy are of pivotal importance for modelling phase equilibria and processes in both nature and industry. This work aims at contributing to the thermodynamic characterisation of the most common mineral group in Earth's crust, namely feldspar. The focus is on the alkali feldspar solid solution, the endmembers of which are Albite ($NaAlSi_3O_8$) and Orthoclase ($KAlSi_3O_8$), and on the quantification of its molar heat capacity c_p and vibrational entropy S^{vib} as functions of composition X_{Or}.

Gem quality sanidine from Volkesfeld, Germany, with a composition of $X_{Or} = 0.85$ was used as starting material for cation exchange with a (Na,K)Cl salt melt. A total of 14 feldspar samples together with different (Na,K)Cl salt mixtures were held at 900 °C for a duration of 30 to 45 days in order to reach equilibrium. The resulting series was analysed on the EPMA Cameca SX Five FE at the University of Vienna and represents the composition of the whole binary.

10 of these samples have already been analysed via heat pulse calorimetry using the Physical Property Measurement System (PPMS) by Quantum Design at Salzburg University. Cp data were obtained for the temperature range from 2 to 300 K. S^{vib} was subsequently calculated by numerical integration of cp/T and is shown in Tab. 1. The corresponding plot can be found in Fig. 1. The relative error for S^{vib} is estimated at ± 0.7 % (Dachs & Bertoldi 2005).

These preliminary results yield a positive excess entropy with a maximum of $S^{ex} \approx 2$ J mol^{-1} K^{-1}. Further samples are being prepared for calorimetric analysis to close the current gap at $X_{Or} = [0.1, 0.3]$. As soon as the missing calorimetric data is available a Margules mixing model will be fitted to the data in order to obtain S^{vib} and S^{ex} as a function of X_{Or}.

Table 1. Vibrational entropy S^{vib} at T = 298.15 K

X_{Or} [ ]	S^{vib} [J mol^{-1} K^{-1}]
0.06	207.0
0.33	211.2
0.40	211.4
0.50	212.2
0.56	212.4
0.60	211.9
0.68	212.7
0.83	212.9
0.93	212.9
1.00	213.1

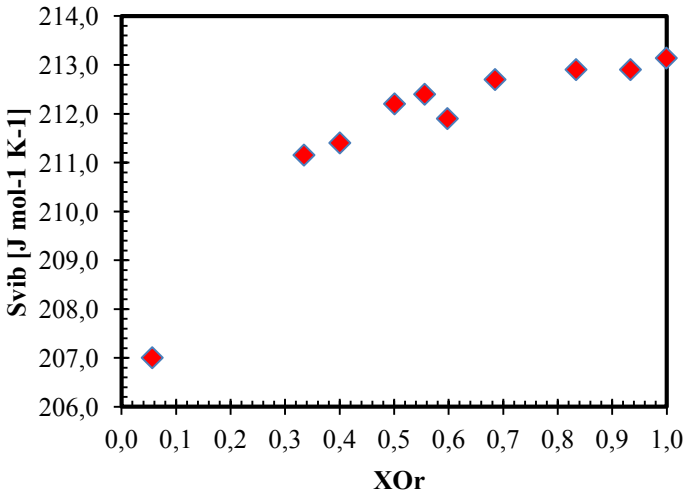

Figure 1. Vibrational entropy S^{vib} at T = 298.15 K

Dachs E, Bertoldi C (2005): Precision and accuracy of the heat-pulse calorimetric technique: low-temperature heat capacities of milligram-sized synthetic mineral samples. – Eur J Mineral 17, 251-261

Impurities in quartz from Amazon river sands

D. Jaeger[1], T. Ludwig[2], S. Andó[3], E. Garzanti[3], A.O. Sawakuchi[4], C. Chiessi[4], M. Strasser[1], R. Stalder[1]

[1]University of Innsbruck
[2]Heidelberg University
[3]University of Milano
[4]University of São Paulo
e-mail: roland.stalder@uibk.ac.at

Incorporation of impurities in quartz is primarily controlled by (1) the availability of the respective impurity in the chemical system and (2) the crystallisation condition. Even if the concentration of some of the impurities (such as OH species) may later be affected by metamorphic overprint, the total impurity inventory of each individual grain reflects its geological history. As the impurities are rather stable throughout sedimentary processes, quartz from siliciclastic sediments may thus serve as archive for the crystallisation conditions of the rocks in the source area. As hydrous defects are usually charge balanced by trace metals, concentrations in the most important charge balancing elements (Al, Li, B) may be reflected in the IR spectra, unless the sample lost OH by diffusion during metamorphic dehydration.

In this study quartz from several sediment samples from the lower Amazon and from three major tributaries of the Amazonian river system were analysed by FTIR spectroscopy and secondary ion mass spectrometry (SIMS) in order to characterise individual grains with respect to hydrous defects and trace metal contents.

Differences between the four samples are subtle but discernable. Trace element contents relevant for hydrous defects (Al, Li, B) are in general lower in quartz from the rivers draining the old continental shields (Xingu and Rio Negro) compared to quartz from the lower Amazon River; grains from Solimões, partly drained from the Andean orogeny, exhibit in general the highest trace element concentrations. The trace element contents are partly reflected in the OH signatures of quartz: samples from Solimões and lower Amazon exhibit a larger fraction of OH-rich grains, and the Li- and Al-specific absorption bands is less evolved in grains from Xingu and Rio Negro.

Taking into account trace element contents and OH signatures in quartz, quartz grains from the lower Amazon sample represent a mixture with significant contributions from Andean and shield sources. Conversely, heavy-mineral analysis indicates the Solimões River as the dominant source of sediment. This apparent discrepancy is reconciled considering that Andean detritus has a much higher heavy-mineral concentration than detritus recycled from siliciclastic rocks exposed in the Andean foothills, siliciclastic covers of the Brazilian-Guiana Shield, and quartz-rich sediments incised all across the retroarc basin and Amazonian lowlands.

Structure and vibrational properties of hydrous and anhydrous amorphous SiO_2 at high pressures

S. Jahn[1], M. Herrmann[1], M. Schulze[1], J. Dreschmann[1], W. Morgenroth[2], G. Garbarino[3], M. Mezouar[3], M. Wilke[2]

[1] Institut für Geologie und Mineralogie, Universität zu Köln, Zülpicher Straße 49b, 50674 Köln, Germany
[2] Institut für Geowissenschaften, Universität Potsdam, Karl-Liebknecht-Str. 24, 14476 Potsdam, Germany
[3] ESRF, CS 40220, 38043 Grenoble Cedex 9, France
e-mail: s.jahn@uni-koeln.de

Volatiles such as H_2O are important components in natural silicate glasses and melts. Their solubility and structural incorporation mechanisms depend on many parameters, and they change continuously with pressure and temperature. For a systematic understanding of those changes, in situ measurements are required. Here, we study the pressure-induced structural evolution of hydrous amorphous SiO_2 in diamond and moissanite anvil cells up to 40 GPa by Raman spectroscopy and X-ray diffraction, and compare the results to those from the respective anhydrous samples. The hydrous sample contains 10 wt% H_2O. Both hydrous and anhydrous samples show the characteristic features of the 4-fold to 6-fold Si coordination transition, which is essentially completed at the highest pressures of this study. Raman spectra indicate the predominance of molecular H_2O species over hydroxyl groups in the whole pressure range. However, the spectra change significantly at wavenumbers in the range of the O-H stretching vibrations. By analogy to spectra of pure liquid and crystalline H_2O, a transition from water-like to ice-VI-like behavior is observed, before the spectra become very broad at the highest pressures. The interpretation of the experimental data is supported by *ab initio* molecular dynamics simulations.

This work was supported by BMBF project 05K19PK2. Simulations were performed on the JUWELS supercomputer at Jülich Supercomputing Centre (JSC).

$Ca_2(Mn,Ti)O_4$, a potentially new mineral with the Ruddlesden-Popper structure

R. Juroszek[1], B. Krüger [2], G. Cametti[3]

[1] Institute of Earth Sciences, University of Silesia, Katowice, Poland
[2] Institute of Mineralogy and Petrography, University of Innsbruck, Innsbruck, Austria
[3] Institute of Geological Science, University of Bern, Bern, Switzerland
e-mail: rafal.juroszek@us.edu.pl

A potentially new mineral $Ca_2(Mn,Ti)O_4$, was found within the xenolith sample from the Bellerberg volcano in Germany. It is an accessory phase in partially altered xenolith composed mainly of cuspidine, fluorapatite, and gehlenite. It forms flat plate dark-brown crystals up to 100 μm in size. The empirical formula, established by electron microprobe analyses, is $(Ca_{1.98}Ce_{0.06})_{\Sigma 2.04}(Mn^{4+}_{0.36}Ti_{0.35}Fe^{3+}_{0.19}Al_{0.09})_{\Sigma 0.99}O_4$.

This mineral exhibits a Ruddlesden-Popper type structure characteristic for perovskite-like layered oxides of general formula $A_{n+1}M_nO_{3n+1}$, where A is typically an alkaline or rare earth ion, and M is a transition or post-transition metal ion (Ruddlesden and Popper, 1957). The diffraction pattern of the analysed crystal reveals a tetragonal lattice with unit cell parameters a = 3.7666(2) Å, c = 11.9861(8) Å, and volume V = 170.050(17) Å^3. The A site was refined with Ca^{2+} and Ce^{3+} scattering factors, whereas for the M site, a mixed scattering curve was used (0.55 Mn/Fe + 0.36 Ti + 0.09 Al) according to the chemical analyses. The final structure refinement converged to R = 2.74%. The crystal structure of $Ca_2(Mn,Ti)O_4$ exhibits a modular nature and consists of $Ca(Mn,Ti)O_3$ perovskite layers, which are packed between CaO rock-salt layers arranged along the c-axis (Fig. 1).

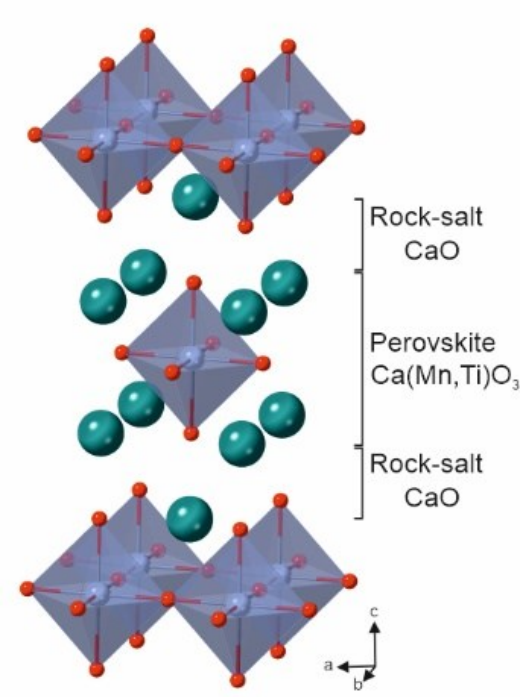

Figure 1. The $Ca_2(Mn,Ti)O_4$ phase with Ruddlesden-Popper structure, comprising rock-salt (CaO) and perovskite layers $Ca(Mn,Ti)O_3$ build by Ca-green spheres and $(Mn,Ti)O_6$ octahedra.

Previous reports indicate that Ruddlesden-Popper calcium manganates exhibit functional electronic properties and are interesting for various electronic phenomena, such as insulator-to-metal transitions, charge-ordering, and colossal magnetoresistance effect (Fawcett et al. 1998; Autret et al. 2004).

The investigation was partially supported by the National Science Center of Poland Grant (grant number 2021/41/B/ST10/00130).

Autret C, Martin C, Hervieu M, Retoux R, Raveau B, André G, Bourée F (2004): Structural investigation of Ca_2MnO_4 by neutron powder diffraction and electron microscopy. – J Solid State Chem 177, 2044-2052

Fawcett I.D, Sunstrom J.E, Greenblatt M, Croft M, Ramanujachary K.V (1998): Structure, magnetism, and properties of Ruddlesden-Popper calcium manganates prepared from citrate gels. – Chem Mater 10, 3643-3651

Ruddlesden S, Popper P (1957): New compounds of the K_2NiF_4 type. – Acta Crystallogr 10, 538-539

Interstitial diamonds reveal dry exhumation of UHP metamorphic rocks - insights from 3-D spatially resolved X-ray microtomography data

W.-A. Kahl[1] , H.-P. Schertl[2]

[1]MAPEX Center of Materials and Processing, Universität Bremen, 28359 Bremen, Germany,
[2]Institute of Geology, Mineralogy and Geophysics, Ruhr-University Bochum, 44780 Bochum, Germany
e-mail of communicating author: wakahl@uni-bremen.de

The Kokchetav Massif of northern Kazakhstan is part of one of the largest suture zones in Central Asia and contains slices of HP and UHP metamorphic rocks. The Kumdy Kol area is the first recorded locality of diamondiferous UHP rocks (Sobolev & Shatsky 1990) that were formed due to subduction processes at mantle depths. The diamond grains in these rocks are exceptionally large for such an environment reaching 200 µm. In a calcsilicate rock studied they form inclusions within Grt or Cpx, or occur as interstitial grains along Grt-Cpx boundaries. Such diamonds were reported to have formed by C-O-H fluids, but is it possible to identify potential fluid pathways? Our true spatially resolved tomography data of a piece of rock indicate, that the location of diamonds is related to a network of deformational microcracks. Local hydrothermal alteration in parts accompanied by Hbl-formation refers to a late event. Our data corroborate a diamond formation by fluids and an early dry exhumation history after peak metamorphic conditions were reached.

Sobolev NV, Shatsky VS (1990): - Nature 343, 742–746

Please add – many thanks:

---- Name of the abstract file: Kahl_W-A_InterstitialDiamonds_AbsForm2

The abstract file should be named according to the first author's last name (e.g., Zemann.docx). Only doc or docx formats are accepted. The abstract should be sent as an attachment to an e-mail to minwien2023.mineralogie@univie.ac.at

---- Presenting author: Wolf-Achim Kahl

Please indicate your preferences for the presentation of your contribution:

---- Preferred presentation: □ Oral **x** Poster

---- Preferred session of the contribution

	first - second choice
Young Scientist Session. Chairs: L. Czekay (Bayreuth), R. Volkmann (Potsdam)	□ □
Metal enrichment processes - latest advances in the understanding of ore formation. Chairs: M. Wilke (Potsdam), J. Michaud (Hannover), M. Korges (Potsdam)	□ □
The co-evolution of Earth's atmosphere, oceans, continents, and life from the early Archean until today. Chairs: S. Viehmann (Hannover), A.S. Rodler (Vienna), S.V. Hohl (Shanghai, China)	□ □
Carbonates in natural and technical environments – Precipitation mechanisms, monitoring and applications. Chairs: R. Boch (Graz), P. Németh (Budapest, Veszprém), M. Dietzel (Graz)	□ □
Interplay of chemical and mechanical processes across scales. Chairs: S. Schorn (Graz), A. Rogowitz (Graz)	□ □
Chronology of geological processes: past, present, future. Chairs: D. Gallhofer (Graz), E. Skrzypek (Graz)	□ □
Spectroscopic methods in modern geosciences. Chairs: M. Kaliwoda (Munich), J. Göttlicher (Eggenstein-Leopoldshafen)	□ □
Linking microstructures, crystallographic textures, and the nature of interfaces. Chairs: T. Griffiths (Wien), G. Habler (Wien)	□ □
Crystallographic Materials Science: from basics to application. Chairs: S. Schorr (Berlin), C. Weidenthaler (Duisburg-Essen)	□ □
Structure-property relationships of minerals and beyond - Minerals as advanced materials. Chairs: M. Münchhalfen (Bochum), J. Schreuer (Bochum)	□ □
"Early Earth – Crustal evolution, metamorphism and tectonics" Chairs: Thomas Müller (Göttingen), Dominik Sorger (Göttingen), Matthias Willbold (Göttingen)	□ □

Stable and radiogenic isotopes as fingerprints of processes in natural materials
Chairs: Johannes Pohlner (Frankfurt) & Chunhui Li (Cologne/Chengdu) □ □

Mineral history & teaching - Geoscientific collections & museums
Chairs: Vera Hammer (Wien), Christin Kehrer (Freiberg),
Dorothée Kleinschrot (Würzburg), Birgit Kreher-Hartmann (Jena) □ □

Oral contribution & panel discussion
Turning toolboxes into an ecosystem: How to make research software interoperable?
Chairs: T. Rose (Frankfurt), D.C. Hezel (Frankfurt) □ □

You do not find a suitable session for your abstract here - please suggest an additional symposium. The list of sessions is completed regularly at https://minwien2023.univie.ac.at/abstracts.html

---- Further session topics – please mark your preferences (first and second choice)

Mineralogy and Crystallography □ □
- Properties of minerals & materials - Physics and chemistry of minerals
- Crystal structures of minerals and related compounds
- Topology and modular aspects of crystal structures - Aperiodic & quasi-crystals
- (New) minerals and mineral classification
- Phase transitions and high-pressure / high-temperature mineralogy
- Neutron and electron scattering – Microstructures & textures of minerals
- Recent analytical developments used in the Earth sciences

Applied and Technical Mineralogy □ □
- Environmental mineralogy and technical applications
- Forensic mineralogy - archeometry and cultural heritage
- Cements, ceramics, glasses and building stones
- Biomineralogy and biomineralization
- Mineralogical aspects related to climate change (carbon cycle)

Environmental and medical mineralogy □ □
- Biosphere-geosphere interactions: environmental aspects
- Weathering, dissolution, adsorption, and transport processes
- Developments and applications of analytical methods
- Stable isotopes in biogeochemistry: experiment and theory
- Biogenic substances - CO_2 cycle and storage - anthropogenic environments
- Biogeochemical interfaces and environmental mineralogy

Petrology and Geochemistry **x** □
- From melts to rocks and P-T evolution of rocks
- Timing and duration of metamorphic events and reactions
- Transport reactions, fluid—mineral—rock interactions and interfaces

Stable and radioactive isotopes: clocks & tracers of rock formation/evolution
Geochronology and petrochronology - fluid processes in the crust and mantle
Sedimentology and weathering of rocks - thermodynamics and phase equilibria
Experimental mineralogy, petrology and geochemistry - the deep Earth and beyond
Astromineralogy, early solar system and the mineral record of impact events

Economic Geology and Ore Deposits □ □

Raw materials & metals - Industrial, economic and ore minerals
Critical geomaterial - (Deposit) modelling and mapping
Geometallurgical aspects in the beneficiation of metallic ore deposits
Genesis of ore & mineral deposits - Field studies - Supergene enrichments

Open Sessions □ □

Computer programmes - gemmology and gemstones
Mineral history & teaching - mineralogical museums and collections
Other general aspects of mineralogy, petrology, and geochemistry

Amphibole megacrysts with cavities reveal rapid crystal growth at mantle depth during the 1951 eruption of Fogo (Cape Verdes)

W.-A. Kahl[1], A. Klügel[2]

[1]MAPEX Center of Materials and Processing, Universität Bremen, 28359 Bremen, Germany
[2] Faculty of Geosciences, Universität Bremen, 28359 Bremen, Germany
e-mail: wakahl@uni-bremen.de, akluegel@uni-bremen.de

The late basaltic deposits of the 1951 Fogo eruption contain peridotite xenoliths, ultramafic cumulate xenoliths, and euhedral kaersutite megacrysts up to 12 cm in size. The megacrysts contain abundant of cavities that locally contain vesicular basaltic glass with small clinopyroxene phenocrysts, with compositions more primitive than the host magma. Some of these cavities remind of hopper textures. Micro-CT analyses reveal that the cavities are only in part interconnected and in some cases form funnel-like openings to the crystal surface. In addition to some spinel and clinopyroxene inclusions, the kaersutite contain numerous pyrrhotite rods aligned perpendicular to the crystal surface, and some pyrrhotite blebs. We interpret these structures to result from rapid crystal growth in a volatile-rich silicate melt with abundant droplets of exsolved sulfide melt. Barometric data indicate that this rapid growth occurred in the uppermost mantle. Possible causes for the rapid growth event include magma mixing or sudden H_2O loss to raise the liquidus.

Structural news from the quaternary system Na_2O-K_2O-CaO-SiO_2

V. Kahlenberg[1], H. Krüger[1], S. Garber[1], J. Aschauer[1]

[1]*University of Innsbruck, Institute of Mineralogy and Petrography, Innrain 52, 6020 Innsbruck, Austria*
e-mail: volker.kahlenberg@uibk.ac.at

The crystalline compounds and sub-solidus equilibria in the ternary subsystems Na_2O-CaO-SiO_2 and K_2O-CaO-SiO_2 have been studied frequently in the past. On the contrary, the quaternary system containing both alkali oxides is rather uncharted territory and no thermodynamic or detailed phase-analytical data are available. So far, only a few potassium-sodium-calcium silicates such as $K_{1.08}Na_{0.92}Ca_6Si_4O_{15}$ (Kahlenberg et al. 2018a) or $Na_{1.5}K_{0.5}Ca_6Si_4O_{15}$ (Kahlenberg et al. 2018b) or $NaKCa_4[Si_9O_{23}]$ (Kasatkin et al. 2019) have been structurally characterized. While the first two members are mixed-anion silicates and isostructural with ternary phases, the latter compound corresponding to the mineral patynite represents a previously unknown structure type and belongs to the group of tubular inosilicates.

Our own recent synthesis experiments in the quaternary system K_2O-Na_2O-CaO-SiO_2 proved that there exists a complete solid-solution series between $Na_4CaSi_3O_9$ and its K-counterpart: $Na_{4-x}K_xSi_3O_9$. Lattice parameters of the cubic materials (space group $Pa\bar{3}$) obtained in polycrystalline form from solid-state reactions vary between 15.0998 (x = 0) and 15.9472 (x=4) Å. The silicate anions form strongly corrugated 12-membered tetrahedral rings.

Furthermore, we were able to prepare a previously unknown compound with composition $K_{0.72}Na_{1.71}Ca_{5.79}Si_6O_{19}$. Single-crystals of sufficient size and quality could be retrieved from a starting mixture with a K_2O:Na_2O:CaO:SiO_2 ratio of 1.5:0.5:2:3. The crystal structure was determined by direct methods at 25 °C from single crystal X-ray diffraction data (tetragonal symmetry, space group $P4_122$, a = 7.3659(2) Å, c = 32.2318(18) Å, V = 1748.78(12) Å^3, Z = 4, R_1 = 0.026, wR_2 = 0.063, for 1690 observed reflections with I > 2σ(I)). The silicate anion consists of highly puckered unbranched six-membered oligogroups of composition $[Si_6O_{19}]$ having point-group symmetry 2 (C_2). Even though several thousands of natural and synthetic oxidosilicates have been structurally characterized, the present compound is the first representative for this type of catena-hexasilicate anion - at least to the best of our knowledge.

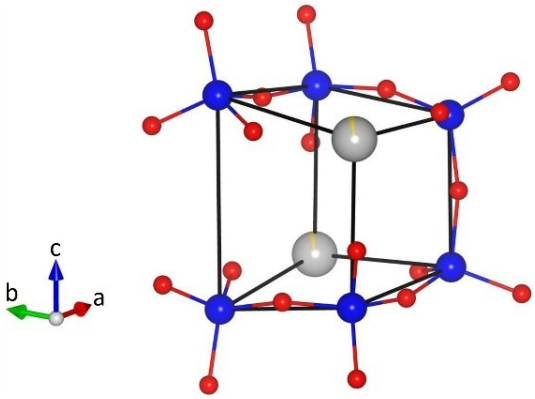

Figure 1. Conformation of a single $[Si_6O_{19}]$ group in $K_{0.72}Na_{1.71}Ca_{5.79}Si_6O_{19}$. The six Si atoms (blue) can be thought of as being located at the corners of an imaginary distorted cube with edge lengths between 3.22 and 4.60 Å. The remaining two corners are occupied by Na/Ca cations (grey/yellow). Oxygen atoms are shown in red.

Kahlenberg V, Mayerl MJP, Schmidmair D, Krüger, H (2018a): First investigations on the quaternary system Na_2O-K_2O-CaO-SiO_2: synthesis and crystal structure of $K_{1.08}Na_{0.92}Ca_6Si_4O_{15}$. - Miner Petrol 112, 219-228

Kahlenberg V, Mayerl, MJP, Schmidmair D, Krüger H, Tribus M (2018b): Preparation and characterization of $Na_{1.5}K_{0.5}Ca_6Si_4O_{15}$ and $Na_{1.41}K_{0.19}Ca_{2.20}Si_2O_7$: two new phases in the system Na_2O–K_2O–CaO–SiO_2. - Eur J Mineral 30, 957-966

Kasatkin AV, Cámara F, Chukanov NV, R. Škoda, F. Nestola, AA Agakhanov, DI Belakovskiy, V.S Lednyov (2019): Patynite; $NaKCa_4[Si_9O_{23}]$, a new mineral from the Patynsky massif. - Minerals 6, 611, 18 pp

3D electron and powder X-ray diffraction: the best of both worlds to study the crystal structure of γ-$Na_2Ca_6Si_4O_{15}$

V. Kahlenberg[1], H. Krüger[1], J. Vinke[1], S. Ito[2], C.J. Schürmann[3]

[1]Institute of Mineralogy and Petrography, University of Innsbruck, Innrain 52, 6020 Innsbruck, Austria
[2]Rigaku Corporation, 3-9-12 Matsubaru-cho, Akishima, Tokyo 196-8666, Japan
[3]Rigaku Europe SE, Hugenottenallee 167, 63263 Neu Isenburg, Germany
e-mail: volker.kahlenberg@uibk.ac.at

Phase assemblages of mixtures containing Na_2CO_3, $CaCO_3$, and SiO_2 in the molar ratio 1:3:2 have been studied at elevated temperatures. Synthesis experiments have been performed at 1000, 1100 and 1200 °C within a DTA-TGA apparatus. Mass losses during heating and annealing periods of the high-temperature treatment have been studied *in-situ* using thermogravimetry. For the run at 1200 °C, the solid-state reactions resulted in almost phase pure polycrystalline material of a previously unknown high-temperature polymorph of $Na_2Ca_6Si_4O_{15}$, whose formation was triggered by significant Na_2O losses at the reaction temperature. The new so-called γ-phase has been structurally characterized by a combination of 3D single-crystal electron and powder X-ray diffraction.

Basic crystallographic data at ambient conditions are as follows: monoclinic symmetry, space group *C*2, a = 17.2066(1) Å, b = 5.47863(3) Å, c = 7.32583(4) Å, β = 91.435(4)°, V = 690.38(1) $Å^3$, Z = 2. Structure solution was accomplished by electron diffraction, whereas the subsequent refinement calculations were based on the Rietveld method using high-resolution data from a laboratory powder diffractometer. Similarly to the two already known $Na_2Ca_6Si_4O_{15}$ modifications, the crystal structure of the γ-phase contains both [Si_2O_7] dimers and insular [SiO_4] moieties. Tetrahedra and [CaO_6] octahedra form a three-dimensional framework whose topological characteristics have been studied. The remaining Ca and Na cations are located on five symmetrically independent positions in the cavities of the network.

There are sufficiently strong arguments that previously described "triclinic $Na_2Ca_3Si_2O_8$" is actually misinterpreted γ-$Na_2Ca_6Si_4O_{15}$ and that a sodium calcium silicate with a molar ratio of Na_2O:CaO:SiO_2 = 1:3:2 probably does not exist. Our investigation is an excellent example that 3D electron diffraction has transformed from an exotic technique for crystal-structure determination into an indispensable method for problems where small sizes of the crystallites is an issue.

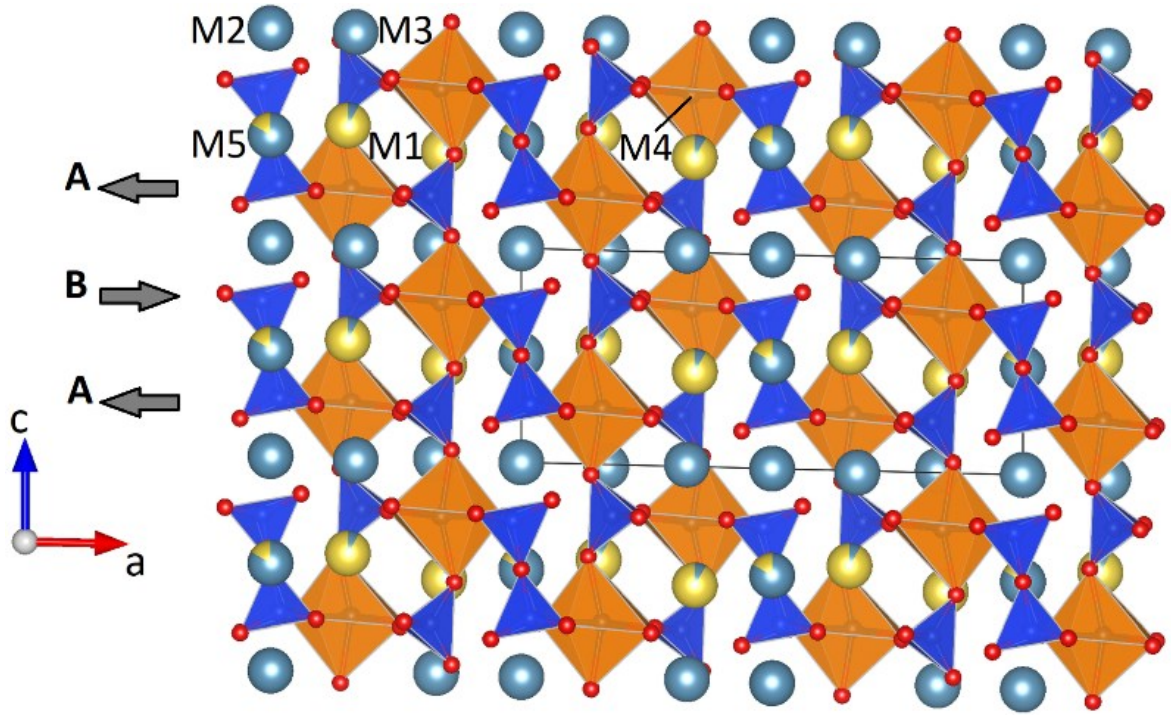

Figure 1. Projection of the whole crystal structure of γ-$Na_2Ca_6Si_4O_{15}$ (moooclinic) along [$0\bar{1}0$]. [SiO_4] tetrahedra and calcium dominated [$M4O_6$] octahedra are shown in dark blue and orange, respectively. Small red spheres represent oxygen atoms. Interstitial Ca and Na atoms are given in light blue and yellow. Bi-colored spheres indicate mixed Ca-Na positions. The alternating …ABA… stacking sequence of adjacent layers building up the network as well as the relative shift vectors are indicated.

Children's and teenagers' geoscience projects at the Mineralogical State Collection Munich (MSM)

M. Kaliwoda[1,2], M. Junge[1,2], F. Hentschel[1], F. Joseph[1], W.W.Schamahl[1,2]

[1]Mineralogical State Collection Munich, SNSB
[2] Department of Earth and Environmental Sciences, LMU, Ludwig Maximilians University, Munich
e-mail: kaliwoda@snsb.de

The Museum Mineralogia München is the publicly accessible part of the Mineralogical State Collection Munich (MSM), which belongs to the Bavarian State Natural Science Collections (SNSB). The aim of the State Collection is to impart knowledge in the STEM subjects, i.e. especially in the field of geosciences. The MSM has been trying to fulfil this task for more than 16 years and has thus gained a great amount of experience in the teaching-learning field.

Since the geosciences are unfortunately not a school subject, but geoscientific topics are becoming more and more relevant for socio-political concerns, it is important to sensitize and inspire children and young people for the geosciences at an early age.

The Museum Mineralogia therefore offers a variety of activities on topics such as (1) volcanism, (2) the cycle of rocks, (3) meteorites, (4) the construction of a smartphone and critical raw materials. In addition, there are special exhibits each year on a variety of earth science topics that are incorporated into the student projects and tours. All projects offered can also be booked as school and kindergarten projects, if there is capacity. In addition, there is a network with other science laboratories for schoolchildren both in Munich (Muc-Labs) and throughout Germany (LeLa). Participation (e.g., in Girls'Day, Science Days (Forscha), or the Children's Culture Summer) as well as many different projects in Munich and the surrounding area with other museums and research institutes also strengthen the reach. In addition to national projects, international projects (e.g. with Austria, Italy, Norway) are carried out.

As a further concept, internships are also offered for school students from the age of 14. In addition, the Mineralogische Staatssammlung Munich has successfully participated in two funded programs on ease-Corona (BMBF - catching up after Corona). Here, especially children and teenagers who show Corona and Lock-down induced learning deficits should be supported.

Raman spectroscopy as an important tool for the petrological study of different meteorite samples

M. Kaliwoda[1,2], I. Drozdovsky[3], F. Joseph[1], F. Dellefant[2], W.W. Schmahl[1,2]

[1]Mineralogical State Collection Munich, SNSB, Munich, Germany
[2]Departnemt of Earth and Environmental Sciences, LMU, Ludwig Maximilians University, Munich, Germany
[3]European Astronaut Centre (EAC) - European Space Agency, Cologne, Germany
e-mail: kaliwoda@snsb.de

Spectroscopic methods with their capability to gain information on different rocks and minerals as well as on fluids and other types of inclusions are becoming more and more relevant in earth sciences in order to open up new fields of research and providing solutions to problems in various scientific disciplines.

Raman spectroscopy represents a fast and at the same time precise method to characterize materials in different types of environments. Furthermore, Raman spectroscopy can be an important tool to investigate extraterrestrial bodies, because the measurements are more or less independent of the surrounding environmental effects including the temperatures. Therefore, it will be an important goal to gain as much experience as possible by Raman measurements of meteorites in order to be able to apply this experience to extraterrestrial bodies.

At the mineralogical state collection Munich (MSM) Raman spectroscopy is used to characterize different meteorites, with main focus to mars, moon and vesta, in order to find out the composition of the various minerals, the high pressure phases, the possible glass components and the inclusions. All the measured phases are collected in an in-house Raman database (Kaliwoda et al. 2013, 2021; Drozdovsky et al. 2020).

Raman spectroscopy make it possible to gain more information about the mineral composition and the original pressure and temperature conditions on these extraterrestrial bodies. In addition, it is possible to draw parallels to the composition and to the formation history of the early earth. In another Raman study we aim at getting more detailed information about the earth mantle and investigate therefore mantle-xenoliths and ophiolitic mantle sections.

One examples of our research targets is NWA11266 meteorite, discovered in 2017, that has already been classified as lunar feldspar breccia (Gattacceca et al., 2019). In the MSM we did further investigations with Raman spectroscopy. The main minerals are mafic olivines and pyroxenes, beside anorthitic feldspar minor graphite and tiny little glass patches. Furthermore, metallic components and accessory phases like apatite and zircon could be identified. In addition, we like to compare brecciated meteorites with other terrestrial Breccias, like those from the Nördlinger Ries.

Drozdovskiy I, Ligeza G, Jahoda P, Franke M, Lennert P, Vodnik P, Payler SJ, Kaliwoda M, Pozzobon R, Massironi M, Turchi L, Bessone L, Sauro F (2020): The PANGAEA Mineralogical Database. - Data in Brief 31, S2352-3409(20), 30879-9, https://doi.org/10.1016/j.dib.2020.105985

Gattacceca J, Bouvier A, Grossman J, Metzler K, Uehara M (2019): The meteoritical bulletin, no. 106. -Meteorit Planet Sci 54, 469–471

Kaliwoda, M, Giordano, D, Krüger ME, Uysal I, Akmaz MR, Hoffman, V, Hochleitner R, Schmahl WW (2021): Raman spectroscopy as a tool for the quantitative estimate of chromium aluminium oxide content in chromite. - Spectroscopy 36, 17-23

Kaliwoda M, Hochleitner R, Hoffmann VH, Mikouchi T, Gigler AM, Schmahl WW (2013): New Raman spectroscopic data of the Almahata Sitta Meteorite. - Spectroscopy letters 46, 141-146

Investigation of Martian and other meteorites using Raman spectroscopy

M. Kaliwoda[1,2], F. Joseph[1,2], V. Helmbrecht[2], J. Zuncke[1,2], A. Nömer[2], L. Eckle[2], I. Drozdovsky[3]

[1]Mineralogical State Collection Munich (SNSB)
[2]Departnemt of earth and environmental sciences, LMU, Ludwig-Maximilians University
3European Astronaut Centre (EAC) - European Space Agency (Linder Höhe, D-51147 Cologne, Germany
e-mail: kaliwoda@snsb.de

Our solar system consists of a wide range of different objects. Planet Mars is one of them, and its proximity to Earth makes it an important place to study. Investigations are currently related to rover missions; human missions are planned, and, in addition, the study of meteorites provides us with a lot of new data. Martian meteorites deliver us a sample in a "nutshell" that can tell us about (1) the composition of the Martian surface, (2) the chemical composition of minerals, (3) rock temperatures and pressures during formation, (4) and possible melting processes.

In the Mineralogical state collection Munich (MSM) there are several Martian but also other meteorites, i.e. from the Moon, Vesta or other extraterrestrial bodies for investigation with Raman-Spectroscopy, SEM and electron microprobe. In the following context, we want to present two Martian meteorites NWA13366 and NWA7032. Our first investigations belong to NWA13366, this meteorite is composed of olivine with 55 vol.-% and pyroxene with 35 vol.-%. Olivine is generally Mg-rich and pyroxenes have a enstatititic composition Another present phase is maskelynite with 5 vol.-% next to older feldspar grains. Maskelynite is a plagioclase glass that possibly formed during a high-pressure impact. Minor amounts of ilmenite, chromite, hematite, iron sulfide (possibly troilite), calcite, and calcium phosphate (possibly merrillite) also occur in the NWA 13366, the meteorite belongs furthermore to the shergottite group of Martian meteorites. NWA 13366 has a bimodal texture of poikilitic and non-poikilitic areas. Poikilitic domains consist of mm-sized anhedral magnesian low-Ca pyroxene crystals (oikocrysts) and smaller interlocked subhedral to euhedral Mg-rich olivine crystals (chadacrysts). Cr-rich chromite is also present. Olivine grains show chemical zoning from Fe-rich rims to Mg-rich cores in poikilitic domains. Pyroxene in poikilitic areas might be zoned as well. Non-poikilitic domains contain smaller olivine and pyroxene grains, that are chemically more evolved with higher Fe- and Ca-contents. Calcium carbonate (calcite) is present in fracture zones. It could originate from primary Martian aqueous or hydrothermal alteration or due to secondary alteration on Earth. The meteorite shows many features indicative of high shock stages. The chemical differences and the bimodal texture in the shergottite indicate a complex crystallization history of the meteorite. NWA7032 belongs also to the Martian group of meteorites and shows gabbroitic compositions. The rock is at the moment under investigation, more details will be shown later on. The detailed investigation of meteorites helps us to understand the composition of the Martian surface and besides this gives us important data for the in-house Raman database (MSM-MRD), which also takes part in the Raman database of the ESA [1].

Drozdovskiy I, Ligeza G, Jahoda P, Franke M, Lennert P, Vodnik P, Payler SJ, Kaliwoda M, Pozzobon R, Massironi M, Turchi L, Bessone L, Sauro F (2020): The PANGAEA Mineralogical Database. - Journal D i Brief S2352-3409(20), 30879-9, https://doi.org/10.1016/j.dib.2020.105985

Crystal-chemical effects of high-temperature treatment on Mg-dominant tourmalines

P. Kardošová[1], P. Bačík[1,2], J. Fridrichová[1], O. Rybnikova[1], M. Miglierini[3], T. Mikuš[4]

[1]Comenius University in Bratislava, Faculty of Natural Sciences,
Department of Mineralogy, Petrology and Economic Geology, Bratislava, Slovak Republic
[2]Earth Science Institute of the Slovak Academy of Science, Bratislava, Slovak Republic
[3]Slovak University of Technology, Faculty of Electrical Engineering and Information Technology
Institute of Nuclear and Physical Engineering, Bratislava, Slovak Republic
[4]Earth Science Institute of the Slovak Academy of Science, Bratislava, Slovak Republic
e-mail: kardosova6@uniba.sk

We present a detailed study of oxidation-induced deprotonation and its influence on tourmaline breakdown. The crystal-chemical effects of high-temperature treatment on Mg-dominant tourmalines, the oxidation of Fe^{3+} associated with the deprotonation of OH^- groups and its subsequent effect on the breakdown of tourmaline. Tourmaline samples were studied using a wide range of analytical methods. The chemical composition of all samples is Mg dominant, but with variable X_{Mg} [Mg/(Mg+Fe)]: TSCH – schorlitic dravite from Tanzania with X_{Mg} of 0.5-0.8; CHD – Mg-dominant dravite from China with $X_{Mg} > 0.9$; TUV – Cr- bearing uvite from Tanzania with $X_{Mg} > 0.98$). Tourmaline samples were heat-treated in air at atmospheric pressure at temperatures from 700 to 1000 °C to obtain information on the effect of oxidation on the deprotonation of OH groups.

The majority of Fe was oxidized after heating at 800 °C which was observed in the Mössbauer spectrum of TSCH and optical spectrum of CHD. This CHD sample had insufficient Fe content for Mössbauer spectroscopy but changes in the optical spectrum indicated partial Fe oxidation – an increase in band intensity at 750 nm and the shift of the absorption edge to the green region due to electron interactions between Fe^{2+} and Fe^{3+} ions. The influence of the possible cation oxidation on the OH^- groups bonded at the edges of YO_6 octahedra was determined by IR spectroscopy. The TSCH sample shows a significant decrease in absorbance of OH^- bands which indicates deprotonation induced by Fe oxidation, the absorbance decrease in the CHD spectra is less pronounced, and TUV does not show any decrease in absorbance suggesting no oxidation could take place due to a very low Fe, Mn, and V content. This influenced the appearance of samples after the structural breakdown: TSCH heated at 1000 °C changed appearance and cracked but there were no volumetric changes; CHD and TUV samples expanded. This suggests that before the structural breakdown, TSCH released water gradually due to Fe oxidation but CHD and TUV samples kept a majority of water in the structure due to the low content of Fe and released at one moment causing the expansion of samples.

However, the CHD and TUV samples retained most of the water in the structure due to the low Fe content that could oxidize, so the OH^- groups were not significantly deprotonated. Deprotonation occurred in one sudden moment as the structure broke down, with the released water escaping rapidly in the form of steam in all directions, causing the samples to expand. The contents of chromophores in the samples were too low to colour the resulting products in the new forms.

Meta-igneous rocks from the Kaintaleck Metamorphic Complex as indicators of a Variscan Ocean within the Eastern Alps

K. Karner-Rühl[1], C.A. Hauzenberger[1], E. Skrzypek[1], H. Fritz[1]

[1]University of Graz, Universitaetsplatz 2, 8010 Graz, Austria
e-mail: kevin.karner-ruehl@edu.uni-graz.at

The Kaintaleck Metamorphic Complex is part of the Eastern Greywacke Zone, Eastern Alps. The Eastern Greywacke Zone is subdivided into three Alpine nappes, with the Veisch nappe being overlaid by the Silbersberg and Noric nappe. The Silbersberg nappe contains intercalated crystalline fragments of Variscan age, the Kaintaleck Metamorphic Complex. It is represented by a mafic suite, comprising amphibolite, garnet-amphibolite, greenschist and serpentinite, and a felsic suite, that consists mostly of gneiss and mica schist, some of them garnet-bearing. Petrological, geochemical and geochronological investigations were carried out to provide new insights into the metamorphic and tectonic evolution of the Kaintaleck Metamorphic Complex. Geochemical results indicate, that the mafic suite originates from tholeiitic basalts. Amphibolites from the locality of Frauenberg show an enrichment in LREE indicative for either an E-MORB or OIB affinity. Garnet-amphibolites, amphibolites, and greenschists from the localities of Prieselbauer, Oberdorf, Unteraich, Kalwang, Arzbach and Schlöglmühl show flat REE patterns with only a slight depletion in HREE and resemble T-MORB. Samples from the localities of Stübminggraben and Utschgraben are depleted in LREE, typical for N-MORB affinity. U-Pb zircon dating of a garnet-amphibolite sample from the locality of Prieselbauer yields an Early Devonian age of 414.2 ± 5.6 Ma, interpreted as the age of protolith formation. Garnets from these garnet-amphibolites show distinct plagioclase-epidote-rich symplectitic coronae, indicating decompression from former high-pressure metamorphic conditions. The evolution of the Kaintaleck Metamorphic Complex might be related to the opening and closure of the short-lived Balkan-Carpathian Ocean. The onset of rifting might be due to slab roll-back and back-arc spreading during Late Ordovician and Early Silurian. During the Late Devonian and Early Carboniferous, the Balkan-Carpathian Ocean was subducted. The mafic suite of the Kaintaleck Metamorphic Complex, comprising the oceanic crust of the Balkan-Carpathian Ocean, was dragged into the subduction channel and underwent HP metamorphism with conditions of ~ 550°C and ~ 1.7-2.2 GPa. Subsequent exhumation resulted in a near isothermal decompression. Further relics of Devonian age are exposed in the North-Gemeric Klatov and Rakovec Complexes in the Western Carpathians (Putiš et al. 2009). Neubauer et al. (2022) propose, that the Klatov and Rakovec Complexes are small remnants of the Balkan-Carpathian Ophiolite, dated with an age of 405.0 ± 2.6 Ma by Zakariadze et al. (2012). Similarities in their age, the affinity to MORBs, the presence of serpentinite and the general conception, that the Klatov Complex might be a continuation of the Kaintaleck Metamorphic Complex within the Western Carpathians, might relate the mafic suite of the Kaintaleck Metamorphic Complex to the Balkan-Carpathian Ocean.

Putiš M, Ivan P, Kohút M, Spišiak J, Siman P, Radvanec M, Uher P, Sergeev S, Larionov A, Méres Š, Demko R, Ondrejka M (2009): Meta-igneous rocks of the West-Carpathian basement, Slovakia: indicators of Early Paleozoic extension and shortening events. - Bull Soc Géol Fr 180, 461–471

Neubauer F, Liu Y, Dong Y, Chang R, Genser J, Yuan S (2022): Pre-Alpine tectonic evolution of the Eastern Alps: From Prototethys to Paleotethys. - Earth-Science Reviews 226, doi:10.1016/j.earscirev.2022.103923

Zakariadze G, Karamata S, Korikovsky S, Ariskin A, Adamia S, Chkhotua T, Sergeev S, Solov'eva N (2012): The Early−Middle Palaeozoic Oceanic events along the Southern European Margin : The Deli Jovan Ophiolite Massif (NE Serbia) and Palaeo-oceanic Zones of the Great Caucasus. - Turkish J Earth Sci 21, 635–668, doi:10.3906/yer-1011-2

Antimony isotope evolution during hydrothermal precipitation and during oxidative weathering of diverse antimony mineralization in the Western Carpathians (Slovakia)

A. Kaufmann[1,2], M. Lazarov[1*], S. Weyer[1], J. Majzlan[2]

[1] *Institute of Mineralogy, Leibniz University Hannover, Germany*
[2] *Institute of Geosciences, Friedrich Schiller University Jena, Germany*
**e-mail: m.lazarov@mineralogie.uni-hannover.de*

Numerous hydrothermal Sb or Sb-Au mineralization and ore deposits are seated in a Variscan basement of the Western Carpathians (Slovakia). Stibnite is the most common mineral in all of them. However, each deposit has its specific mineralization association and Sb is found in a variety of sulfides, sulfosalts, or oxides, in combination with Cu, Pb, Fe, or Ag. All these minerals, on macro- or microscale, carry information about the ore-forming processes. In this study, a variety of Sb minerals from four ore deposits: Dve Vody, Magurka, Dúbrava and Pezinok, are investigated for their Sb isotope composition. Measurements were conducted *in-situ* by deep UV-fs laser ablation system coupled with MC-ICP-MS following the procedure of Kaufmann et al. (2021).

The δ^{123}Sb values of all investigated primary hydrothermal minerals show a range of -0.8 to +1.0 ‰. Variations of δ^{123}Sb for each deposit do not exceed 0.8 ‰. Combining information from textural relationships and Sb isotope compositions, in some cases also mineral trace-element contents, implies that mineral δ^{123}Sb can be correlated with the mineral precipitation sequence. This relationship can be observed on hand-specimen as well as on ore body and ore deposit scale. The systematic increase of δ^{123}Sb values during progressive precipitation of primary Sb minerals can be rationalized by a Rayleigh crystallization model, applying a uniform isotope fractionation factor for all minerals that was determined for stibnite by Zhai et al. (2021).

Each ore deposit has its own distinct mean of δ^{123}Sb. Dúbrava displays the lowest values of around -0.11 ±0.56 ‰, followed by Magurka and Pezinok with a mean of 0.08±0.59 ‰ and 0.24±0.48 ‰, respectively. The overall heaviest isotopic compositions are observed for Dve Vody ~ 0.53±0.88 ‰. These differences may indicate that either different sources or differently developed fluids, or both were responsible for each deposit formation.

A similar spread of δ^{123}Sb (-0.50 to +0.8 ‰) was observed for secondary Sb minerals formed near surface as the result of weathering. Depending on the amount of leached, primary mineral, and redox changes during transport and formation of secondary minerals, Sb isotope fractionation of more than 0.3 ‰ was observed. While the Sb oxides tend to become isotopically heavier, Sb hydroxides, Fe,Sb oxides or silicates prefer the ^{121}Sb isotope and display lower δ^{123}Sb signatures, compared to the coexisting primary minerals.

Thus, considering all studied deposits, mineral δ^{123}Sb may help to constrain the precipitation sequences in primary ore deposits, to decipher hydrothermal remobilization or near-surface weathering of primary ores and to constrain the potential source(s) of the metalloid.

Kaufmann AB, Lazarov M, Kiefer S, Majzlan J, Weyer S. (2021): In-situ determination of antimony isotope ratios in Sb minerals by femtosecond LA-MC-ICP-MS. - JAAS 36, 1554-1567

Zhai D, Mathur R, Liu SA, Liu J, Godfrey L, Wang K, Vervoort J. (2021): Antimony isotope fractionation in hydrothermal systems. - Geochim Cosmochim Acta 306, 84-97

Isotope fractionation of antimony during oxidative weathering of stibnite (Sb_2S_3)

A.B. Kaufmann[1,2], M. Lazarov[2], J. Majzlan[1], S. Weyer[2]

[1]Friedrich-Schiller University Jena
[2]Leibniz University Hannover
e-mail: a.kaufmann@mineralogie.uni-hannover.de

Antimony (Sb) has two stable isotopes with almost equal abundances (^{121}Sb = 57.213 %, ^{123}Sb = 42.787 %). Similar to Mo, V, Fe and U, Sb is redox-sensitive, however, with a higher redox potential (Eh value) than the aforementioned elements. It can occur in four formal (-I, 0, +III, +V) oxidation states with commonly +III and +V encountered in nature. Therefore, stable Sb isotope signatures could have great potential as a redox proxy in low-temperature surface studies to reconstruct the weathering conditions of recent and Early-Earth environments. The transport of Sb in the environment (including soils, water and sediment) was reviewed by Herath et al. (2017), however, only scarce experimental data exist, regarding the environmental release of Sb (e.g., Biver et al. 2012) under different Eh conditions.

In this study, we experimentally explored the leaching behaviour of stibnite (Sb_2S_3), the most common Sb mineral in nature, and associated isotope fractionation. For this, we performed leaching experiments with an isotopically homogeneous stibnite powder (0.14 g) and three different acids (0.05 M HCl, 0.5 M HNO_3 and 0.1 M oxalic acid) with a volume of 200 ml each. Antimony concentration, isotope composition, pH, and Eh values were determined at selected time steps in a time interval from 30 minutes to 13 days. During the leaching experiments, the pH value of oxalic acid and HCl solutions remained constant at 1.4 and 1.5, respectively, whereas that of HNO_3 rapidly increased from 0.7 to 1.2 and stabilized at 1. The Eh of the HCl solution was adjusted at 570 mV during the first 20 hours, whereas the Eh of HNO_3 and oxalic acid decreased to <630 mV till the end of the experiment. During the first 6 hours, with high Eh (>730 mV) for HNO_3 and oxalic acid, stibnite released almost 1% of Sb (>900 µg), resulting in ~0.1 ‰ heavier and ~0.3 ‰ lighter δ^{123}Sb for oxalic acid and HNO_3, respectively. In comparison, HCl, without large Eh changes, preferentially mobilized the lighter Sb isotope, resulting in δ^{123}Sb ~ -0.4 ‰ compared to the precursor material (δ^{123}Sb = -0.21 ‰). In the HCl experiment, equilibrium was achieved after 20h with constant Sb concentration and δ^{123}Sb. Conversely, progressive leaching with HNO_3 and oxalic acid, accompanied with a Eh drop, resulted in an increase of the Sb content (>2 %) with preferential mobilisation of the heavy Sb isotope.

The leachate for the first 20 hours of leaching is marked by <0 saturation indexes relative to Sb oxides, resulting into progressive dissolution of Sb. After a further slight decrease of Eh values (e.g. from 630 mV to down to 565 mV for oxalic acid) at >20 hours, the leachate became alternately over- and undersaturated relative to Sb oxides, resulting in the precipitation of Sb oxides along with additional Sb leaching. In comparison, natural secondary minerals show an isotopic variation of -0.5 to +0.3 ‰ with also preferentially enrichment of light Sb isotope compared to primary minerals (isotopic range: -0.4 to +0.8) that are consistent with our leaching results with weak acids of HNO_3 and HCl, which generates heavy isotopic Sb enriched residues. With this in mind, our first results indicate the potential of Sb isotopes as a new proxy to interpret modern and past weathering and hydrothermal alteration environments.

Biver M, Shotyk W (2012): Stibnite (Sb_2S_3) oxidative dissolution kinetics from pH 1 to 11. – Geochim Cosmochim Acta 79, 127-139

Herath I, Vithanage M, Bundschuh J (2017): Antimony as a global dilemma: Geochemistry, mobility, fate and transport. – Environmental Pollution 223, 545-559

Reconstruction of a 3.5-billion-year-old marine environment: Evidence from trace element data of iron formation from the Daitari Greenstone Belt, Singhbhum Craton, India

S. Kienle[1], S. Viehmann[2], J. Jodder[3,4], A. Hofmann[4], T. Schulz[1], C. Koeberl[1]

[1]Department of Lithospheric Research, University of Vienna, Austria
[2]Institute of Mineralogy, Leibniz University Hanover, Germany
[3]Evolutionary Studies Institute, University of the Witwatersrand, South Africa
[4]Department of Geology, University of Johannesburg, South Africa
e-mail: a01616435@unet.univie.ac.at

Banded Iron Formations (BIF) are marine chemical sedimentary rocks common in Precambrian volcano-sedimentary sequences. BIFs serve as geochemical archive of the composition of Precambrian seawater, and their trace element composition aids to investigate the geochemical evolution of the early Earth.

The Daitari Greenstone Belt (DGB) in the Singhbhum Craton of India hosts a ca. 3.5–3.3 Ga old volcano-sedimentary sequence with BIFs preserved within the Tomka Formation (Jodder et al. 2023). The DGB has only experienced greenschist-facies metamorphic conditions (Hofmann et al. 2022) providing a unique record for marine chemical sediments from the early Archean. Here we studied the Tomka BIF, which might serve as an excellent geochemical archive to reconstruct physico-chemical conditions of the 3.5-billion-year-old marine environment in the Daitari area. It may provide unique insights into the state of Earth's oceans, continents, and atmosphere within this critical time window.

Trace element compositions of high pressure-high temperature digestions of individual chert-, Fe- and mixed Fe- and chert-microbands were determined via quadrupole ICP-MS following the protocol described in Viehmann et al. (2016). Trace element compositions of chemical sediments can be used to reconstruct the depositional environment and physico-chemical conditions of the ambient atmosphere and hydrosphere. The Tomka BIF samples have very low concentrations of incompatible elements such as Al, Hf, Th, and Zr. In addition, the concentrations of rare earth elements and yttrium (REY) show no correlations with fluid-mobile elements such as Sr. The chemical compositions thus highlight their usefulness as a geochemical archive of Paleoarchean seawater. Pure chert, Fe- and mixed layers of the Tomka BIF display typical REY distribution patterns of Archean seawater (e.g., Alexander et al., 2008) and shale-normalized (subscript SN) REY_{SN} patterns similar to modern seawater, i.e., enrichment of heavy to light REY_{SN} (Yb_{SN}/Pr_{SN}: 2.67-20.4), positive La_{SN} (La_{SN}/La_{SN}*: 1.43-3.43) and Gd_{SN} (Gd_{SN}/Gd_{SN}*: 1.12-1.64) anomalies and super-chondritic Y/Ho ratios (41.2-66.7). The presence of positive Eu_{SN} (Eu_{SN}/Eu^*_{SN}: 1.37-3.17) anomalies indicate REY contributions from high-temperature hydrothermal fluids in seawater of the Tomka depositional environment. The lack of negative Ce_{SN} (Ce_{SN}/Ce^*_{SN}: 0.67-1.37) anomalies suggests anoxic atmospheric-hydrospheric conditions during BIF deposition.

The presence or absence of Eu anomalies in chondrite-normalized (subscript CN) REY patterns of BIFs can be used to distinguish between Archean and Post-Archean chemical sedimentary rocks. REY data of pure BIFs show that Eu_{CN}/Eu^*_{CN} ratios of Precambrian seawater follow a general global evolution curve with BIFs displaying strong positive Eu_{CN} anomalies in the Eoarchean, followed by decreasing Eu_{CN}/Eu^*_{CN} ratios until the Neoarchean (Viehmann et al. 2015). Eu data from BIFs in the time frame around 3.5 Ga, however, are lacking to date. Eu_{CN}/Eu^*_{CN} ratios of the Tomka BIF that fall into this time window do not follow the global seawater Eu curve but show significantly lower Eu_{CN}/Eu^*_{CN} values than expected. These values may indicate a less pronounced flux of high-temperature hydrothermal REY to the Archean ocean 3.5 Ga ago.

Alexander BW, Bau M, Andersson P, Dulski P (2008): Continentally-derived solutes in shallow Archean seawater: Rare earth element and Nd isotope evidence in iron formation from the 2.9 Ga Pongola Supergroup, South Africa. - Geochim Cosmochim Acta 72(2), 378–394

Hofmann A, Jodder J, Xie H, Bolhar R, Whitehouse M, Elburg M (2022): The Archaean geological history of the Singhbhum Craton, India – a proposal for a consistent framework of craton evolution. - Earth-Science Reviews 228, 103994

Jodder J, Hofmann A, Xie H, Elburg MA, Wilson A 2023: Geochronology of the Daitari Greenstone Belt, Singhbhum Craton, India. - Precamb Res 388, 106997

Viehmann S, Bau M, Bühn B, Dantas EL, Andrade FRD, Walde DHG (2016): Geochemical characterisation of Neoproterozoic marine habitats: Evidence from trace elements and Nd isotopes in the Urucum iron and manganese formations, Brazil. - Precamb Res 282, 74–96

Viehmann S, Bau M, Hoffmann JE, Münker C (2015): Geochemistry of the Krivoy Rog Banded Iron Formation, Ukraine, and the impact of peak episodes of increased global magmatic activity on the trace element composition of Precambrian seawater. - Precamb Res 270, 165–180

Special exhibitions are suitable for knowledge transfer

D. Kleinschrot[1]

[1]University of Wuerzburg
e-mail:kleinschrot@uni-wuerzburg.de

The most beautiful exhibits are in the showcases of our museum and attract numerous visitors who want to see these original objects from locations all over the world. The permanent exhibition can be visited at any time during opening hours and gives visitors enough time and space to learn more about the objects or to deal with a specific topic. In the temporary exhibitions of the Mineralogical Museum, for example, current topics such as raw materials in smartphones are dealt with. Scientists take the opportunity to present their research results to a broad public and thus emphasize their importance for society. In 2007 we presented 25 years of Antarctic research. Mining in Namibia and the exploration of eclogite and gold were also themes of exhibitions. Collaborations with various artists attract visitors to the museum who previously had little or no interest in geosciences. Together with other institutions, museums, and students, we organized an interdisciplinary exhibition project that showed the different aspects of color. Today we are still showing a showcase from this exhibition. The formats of the respective exhibitions are different. We have the showcase that changes quarterly, showing a mineral's properties, its origin and use as a raw material. Every one to two years we create larger exhibitions lasting 6 to 12 months. The museum team conveys the complex content in easy-to-understand exhibition texts, organizes lectures, guided tours, action Sundays for families and hands-on stations in order to reach a broad target group and, above all, to introduce young people to science. The amount of work is enormous and a temporary exhibition is usually associated with high costs. In order to convince sponsors of our work, we carried out visitor statistics, among other things. We can thus show that the number of visitors is increasing during special exhibitions and that the accompanying program is being used for further training by school classes and individuals of different ages.

GEOROC 2.0: A globally connected geochemical database to facilitate interdisciplinary, data-driven research

M. Klöcking[1], A. Sturm[2], B. Sarbas[1], L. Kallas[1], S. Möller-McNett[1], K. Lehnert[3], K. Elger[4], W. Horstmann[2], D. Kurzawe[2], M. Willbold[1], G. Wörner[1]

[1]Geoscience Centre, Universität Göttingen
[2]Göttingen State and University Library
[3]Columbia University, New York
[4]GFZ Data Services, Potsdam
e-mail: gwoerne@gwdg.de

The GEOROC database is one of the leading, open-access sources of geochemical and isotopic datasets that provides access to curated compilations of igneous and metamorphic rock and mineral compositions from >20,600 publications. It is an international data resource that supports hundreds of new research publications each year across multiple geoscientific and related disciplines (Chamberlain et al., 2021; Klöcking et al., 2023).
In this context, the Digital Geochemical Data Infrastructure (DIGIS) initiative is currently developing a new IT and data infrastructure for GEOROC 2.0 to facilitate modern solutions to data submission, discovery and access (Fig. 1). GEOROC data compilations are made accessible via a web search interface and trough a dedicated API. DIGIS also maintains a direct data pipeline of GEOROC compilation data to the EarthChem Portal (Fig. 2), which enables combined searches across six distinct geochemical databases. The DIGIS infrastructure further includes a domain repository for direct submission of geochemical datasets by the community (Fig. 2). This repository is hosted and curated in partnership with the GFZ Data Services of the GFZ (German Research Centre for Geosciences) in Potsdam. In addition, this repository can also be used for archiving citeable database versions.

Fig. 1: Setup and IT-environment of the GEOROC database

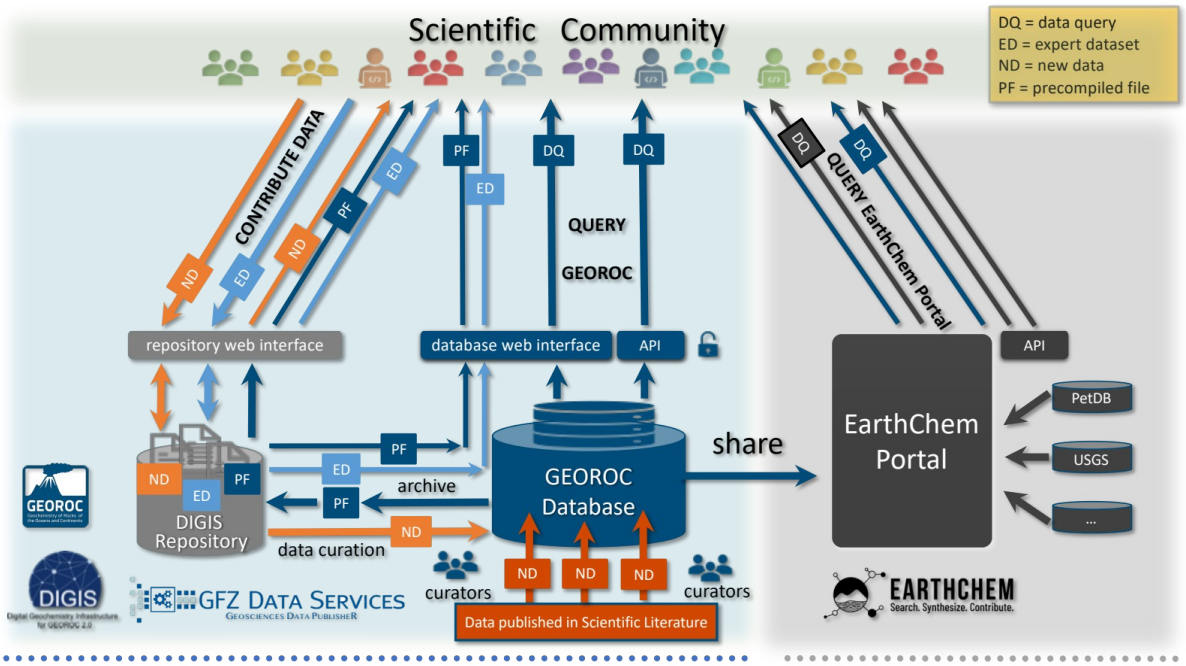

Fig. 2: The GEOROC data base and links to geochemical data services

In an effort to standardise geochemical data reporting, DIGIS collaborates with EarthChem, Astromat, and MetBase to develop common vocabularies that will enhance international interoperability of geo- and cosmochemical data systems. Part of this cooperation is the development of a joint, browser-based data entry tool for the GEOROC, PetDB and Astromat synthesis databases, which will avoid duplication of data and ensure consistent data and metadata quality through common curation policies. With these efforts, and as a participant of the "OneGeochemistry" initiative, DIGIS is working towards the goal of globally harmonised and FAIR geochemical data and support interdisciplinary, data-driven research.

Klöcking M, Wyborn L, Lehnert K, Ware B, Prent A, Profeta L, Kohlmann F et al. (2023) Community recommendations for geochemical data, services and analytical capabilities in the 21st century. - Geochim Cosmochim Acta 351, 192-205. DOI: https://doi.org/10.1016/j.gca.2023.04.024

Chamberlain KJ, Lehnert KA, McIntosh IM, Morgan DJ, Wörner G (2021) Time to change the data culture in geochemistry. - Nat Rev Earth Environ (2021), https://doi.org/10.1038/s43017-021-00237-w

The anatectic genesis of lithium pegmatite from the Austroalpine Unit Pegmatite Province

T. Knoll[1], B. Huet[2], R. Schuster[1], H. Mali[3]

[1] Division of Geophysical and Applied Geological Services, Geosphere Austria, Neulinggasse 38, 1030 Vienna, Austria
[2]Division of Basic Geological Services, Geosphere Austria, Neulinggasse 38, 1030 Vienna, Austria
[3]Department of Applied Geosciences and Geophysics, Montanuniversitat Leoben Peter-Tunnerstraße 5, 8700 Leoben, Austria
e-mail: tanja.knoll@geosphere.at

Whether rare element pegmatites are always related to fractional crystallization of melts derived from large fertile granite bodies or they can also form directly from limited portions of enriched anatectic melt is since long a debated topic (e.g. Stewart 1978; Cerný 1991). We here present the results of a recent case study that documents continuous evolution from anatectic melt generated in staurolite-bearing micaschist to albite-spodumene pegmatite (Knoll et al., 2023). The investigated Austroalpine Unit Pegmatite Province (AUPP, Eastern Alps) formed in the Adria crust during Permian lithospheric extension (Figure 1a, Schuster & Stüwe 2008) and all levels of the Permian crust are now accessible in a Cretaceous nappe stack (Froitzheim et al. 2008).

It can be shown that the Permian pegmatites of the AUPP are neither spatially nor genetically related to large fertile granite bodies. Geochronological data proofs that emplacement of pegmatite and leucogranite is broadly contemporaneous with high temperature-low pressure metamorphism of the country rocks in a time range between 247 and 288 Ma (Knoll et al. 2023; and references therein). Permian albite-spodumene pegmatites are restricted to certain lithostratigraphic complexes (e.g. Rappold Complex, Strieden Complex or Silvretta Complex; Schuster et al. 2001; Knoll et al. 2018). Pegmatite-bearing units mainly consist of aluminosilicate-bearing partly migmatitic micaschist and paragneiss as well as staurolite-bearing micaschist. Field observations give clear evidence of a genetic link between simple pegmatite, leucogranite, evolved pegmatite and albite-spodumene pegmatite, on the one hand, and the subsolidus or suprasolidus metasediment hosting them on the other hand. These relationships are supported by geochemical investigations of major and trace elements in all mentioned rock types and the minerals they contain.

The Li source rock is found to be an Al-rich metapelite, richer in Li (70-270 ppm) than the average upper continental crust. The primary Li-carrier is staurolite with up to 3000 ppm Li. The pegmatite and leucogranite are derived from anatectic melts that formed at 0.6-0.8 GPa and 650-750 °C, corresponding to 18-26 km depth. During melt formation staurolite was consumed by sillimanite forming reactions. Subsequently, the melts were enriched in Li during their ascent to higher crustal levels by fractional crystallization of quartz and feldspar. While simple pegmatite and inhomogeneous leucogranite formed in lower and intermediate levels, evolved and albite-spodumene pegmatite crystallised at high levels at 0.3-0.4 GPa and 500-570 °C, corresponding to about 12 km depth.

On the basis of this data we developed a geochemical model showing that Li can be transferred from a metasediment into an anatectic melt if Li-bearing staurolite is stable or metastable at the onset of melting (Figure 1b). Such a melt can initially contain between 200

and 1000 ppm Li and be further enriched by fractional crystallization, with up to 5000-10000 ppm Li allowing crystallization of spodumene (Figure 1c). Estimated fractionation degrees vary between 81 and 99 %, depending on the protolith composition, the melting scenario and the partitioning coefficients. Li-Al-rich metasediments are therefore a significant source of Li when they first melt. This anatectic model provides an alternative explanation for the formation of Li-rich pegmatite if no fertile parent granite can be identified.

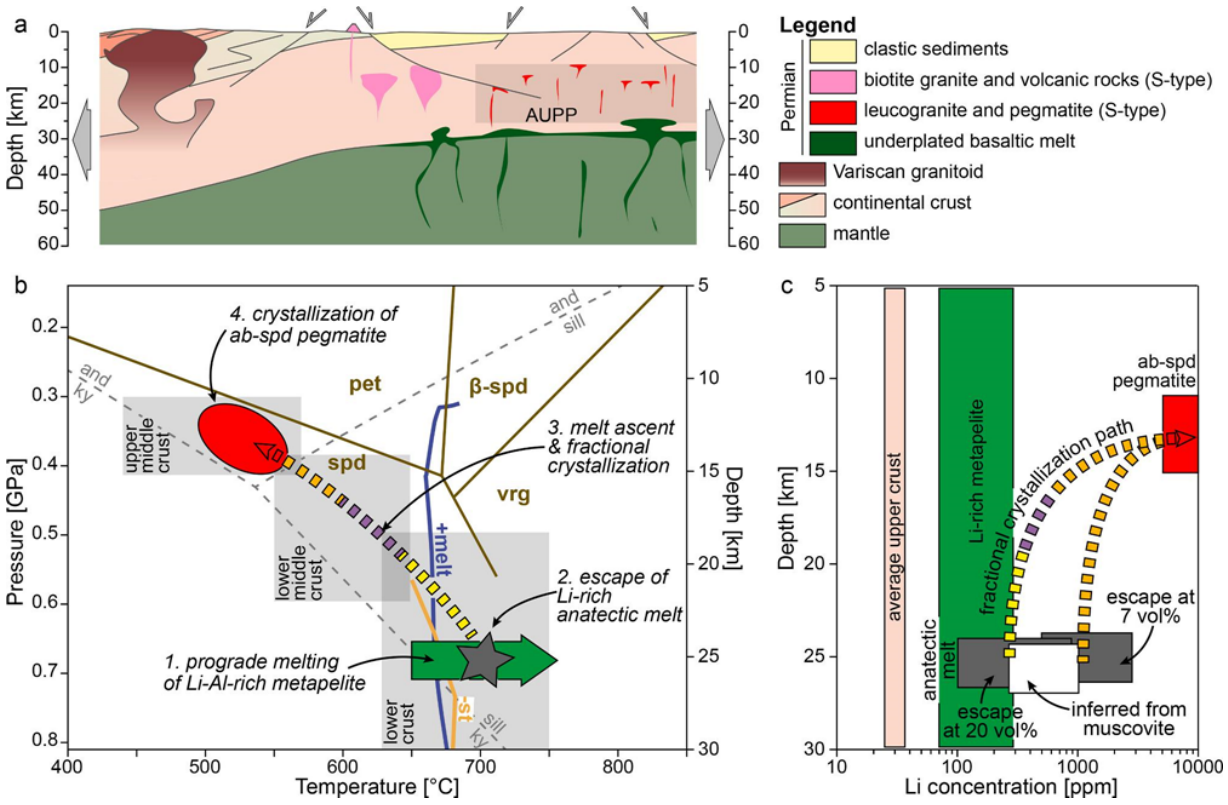

Figure 1. a. Position of the Austroalpine Unit Pegmatite Province (AUPP) within the Adria continental crust during Permian lithospheric extension. b. The main processes of the genetic model placed on a pressure–temperature diagram: 1. Prograde melting of Li-Al-rich metapelite in the lower crust. 2. Escape of Li-rich anatectic melt from the migmatite of the lower crust. 3. Ascent of the melt through the lower middle crust and progressive fractional crystallization. 4. Crystallization of residual melt as albite-spodumene pegmatite in the upper middle crust. c. Postulated evolution of Li concentration in anatectic melt during ascent (see also Knoll et al. 2023).

Cerný P (1991): Rare-element granitic pegmatites. Part I: Anatomy and internal evolution of pegmatite deposits. - Geosci Canad 18, 49–67

Froitzheim N, Plasienka D, Schuster R (2008): In: McCann, T. (Ed.), The Geology of Central Europe, 2. Mesozoic and Cenozoic. - J Geol Soc 1141–1232

Knoll T, Schuster R, Huet B, Mali H, Onuk P, Horschinegg M, Ertl A, Giester G (2018): Spodumene Pegmatite and Related Leucogranite from the Austroalpine Unit (Eastern Alps, Central Europe): Field Relations, Petrography, Geochemistry, and Geochronology. - Canad Mineral 56, 489–528

Knoll T, Huet B, Schuster R, Mali H, Ntaflos T, Hauzenberger C (2023): Lithium pegmatite of anatectic origin-A case study from the Austroalpine Unit Pegmatite Province (Eastern European Alps): geological data and geochemical model. - Ore Geol Rev 154, 105298

Schuster R, Scharbert S, Abart R, Frank W (2001): Permo-Triassic extension and related HT/LP metamorphism in the Austroalpine-Southalpine realm. - Mitt Ges Geol Bergbaustud Österr 45, 111–141

Schuster R, Stüwe K (2008): Permian metamorphic event in the Alps. - Geology 36, 603–606

Stewart D B (1978): Petrogenesis of lithium-rich pegmatites. - Amer Mineral 63, 970–980

Petrogenetic information stored in needle-shaped rutile inclusions in pegmatoid garnet

V. Kohn[1], T. Griffiths[1], E. Libowitzky[1], O. Ageeva[1], R. Abart[1], G. Habler[1]

[1] *University of Vienna, Josef-Holaubek-Platz 2, 1090, Wien, Austria*
e-mail: victoria.kohn@univie.ac.at

We investigate the petrogenetic information stored in needle-shaped rutile inclusions hosted by garnet. For this purpose, microstructural and compositional zoning of almandine-spessartine garnet (Grt) in a pegmatoid from the Gföhl Unit (Bohemian massif, AT) is correlated with host-inclusion crystallographic and shape orientation relationships along the transition between microstructurally distinct garnet growth zones. The transition from the Grt core to the garnet rim (R1) is defined by a gradual increase in the aspect ratio of rutile (Rt) inclusions accompanied by a reduction in Grt colour intensity. The coloured outer core of Grt hosts equant rutile inclusions, whereas the uncoloured Grt zone R1 contains rutile needles of c. 100 – 150 μm length (Figure 1).

More than 11 different crystallographic orientation relationships (CORs) between Grt host and Rt inclusions are known (Hwang et al. 2016; Griffiths et al. 2016). The new dataset documents a systematic correlation of the shape preferred orientations (SPOs) of rutile inclusions in garnet, and the CORs between the two phases. This allows grouping specific CORs according to the particular crystallographic axes that coincide with the needle elongation directions: Group A Rt⟨103⟩‖Grt⟨111⟩*, Group B Rt⟨001⟩‖Grt⟨111⟩** and Group C Rt⟨001⟩‖⟨100⟩***. The two microstructural domains show remarkable differences in the frequencies of these COR groups. In the outer core of garnet Group A CORs are predominant (> 70%), while Grt zone R1 shows a predominance of Group B CORs, as well as a significantly higher abundance of CORs assigned to Group C, which are almost absent in the outer core.

As the major element profile of garnet along this microstructural transition is continuous, and the trace element distribution in Grt allows us to exclude significant re-equilibration by diffusion, we conclude that other factors than changes in the PT-conditions are responsible for the differences in the garnet microstructure and COR frequencies.

Growth zone R1 is characterized by the exclusive presence of Qtz inclusions and elevated Na_2O and OH^- content compared to the Grt core, implying an increase in the water activity during R1 growth. Hydrogen content in Alm-Sps garnet has been confirmed to increase from wall to core zones of pegmatites and to serve as tracer for their evolution (Arredondo et al. 2001). Consistently, we also observe an increase in anorthite content in matrix plagioclase (Pl). In analogy to basaltic systems, Pl crystallising from a melt at constant or decreasing temperature can be referred to an increase in water activity (Lange et al. 2009, Housh and Luhr, 1991). Therefore, change in Pl-composition caused by increasing water activity could represent the source of Si and Na during R1 garnet growth. In summary, the observed compositional zoning trends of garnet and plagioclase are consistent with an increase in H_2O concentration of the melt, without need for significant changes in PT-conditions during garnet core and R1 growth.

The comparison of the studied sample with a pegmatite garnet from the Koralpe (Eastern Alps, AT) shows remarkable similarities (Griffiths et al. 2014; 2016). There, the coloured garnet core comprises mostly equant rutile inclusions and corundum, while colourless garnet rim domains contain needle-shaped rutile inclusions and aluminosilicates, and are intergrown with Qtz. Most interestingly, the Koralpe pegmatite garnet rim also has a higher abundance of Group B CORs, compared to the garnet core domains of the same sample. We

conclude that the observed microstructural transition is possibly connected with an increase of Si and/or H_2O-concentration in the melt.

As the formation of dispersed needle-shaped rutile inclusions in garnet is often referred to exsolution from the host garnet (Griffin et al. 1971; Gou et al. 2014), the frequencies of shape preferred orientations (SPOs) of rutile in garnet zone R1 were studied on the basis of > 2500 rutile needles. We observe SPOs of rutile along particular garnet crystal directions, where rutile needle elongation parallel to <111>Grt by far exceeds Rt needle elongation direction parallel to <100>Grt. Based on the assumption that the exsolution of rutile inclusions from garnet would lead to equal abundance of SPOs in symmetrically equivalent directions, each individual needle orientation was counted in R1 zones of two {112}Grt growth sectors corresponding to different crystallographically equivalent garnet facets. We find that those rutile needles parallel to <111>Grt with the lowest angle to the garnet growth direction have a higher abundance, whereas rutile needles with their elongation direction parallel to the particular Grt growth facet plane are absent in both studied growth sectors. Due to this growth-related effect on the SPO frequencies we conclude that the rutile needles originate from co-growth with their host crystal (Griffiths et al. 2020).

* Group A contains the specific CORs with a common axial relationship: COR-1, 2, 2', 3, R3a and an undescribed COR defined by Rt ⟨100⟩‖Grt{112} and Rt ⟨320⟩‖Grt{120},
** Group B contains COR-4 and 4b,
*** Group C contains COR-5 and 5a (Hwang et al 2016; Griffiths et al. 2016).

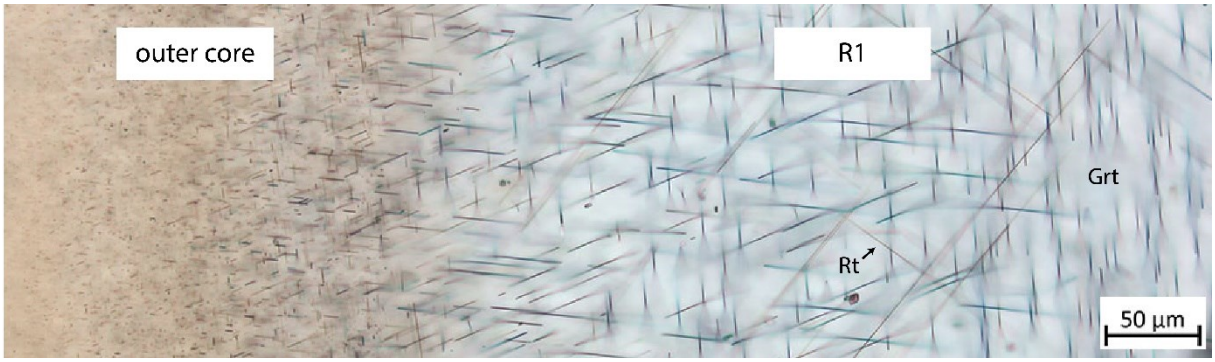

Figure 1. Optical micrograph (plane polarized light) of the microstructural transition from the outer garnet core to the garnet growth zone R1 in a {112}Grt growth sector. Note the increasing aspect ratio of rutile (Rt) inclusions and the decrease in garnet (Grt) colour intensity from the outer core to R1.

Arredondo E, Rossman G, Lumpkin G (2001): Hydrogen in spessartine-almandine garnets as a tracer of granitic pegmatite evolution. - Amer Mineral 86, 485

Gou L, Zhang C, Zhang L, Wang Q (2014): Precipitation of rutile needles in garnet from sillimanite-bearing pelitic granulite from the Khondalite Belt, North China Craton. - Chin Sci Bull 59, 4359

Griffin WL, Jensen BB, Misra SN (1971): Anomalously elongated rutile in eclogite-facies pyroxene and garnet. – N J G 51, 177

Griffiths TA, Habler G, Rhede D, Wirth R, Ram F, Abart R (2014): Localization of submicron inclusion re-equilibration at healed fractures in host garnet. - Contrib Mineral Petrol 168, 1

Griffiths TA, Habler G, Abart R (2016): Crystallographic orientation relationships in host–inclusion systems: New insights from large EBSD data sets. - Amer Mineral 101, 690

Griffiths TA, Habler G, Abart R (2020): Determining the origin of inclusions in garnet: challenges and new diagnostic criteria. - A J S 320, 753

Housh TB, Luhr JF (1991): Plagioclase-melt equilibria in hydrous systems. – Amer Mineral 76, 477

Hwang SL, Shen P, Chu HT, Yui TF (2016): On the forbidden and the optimum crystallographic variant of rutile in garnet. - J Appl Cryst 49, 1922

Lange RA, Frey HM, Hector J (2009): A thermodynamic model for the plagioclase-liquid hygrometer/ thermometer. - Am Mineral 94, 494

The crystal structure of a new natural Na-(Sr,Ba,Ca,K)-Fe-tungstophosphate, a derivative of the betpakdalite-group topology from Le Mazet, Échassières, Allier, France

U. Kolitsch[1,2]

[1]*Mineralogisch-Petrographische Abteilung, Naturhistorisches Museum, Burgring 7, A-1010 Wien, Austria*
[2]*Institut für Mineralogie und Kristallographie, Universität Wien, Josef-Holaubek-Platz 2, A-1090 Wien, Austria*
e-mail: uwe.kolitsch@nhm.at

A new tungstophosphate mineral was found on dumps of the Le Mazet wolframite-bearing quartz vein of the Les Montmins mining district (Échassières, Allier, France). It was not yet found at the nearby, very mineral-rich Ste Barbe vein. The new mineral forms very small, bright yellow to orange-yellow, pseudo-octahedral crystals, indistinct corroded tabular crystals and anhedral grains. The mineral, which shows a vitreous lustre, sits in small voids of a dark pink-grey, fine-grained quartz matrix. The colour of the mineral is somewhat reminiscent of that cyrilovite which also occurs at the locality.

The complex crystal structure was solved from single-crystal intensity data (Mo$K\alpha$; 293 K). The space group is $R\bar{3}m$ (no. 166), with a = 10.874(2), c = 28.243(6) Å, V = 2892.1(1) Å^3; $R(F)$ = 2.1%. The asymmetric unit contains one Na site with refined occupancy $Na_{\sim 0.54(3)}$, one (Sr,Ba,Ca,K) site, two Fe sites, one (P,As) site (refined P:As ratio = 0.719(19):0.281), one W site and nine O sites, four of which represent H_2O molecules. The latter are all partially occupied. The new mineral has the following simplified (and presently tentative) formula: $[Na_{\sim 0.27}(Sr_{0.46}Ba_{0.31}Ca_{0.17}K_{0.08})(H_2O,OH)_{\sim 9.02}][W_3(P,As)Fe^{3+}{}_2O_{16}]$. The $(P,As)O_4$ tetrahedron is, via its basal corners, connected to three $Fe(2)O_6$ octahedra. The remaining apex is shared with a cluster of three edge-sharing, strongly distorted WO_6 "octahedra". This cluster is connected via an $Fe(1)O_6$ octahedron to symmetrically equivalent clusters. Channels and voids in the resulting 3D framework extend along [100] and [110] and are filled with $(Sr,Ba,Ca,K)O_{12-x}$ polyhedra and partially occupied NaO_6 octahedra.

The atomic arrangement is a derivative of that of the members of the betpakdalite group, a group of monoclinic heteropolymolybdates with a pseudohexagonal symmetry of their framework topology (Kampf et al. 2012). A comparison with betpakdalite-CaMg, $[Ca_2(H_2O)_{17}Mg(H_2O)_6][Mo_8As_2Fe^{3+}{}_3O_{36}(OH)]$, shows that the two corner-sharing $Mo(3)O_6$ octahedra, which link adjacent units, are replaced in the new mineral with a single $Fe(1)O_6$ octahedron. The Ca site is replaced with a (Sr,Ba,Ca,K) site, while the Mg site is a Na site in the new mineral.

Further SEM-EDS analyses and additional single-crystal determinations of unit-cell parameters of other samples show that some samples are As-free, and suggest that some may be As-dominant (i.e., a tungstoarsenate). The atomic ratio Sr:Ba:Ca:K is variable, but Sr is always clearly dominant. The Na content is also variable.

Heinz Förch and the late Hans Schmid are thanked for providing samples for study.

Kampf AR, Mills SJ, Rumsey MS, Dini M, Birch WD, Spratt J, Pluth JJ, Steele IM, Jenkins RA, Pinch WW (2012): The heteropolymolybdate family: structural relations, nomenclature scheme and new species. - Mineral Mag 76, 1175-1207

Crystal structure of anthropogenic $Ca_2(OH)(AsO_4)\cdot 2H_2O$ found in the Clara mine, Black Forest, Germany

U. Kolitsch[1,2]

[1]*Mineralogisch-Petrographische Abteilung, Naturhistorisches Museum, Burgring 7, 1010 Wien, Austria*
[2]*Institut für Mineralogie und Kristallographie, Universität Wien, Josef-Holaubek-Platz 2, 1090 Wien, Austria*
e-mail: uwe.kolitsch@nhm.at

The arsenate compound $Ca_2(OH)(AsO_4)\cdot 2H_2O$, known from studies of the system Ca-As-O-H and reported to be stable in the pH range 11-12 (Bothe & Brown 1999, 2002), had a previously unknown unit cell (unindexed powder diffraction pattern ICDD-PDF 18-289) and crystal structure. Its formula was given in the various literature as $4CaO\cdot As_2O_5\cdot 5H_2O$, $Ca_3(AsO_4)_2\cdot Ca(OH)_2\cdot 4H_2O$, or $Ca_4(OH)_2(AsO_4)_2\cdot 4H_2O$.

The anthropogenic occurrence of $Ca_2(OH)(AsO_4)\cdot 2H_2O$ in the famous Clara baryte and fluorite mine, Black Forest, Germany, was reported by Blaß & Graf (1995), based on X-ray powder diffraction data. This occurrence is due to the use of concrete underground; several other Ca arsenates (both crystalline and amorphous) are known to occur in such assemblages (named „Beton-Paragenese“ among collectors). $Ca_2(OH)(AsO_4)\cdot 2H_2O$ was also detected by the present author in 2017 on two samples from the Clara mine. The first sample shows white sprays of colourless, lath-shaped, glassy, transparent crystals up to ~0.3 mm in length. The second sample, erroneously labelled „Calcit, Svabit“, shows pale bluish, blocky, transparent to translucent crystals (up to ~0.5 mm) arranged to form sprays and rounded aggregates. SEM-EDS analyses of carbon-coated fragments showed, apart from Ca, As and O, very minor Si in the first sample, and traces to very minor amounts of Na, Cu, Si and Cl in the second sample

The crystal structure of $Ca_2(OH)(AsO_4)\cdot 2H_2O$ was solved from single-crystal intensity data (Mo$K\alpha$; 293 K). The space group is $P2_1/c$ (no. 14), with a = 6.178(1), b = 15.688(3), c = 6.876(1) Å, β = 99.67(3)°, V = 656.96(19) Å^3; $R(F)$ = 2.1%. The asymmetric unit contains two Ca sites, one As site containing minor Si [refined As:Si ratio = 0.911(2):0.089], seven O sites, one of which represents an OH group and two of which represent water molecules, and five H sites (all detected and refined). The structure is built from an $(As,Si)O_4$ tetrahedron (<As–O> = 1.684 Å) linked to a distorted $^{[6]}CaO_6$ polyhedron and a $^{[7]}CaO_7$ polyhedron. The Ca-O polyhedra share edges with themselves and corners with three of the O ligands of the As atom to form a heteropolyhedral layer parallel to {010}. Hydrogen bonds connect these layers; the “free” O ligand of the As site, O2, is acceptor of three H-bonds of medium strength (2.660 - 2.703 Å).

Heinz Förch and Richard Bayerl are thanked for providing samples for study.

Blaß G, Graf HW (1995): Namibit, ein Neufund aus dem Schwarzwald. - Mineralien-Welt 6, 20-22
Bothe JV, Brown PW (1999): The stabilities of calcium arsenates at 23±1 °C. - J Hazard Mat 69, 197-207
Bothe JV, Brown PW (2002): $CaO\text{-}As_2O_5\text{-}H_2O$ system at 23° ± 1 °C. - J Amer Ceram Soc 85, 221-224

Litharge from El Centenillo and Fuente Espi: A geochemical and mineralogical investigation of Spanish silver processing in the Sierra Morena

P. Krause[1,2], S. Klein[2,3], C. Domergue[4], C. Berthold[5,6], N. Jöns[1]

[1]Institut für Geologie, Mineralogie und Geophysik, Ruhr-Universität Bochum, Universitätsstrasse 150, 44801 Bochum, Germany
[2]Forschungsbereich Archäometallurgie, Deutsches Bergbau-Museum Bochum, Am Bergbaumuseum 31, 44791 Bochum, Germany
[3]Institut für Archäologische Wissenschaften, Ruhr-Universität Bochum, Am Bergbaumuseum 31, 44791 Bochum, Germany
[4]Laboratoire TRACES (UMR 5608 CNRS), Université Toulouse-Jean Jaurès, Allées Antonio Machado, 31058 Toulouse Cédex 9, France
[5]Competence Center Archaeometry, Baden-Wuerttemberg (CCA-BW), Eberhard Karls-Universität Tübingen, Wilhelmstraße 56, 72074 Tübingen, Germany
e-mail: Paul.Krause@ruhr-uni-bochum.de

Galena is treated as the most important silver ore in antiquity and especially in Roman mining history, but many other silver mineralisation and phases occur in the Earth's crust that also contain valuable amounts of silver for exploitation. This study addresses the silver-containing sulfosalts and how to decide between the alternative ores when only metallurgical remains are preserved and the mining context is not evident. Numerous samples of ore minerals, slags, lead metal and stones were collected by one of us (C. Domergue) over several years in the Spanish Sierra Morena, including two Roman foundry sites: Cerro del Plomo and Fuente Espi, both in the mining district of Linares-La Carolina. Cerro del Plomo is closely associated with lead-bearing ore veins near the foundry, while the mines that supplied Fuente Espi with lead ore have not yet been archaeologically explored. The metallurgical remains from the two foundries were analysed for their microstructure, mineralogy and phase composition using microscopy, electron microprobe analysis, and X-ray diffraction. It was hoped that the litharge in particular would provide information about the ores used. Metal inclusions of copper and lead were identified, both still containing some silver. The cooling history and stratigraphy of the litharge cakes were developed and parallels drawn with earlier cupellation models. The litharge cakes from Cerro del Plomo and Fuente Espi are comparable in terms of microstructure and phase composition. Chemical and isotope analysis will follow and be the subject of a separate publication.

The "Societät für die gesammte Mineralogie zu Jena" – Members and minerals from Austria, Slovakia, and Hungary

B. Kreher-Hartmann[1]

[1]*Friedrich-Schiller-University Jena, Mineralogical Collection*
e-mail: Birgit.kreher@uni-jena.de

The "Societät für die gesammte Mineralogie zu Jena" is the first purely geoscientific society in the world. It was founded in 1797 by Johann Georg Lenz (Fig. 1) at the University of Jena, Germany, and its members were scattered all over the globe. Of the more than 2,500 known members, particularly many members came from the then Hungarian region (i.e. today's Slovakia, Hungary, and Romania). These members sent minerals and rocks from their home countries from localities that are often no longer accessible today. The members established networks and in Hungary a Hungarian Mineralogical Society was founded following the Jena model. Famous contemporaries such as Johann Rudolf von Gersdorff, Daniel Mihalyik, or Christian Andreas Zipser can be found among the members. Not all members were mineralogists, many teachers, also theologians, and pharmacists were among them. But the occupation with the formations, parageneses, and formation conditions of the minerals united them.

Figure 1. Johann Georg Lenz (1745-1832).

Domokos Teleki de Szék was elected the first president of the Society. He died unexpectedly already in his first year in office. A gift collection of opals from Červenica, Slovakia, among others, which he had initiated, reached Jena only after his death.

When they arrived at the Mineralogical Collection in Jena, the gift collections received were arranged chronologically, according to their arrival. So were for example K-Feldspars from Karlovy Vary area with pyromorphites from different European areas and granites from Silesia side by side on display. Over the many years and after several moves, these gift suites were torn apart and systematically sorted into the collection that has now existed for more than 240 years. With the help of the catalogs and member letters, more than 6,500 specimen could be reassigned to the original suites in recent years.

Kreher-Hartmann B (2014): Die Mineralogische Societät zu Jena – Beiträge aus den Sammlungen der Universität Jena, Bd. 3

Lenz G Schwabe (1823): Neue Schriften der Großherzoglich-S. - Societät für die Gesammte Mineralogie in Jena 1, Neustadt, O

Mechanical-thermochemical process combination for the recycling of fine fractions from waste treatment plants – A journey into waste mineralogy

T. Kremlicka[1], T. Sattler[1], S. Steiner[2], S. A. Viczek[3], K. P. Sedlazeck[1]

[1]Chair of Waste Processing Technology and Waste Management, Montanuniversitaet Leoben, Leoben, Austria
[2]Institute of Technology and Testing of Construction Materials, Graz University of Technology, Graz, Austria
[3]Holcim (Österreich) GmbH, Trabrennstraße 2A, 1020 Vienna, Austria
e-mail: thomas.kremlicka@unileoben.ac.at

Austria produces approximately 1.5 million tons of municipal solid waste annually. Additionally, about 500,000 tons of slags and ashes from thermal waste treatment plants are generated. There are an estimated 1.9 million tons of fine fractions, which includes one million tons of rubble from construction waste, per year, most of which are landfilled (BMK, 2021).

These fine fractions often contain high amounts of metal and mineral contents, however, they may also include pollutants (Viczek et al. 2021b, Vollprecht et al. 2020). This poses a challenge for recycling, as it is essential to avoid keeping mobile pollutants in the material cycle. Recycling fine fractions can immobilize contaminants, like heavy metals, in stable phases (Sarmiento et al. 2019).

The "MeteoR" project aims to close material cycles by reintegrating these fine fractions as resources and therefore to further develop the circular economy, reduce CO_2 emissions and increase the recycling quota in Austria. The following objectives are pursued:

1. Mineralogical and chemical characterization of fine fractions and mechanical processing.
2. Testing of different thermochemical treatment methods.
3. Investigation of the mineralogy and leachability of the slags resulting from the thermochemical treatment.
4. Removal/immobilization of contaminants in the fine fractions.
5. Life cycle assessment (LCA) of recycling routes and systemic evaluation of waste management.

An interdisciplinary consortium of universities and industrial partners (see Fig. 2) is dedicated to achieving the project's goals.

The first steps will be sampling selected waste streams, chemical and mineralogical analysis. The mineralogical analysis will consist of, but is not limited to, powder X-ray diffraction, X-ray fluorescence and electron probe microanalysis. Mechanical processing is then used to produce concentrates that are analyzed similarly to the sampled waste. These concentrates are then tested by the project partners for suitability for the various recycling routes. The project plan and the resulting dependencies are shown in Fig. 1

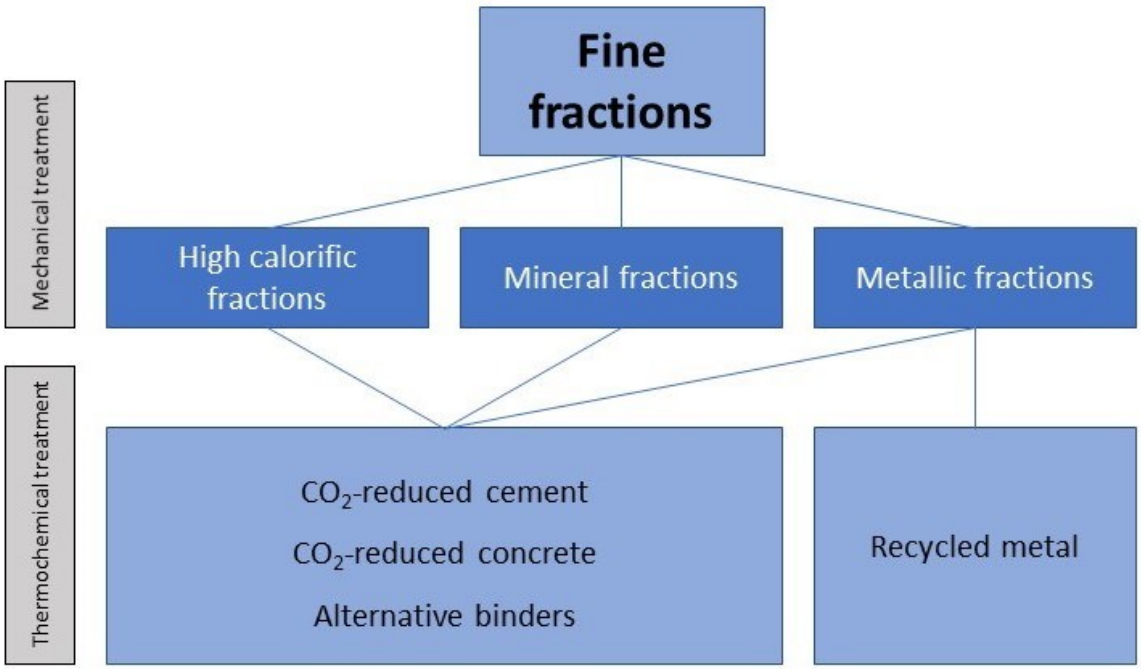

Figure 1. Scheme of the MeteoR project

By achieving the project goals, unused waste fractions containing raw materials can be utilized. Applying waste mineralogy methods, the mineral fractions can be characterized and optimized for reuse. The project enables more efficient use of resources and reintegrating waste into production chains and recycling cycles. This project is funded by the Austrian Research Promotion Agency (FFG, www.ffg.at), grant number 889863.

Figure 2. Logos of the consortium partners, funding agency and ministry of climate action, environment, energy, mobility innovation and technology in random order

Bundesministerium für Klimaschutz, Umwelt, Energie, Mobilität, Innovation und Technologie (BMK) (2021): Die Bestandsaufnahme der Abfallwirtschaft in Österreich – Statusbericht (Referenzjahr 2019)

Sarmiento LM, Clavier KA, Paris JM, Ferraro CC, Townsend TG (2019): Critical examination of recycled municipal solid waste incineration ash as a ineral source for Portland cement manufacture – a case study. - Resour Conserv Recycl 148, 1-10

Viczek SA, Khodier K, Kandlbauer L, Aldrian A, Redhammer G, Tippelt G, Sarc R (2021): The particle size-dependent distribution of chemical elements in mixed commercial waste and implications for enhancing SRF quality. - Sci Total Environ 776, 154343

Vollprecht D, Hernández Parrodi JC, Lucas HI, Pomberger R (2020): Case study on enhanced landfill mining at Mont-Saint-Guibert landfill in Belgium: mechanical processing, physico-chemical and mineralogical characterization of fine fractions <4.5mm. - Detritus 10, 26-43

A potentially new mineral $Ca_2Mg_2Fe_{14}O_{25}$ from Hatrurim Basin, Israel

B. Krüger[1], I. Galuskina[2], M. Tribus[1], G. Cametti[3], Ye. Vapnik[4], E. Galuskin[2]

[1]Institute of Mineralogy and Petrography, University of Innsbruck, Innsbruck, Austria,
[2]Faculty of Natural Sciences, Institute of Earth Sciences, University of Silesia, Poland
[3]Institute of Geological Science, University of Bern, Bern, Switzerland
[4]Department of Geological and Environmental Sciences,
Ben-Gurion University of the Negev Beer-Sheva, Israel
e-mail: biljana.krueger@uibk.ac.at

A potentially new mineral $Ca_2Mg_2Fe_{14}O_{25}$ was discovered in ferrite-rich veins of gehlenite-bearing hornfelses, found near the east slope of Mount Ye'elim in the Hatrurim Basin, Israel (Vapnik et al., 2007; Galuskina et al., 2017). Xenomorphic aggregates of this natural ferrite are observed in association with hematite, magnesioferrite, franklinite, fluorapatite, and minerals of the khesinite-devilliersite series. The empirical formula, established by microprobe analysis is $Ca_2(Mg_{0.61}Cu_{0.48}Zn_{0.41}Ca_{0.32}Ni_{0.13}Mn^{2+}_{0.03}Fe^{2+}_{0.02})_{\Sigma 2}(Fe^{3+}_{13.78}Al_{0.22})_{\Sigma 14}O_{25}$.

The dimensions of the unit cell are a = 5.932 (1) and c = 31.302(7) Å. The space group $P\bar{3}c1$ of natural $Ca_2Mg_2Fe_{14}O_{25}$ correspond to that of the synthetic β-CFF phase $Ca_{2.5}Fe_{15.5}O_{25}$ reported by Arakcheeva & Karpinskii (1983). Its crystalline structure is built by an alternating stacking of spinel blocks and F blocks along the c axis (Fig. 1). The spinel block contains two kagome-type layers with $(Fe,Mg)O_6$ octahedra connected by mixed layers made of $(Fe,Mg)O_6$ octahedra and FeO_4 tetrahedra. In block F, two layers with mixed polyhedra $(Fe,Mg)O_6$, FeO_4, and CaO_7 are connected by a central layer built by trigonal FeO_5 bipyramids.

There are a large number of minerals, in which the triple spinel module intercalates with additional modules, like M-type ferrites (e.g., $BaFe_{12}O_{19}$). However, structurally $Ca_2Mg_2Fe_{14}O_{25}$ is closely related to Y-ferrites, such as $Ba_2Zn_2Fe_{12}O_{22}$, whose natural analogues are still not found. So far, four polytypes of the CFF phase (α, β, γ, and δ) are known, exhibiting different numbers of spinel and F-blocks along the c axis (Arakcheeva & Karpinskii 1989).

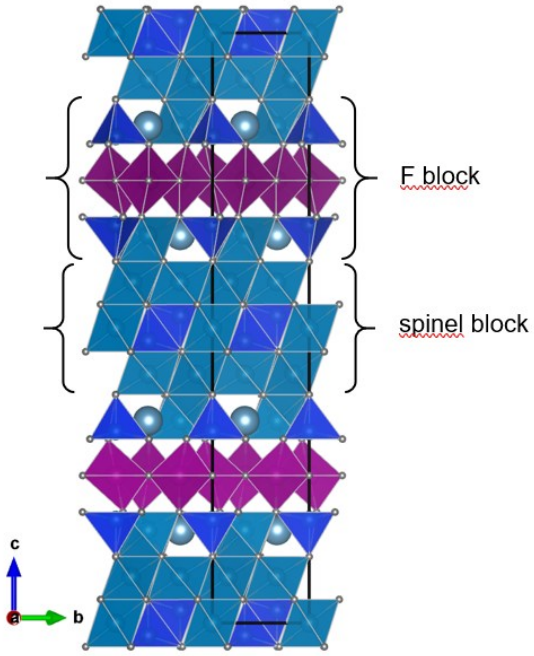

Figure 1. Structure of $Ca_2Mg_2Fe_{16}O_{25}$ - $(Fe,Mg)O_6$ in cyan, FeO_5 in magenta, FeO_4 in blue colour, and Ca as spheres

Arakcheeva AV, Karpinskii OG (1983): Crystal structure of hexagonal ferrite $Ca_{2.95}Fe_{14.85}O_{25}$. - Dokl Akad Nauk SSSR 273, 1127

Arakcheeva AV, Karpinskii OG (1983): Crystal chemical concept of formation of high-ferrous ferrites. - Kristallografiya 35, 1160-1166

Galuskina I, Vapnik Y, Lazic B, Armbruster T, Murashko M and Galuskin E (2014) Harmunite, $CaFe_2O_4$ – a new mineral from the Jabel Harmun, West Bank, Palestinian Autonomy, Israel. - Amer Mineral 99, 965-975

Vapnik, Y, Sharygin, VV., Sokol, EV and Shagam R (2007): Paralavas in a combustion metamorphic complex: Hatrurim Basin, Israel. - Rev Eng Geol 18, 1-21

Incommensurate structure and phase transition of cymrite

H. Krüger[1], K. Skrzyńska[2], R. Juroszek[2]

[1]*Institute of Mineralogy and Petrography, University of Innsbruck, Innsbruck, Austria*
[2] *Institute of Earth Sciences, University of Silesia, Sosnowiec, Poland*
e-mail: Hannes.Krueger@uibk.ac.at

Cymrite, from a hydrothermally altered pyrometamorphic rock of the Hatrurim Complex, found on the east slopes of Mt. Yeelim (Israel), has been investigated using high-temperature single-crystal X-ray diffraction. The empirical formula, as established by electron microprobe analysis, is $Ba_{0.97}Na_{0.01}(Al_{2.00}Si_{2.01})O_8 \cdot 1.48\ H_2O$.

The diffraction pattern of cymrite exhibits a pseudo-hexagonal lattice (a = 5.3 and c = 7.67 Å), with additional satellite reflections in the **a*b***-plane (**q** ≈ 0.125**a***, Figure 1), however, the true symmetry is lower. Some crystals show obvious differences in the intensities of the satellites along the three twin-related directions. A more suitable interpretation of the diffraction pattern is obtained using a (pseudo-orthorhombic) C-centred monoclinic lattice (a = 5.34, b = 9.24, c = 7.69 Å). The satellite reflection can be indexed with **q** = 0.31**b***. A temperature-dependent series of diffraction experiments revealed that the q-vector does not change significantly up to 160 °C. Between 160 and 250 °C, it decreases linearly from 0.31**b*** to 0.26**b***. Above 250 °C, no significant changes are observed until the satellites disappear between 400 and 450 °C and a transformation to a hexagonal structure takes place. At 450 °C, cymrite adopts space group *P6/mmm*.

Earlier studies on cymrite from the Baikal region (Drits 1975) and Alaska (Bolotina 2010) report fourfold superstructures (4×b, with respect to the given monoclinic lattice). The observed temperature-dependent change of the q-vector proves that cymrite from Hatrurim exhibits an incommensurately modulated structure. Possibly, this is related to the water content.

Acknowledgements: KS acknowledges support from Federal Ministry of Education, Science and Research (BMBWF) OeAD – Austria's Agency for Education and Internationalisation (project-No MPC-2022-03371).

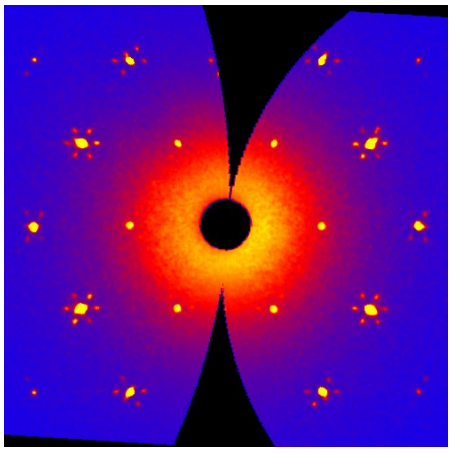

Figure 1. *hk*0-layer (pseudo hexagonal setting) of the diffraction pattern of cymrite from Israel, exhibiting three pairs of satellite reflections for each Bragg spot as a result of twinning.

Drits VA, Kashaev, AA, Sokolova GV (1975): Crystal structure of cymrite. – Sov Phys Crystallogr 20, 171-175
Bolotina NB, Rastsvetaeva RK, Kashaev AA (2010): Refinement of the twinned structure of cymrite from the Ruby Creek Deposit (Alaska). – Crystallogr Rep 55, 569-574

Oriented triphylite rods in apatite (Stankuvatske Li deposit, Ukraine): result of pegmatite–wall rock interaction

S. Kurylo[1], I. Broska[1], R. Gieré[2], N. Lyzhachenko[3]

[1]Earth Science Institute, Slovak Academy of Sciences,840 05 Bratislava
[2]Department of Earth and Environmental Science, University of Pennsylvania, Philadelphia, USA
[3]SI, "Institute of Environmental Geochemistry of the National Academy of Sciences of the Ukraine", UK Kyiv
e-mail: kurylo.sergiy@savbb.sk

Introduction. Exomorphic haloes found around pegmatites in the Stankuvatske Li deposit (SLD) (Ukraine) are enriched in Rb, Cs, Li, Be, Nb and Ta, and such types of haloes around evolved magmatic systems are important for the concentration of critical mineral sources. Metasomatic processes in the SLD can be an example for the formation of apatite as a geochemical barrier with metallogenetic implications, which takes place at the contact between a rare-metal pegmatite and amphibolite. The aim of current report is to describe the unique occurrence at the SLD of oriented triphylite rods in green apatite, resulting from the interaction between pegmatite- and amphibolite-derived fluids. A genetic interpretation of a two-way directed element mobility in an evolved pegmatite are presented here for the first time.

Geological background. The petalite- and spodumene-pegmatite dykes of the SLD are located in the NW part of the Lypniazhka Dome Structure in the western part of the Inhul Domain in the Ukrainian Shield. Pegmatite dykes intruded amphibolite and ultrabasic rocks and were subsequently overprinted by tectonic activity forming metapegmatites. According to the classification of Černý &Ercit (2005), the studied pegmatite dykes show affinity to the rare-element class, and the petalite or spodumene subtype of the LCT family. The general characteristics of the pegmatites have already been reported (Syomka et al. 2022; Kurylo et al. 2022).

Results and discussion. The contact zone was investigated by the drill core materials (No 61-89) on a complete cross section from the host amphibolite to the adjacent metapegmatite dyke. A parallel mineral layering in the metapegmatite endocontact with host amphibolite was formed in the contact zone.

The exocontact *biotite zone* (BT) in the host amphibolite was formed as a result of metasomatic alteration of rock-forming amphibolite by the intruded pegmatite; newly formed biotite (with up to 2.5 wt.% of Rb_2O) and holmquistite are characteristic minerals in this zone. The pegmatite endocontact has a width of ca 8 cm and consists of four thin zones: (1) *aplitic* (APL), (2) *fluorapatite* (AP), which contains apatite with tiny, needle-shaped and oriented parallel c-axis inclusions of triphylite (Figure 1), (3) *triphylite (TR)*, and (4) *transitional zone* (TRN). Within of the endocontact, Nb-Ta-Sn oxides, ilmenite, gahnite, native bismuth, chrysoberyl, and relics of zircon rimmed by brabantite or thorite have been identified. The adjacent metapegmatite (PGM) represents petalite and spodumene bearing metapegmatite. A detailed description of all zones is currently in preparation.

Two stages of metasomatic alteration can be distinguished in the studied metapegmatite – wall-rock amphibolite system: (i) K-Rb-F metasomatism at low P activity, and (ii) the metasomatic Li-P precipitation. The analysis of the studied metasomatic contact zone provides evidence for a two-way directed interaction between host-amphibolite and pegmatite, whereby a fluid derived from the amphibolite infiltrated the adjacent pegmatite while a fluid derived from the pegmatite dykes migrated into the amphibolite.

The presence of TR, AP, and APL zones in the endocontact of the pegmatite offers an understanding of the mobility of Ca, P, and Li in a pegmatite-amphibolite geochemical system. The main source for Ca represents the host amphibolite, which released Ca by alteration of hornblende to biotite. The Ca-enriched fluid was driven towards the pegmatite, which was primarily enriched in P and Li as an evolved system. The interaction of these two fluid systems, one enriched in Ca, the second in P and Li led to the formation of apatite, which represent a geochemical barrier and preserved Li from further migration outside of pegmatite. In such terms, apatite became the main geochemical barrier for the Li flow from the pegmatite towards the host-rock amphibolite, which also indicates the formation of triphylite clusters at the contact with the apatite layer.

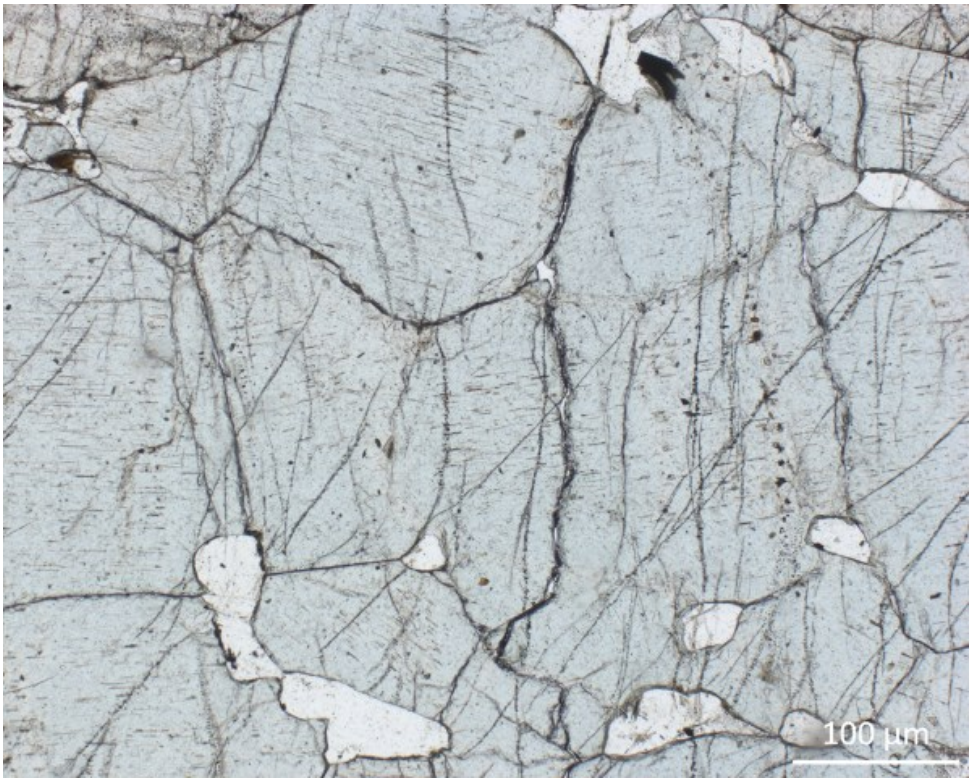

Figure 1. Apatite with needles of oriented triphylite (under plane-polarized light).

Acknowledgement: The authors are grateful for the financial support provided by grant PEGMAT within the ERA MIN2 framework.

Černý P, Ercit S (2005): The classification of granitic pegmatites revisited. - Canad Miner 43, 2005–2026

Kato S, Ikeda S, Saito K, Ogasawara M. (2018): Fe incorporation into hydroxyapatite channels by Fe loading and post-annealing. - J Solid State Chem, 265, 411–416

Kurylo S, Uher P, Broska I, Lyzhachenko N, Bondarenko S, Gieré R. (2022): Fine-grained petalite and spodumene dykes in the Stankuvatske Li-deposit, Ukrainian Shield: products of tectono–metamorphic recrystallisation. - Mineral Mag 86, 863–882

Syomka V, Ponomarenko O, Stepanyuk L, Bondarenko S, Sukach, V, Kurylo S, Donskyi M (2022): Lithium ores of Stankuvatka and Polokhivka ore fields (Ukrainian Shield). - Mineral J 44, 102–124

Tracing high-pressure metamorphism: The spatial evaluation of the Eoalpine metamorphic gradient in the Texel unit (S-Tyrol, Italy)

J. Lanziner-Oberrauch[1], P. Tropper[1], K. Fassmer[2], H. Pomella[2], G. Hoinkes[3]

[1]Institute of Mineralogy and Petrography, University of Innsbruck, Austria
[2]Institute of Geology, University of Innsbruck, Austria
[3]Institute of Earth Sciences, University of Graz, Austria
e-mail: peter.tropper@uibk.ac.at

In the Austroalpine basement west of the Penninic Tauern Window there are four different units that can be attributed to the Upper Austroalpine, but can be distinguished on the basis of their different lithologies and metamorphic histories. These are 1) the Ötztal-Bundschuh nappe system, which includes the Ötztal unit, 2) the Koralpe-Wölz high pressure nappe system including the Schneeberg and Texel units, 3) the Silvretta-Seckau nappe system with the Ortler-Campo unit, and 4) the Drauzug-Gurktal nappe system, which includes the Matsch unit, the Tonale nappe, and the Meran-Mauls nappe stack.

The Texel unit consists of a metasedimentary sequence with intercalating orthogneisses, amphibolites, and eclogites. Previously, the so-called Laas unit was considered both as part of the Texel unit and as an independent unit. However, because of intense Permo-Triassic metamorphism, for which there is as yet no evidence in the rest of the Texel unit, it should be considered as a separate unit called the Lodner unit (Hoinkes et al. 2021). In their present position in the alpine nappe stack, these two units lie in the above of the Ortler-Campo unit and below the Schneeberg and Ötztal units. Based on the Eoalpine age of the eclogites, the Texel unit is considered to be part of the Koralpe-Wölz nappe system and thus an intracontinental subduction-related high-pressure area related to the Neotethys closure. Overall, the Texel unit has been significantly overprinted by Variscan and Eoalpine metamorphism. Only the so-called Lodner unit shows a Permo-Triassic overprint. The Texel unit reached eclogite-facies during subduction. P-T conditions reached 1.2 to 2.2 GPa and 540 to 620 °C or 680 to 730 °C and 2.7 to 2.9 GPa, depending on the author. The age of the pressure maximum of Eoalpine metamorphism in the Texel unit is 85 ± 5 Ma. The eclogites occur only locally in the Texel unit and the question arose whether this "high-pressure memory" is also detectable in the mica schists and paragneisses.

For this purpose 24 metapelite samples (garnet + biotite + plagioclase + muscovite + quartz ± kyanite) were investigated geothermobarometrically (Thermocalc v.3.33, mode 1 and mode 2). It was found that the P-T data can be divided into three groups: P = 0.6-0.8 GPa, P = 0.8-1.2 GPa, and P = 1.2-1.6 GPa, and T = 570-600 °C, T = 600-700 °C, and T > 700 °C. Most pressures were in the range 0.8-1.2 GPa, but some samples taken in the vicinity the eclogites still show elevated P values of 1.2-1.6 GPa. Mineral chemically, a pressure-affected earlier stage of Eoalpine metamorphism can also be detected in the elevated Si contents (3.2-3.3 apfu) of muscovite cores. Regionally, a "central zone" with the highest pressure values in the Texel unit can currently be identified. This correlates spatially with the area in the Texel unit where the eclogites occur. Towards the edge of the Texel unit the pressures decrease again.

Hoinkes G, Krainer K, Tropper P (2021): Ötztaler Alpen, Stubaier Alpen und Texelgruppe. - Sammlung geologischer Führer, Band 112, Gebrüder Bornträger

Characterization of NaOH gas attack on silica bricks by experimental alkali vapour tests and thermochemical modelling by FactSage™

N. Lechner[1]

[1]RHI Magnesita, Technology Center Leoben, Global R&D – Mineralogy,
Magnesitstraße 2, 8700, Leoben, Austria
e-mail: nikolaus.lechner@rhimagnesita.com

Silica bricks are used as refractory lining in the crown area of glass melting furnaces. During glass production the bricks are subjected to highly corrosive NaOH vapour evaporating from the subjacent glass bath. The interaction between NaOH gas and the refractory leads to a lowering of the melting point and the formation of alkali bearing SiO_2-rich melts within the product. A high volumetric amount and loss of the liquid phase appearing in the refractory could decrease the static stability and the lifetime of the glass furnace crown significantly. Thus, a detailed understanding about the atmospheric conditions favouring NaOH gas formation from the glass bath and its consequent interaction with the silica brick crown lining is of crucial importance to avoid lifetime shortening of the refractory. For that purpose, a mineralogical study by using a combination of experimental alkali vapour tests with thermochemical phase equilibrium modelling by FactSage™ and XRD-Rietveld analyses has been executed to evaluate the corrosive behaviour of a NaOH bearing glass furnace atmosphere on silica bricks. It is shown that a varying concentration of gaseous N_2, CO_2 and H_2O in the furnace atmosphere influences (1) the efficiency of Na_2O evaporation into NaOH gas and (2) the NaOH partial pressure that play a major role for the corrosive interaction with the silica bricks. Furthermore, the condensation behaviour of NaOH gas within the refractory and subsequent corrosion by liquid phase formation strongly depends on a temperature gradient developing in the product during operation.

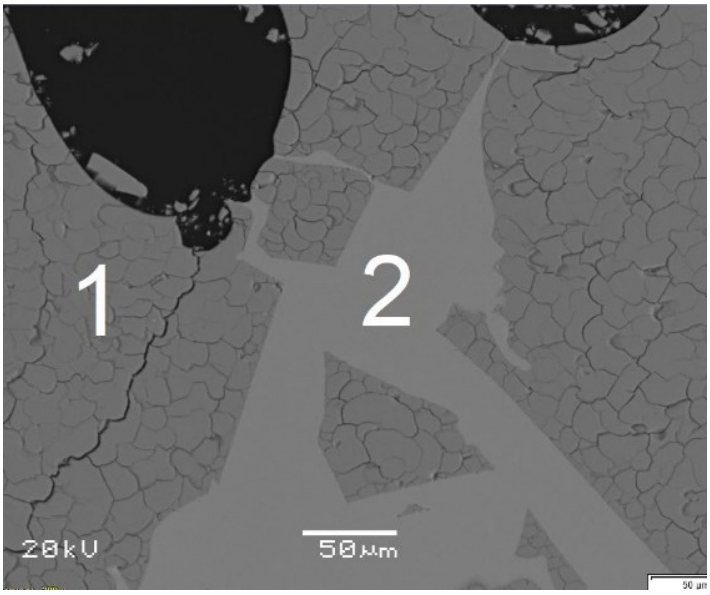

Figure 1. Micrograph of a typical silica brick after use in a glass melting furnace crown lining. Cristobalite (1). Glass phase (2).

Stable Ba isotopes of Apline mantle peridotites

C. Li[1,2,3]

[1]Research Centre for Planetary Science, Chengdu University of Technology, Chengdu, China
[2]School of Earth and Space Science, University of Science and Technology of China, Hefei, China
[3]Insitut for Geologie und Mineralogie, Universität Köln, Germany
email: lichunhui@cdut.edu.cn

Barium is a highly incompatible and fluid-mobile lithophile element. Previous studies on basalts and metamorphic rocks from subduction zones have shown that Ba isotopes can revealed more details of recycle of surface materials into the mantle. However, to our knowledge Ba isotopic data of mantle peridotites have not been investigated in detail. In this session,we report our new measurement of Ba isotope compositions of Alpine mantle peridotites. These samples include lherzolite, harburgite and pyroxeneite which were not thought to have contain crustal and surface materials. The Ba isotopes compositions of the investigated samples show large variations which we interpret as results of modifications by subduction and contamination of continental crust during the up-welling of the mantle materials. Our data suggest mantle peridotites, even the most clean and pristine ones, may have recorded mantle-crust interaction.

Bismoclite BiOCl from the Jean Baptiste mine, Lavrion area, Greece

I. Liebhart[1], B. Rieck[1], M. Zeug[1, 2], G. Giester[1]

[1]Department of Mineralogy and Crystallography, University of Vienna, Josef-Holaubek-Platz 2, 1090 Vienna
[2]Landesamt für Geologie und Bergwesen, An der Fliederwegskaserne 13, 06130 Halle (Saale), Germany
e-mail: gerald.giester@univie.ac.at

Bismoclite was first discovered and described from a museum specimen No 4465 in the McGregor Museum, Kimberly. The sample is from Jakkalswater, South Africa (Mountain, 1935). Chemical analysis resulted in Bi_2O_3 89.41, Cl 13.67, less O=Cl_2 3.08, sum 100 wt. % (Mountain, 1935). In the same year, Bannister & Hey (1935) synthesised the compound BiOCl and named it bismoclite. The crystal structure was solved on synthetic samples in space group *P*4/*nmm*, with unit cell data a = 3.887(5), c = 7.354(5) Å and refined to R = 9.17% (Keramidas et al. 1993). Furthermore, a sample from a Bi-Cu-Au deposit, Argentina was studied by infrared analysis, thermal analysis using DTA and TGA, chemical analysis using inductively coupled plasma mass spectrometry (ICP-MS) and an instrumental neutron activation analysis (INAA), microscopy analysis using scanning electron microscopy (SEM), and by pXRD (Testa et al. 2016).

Recently, rare bismoclite was discovered at the 2nd level of the Jean Baptiste Mine in the central part of the Agios Konstantinos area, Lavrion mining district, Attica, Greece. Natural bismoclite was investigated for the first time by single-crystal X-ray diffraction, confirming space group *P*4/*nmm* with unit cell parameters a = 3.887 (2), c = 7.357 (5) Å, Z = 2, V = 111.16 (14) $Å^3$ and refined to final values R1 = 0.0134 and wR2 = 0.0363. Examined by Raman spectroscopy, the spectrum shows the most intense Raman band at 144 cm^{-1}, smaller bands were observed at 198 and 396 cm^{-1}.

Figure 1. White, in thin sections colourless bismoclite surrounded by ore minerals. FOV 2.9 mm. Foto: B. Rieck

Bannister FA, Hey MH (1935): The crystal-structure of the bismuth oxyhalides. - Mineral Mag 24, 49–58
Keramidas KG, Voutsas GP, Rentzeperis PI (1993): The crystalstructure of BiOCl. - Z Kristallogr 205, 35–40
Mountain ED (1935): Two new bismuth minerals from South Africa. - Mineral Mag 24, 59–64
Testa FJ, Cooke DR, Zhang L, Mas GR (2016): Bismoclite (BiOCl) in the San Francisco de los Andes Bi–Cu–Au Deposit, Argentina. First occurrence of a bismuth oxychloride in a magmatic–hydrothermal breccia pipe and its usefulness as an indicator phase in mineral exploration. - Minerals 6, 62

In-situ powder diffraction study on the formation and reaction pathways of potassium calcium silicates

H. Liu, V. Kahlenberg, C. Hejny, H. Krüger

University of Innsbruck, Institute of Mineralogy and Petrography, Innrain 52, 6020 Innsbruck, Austria
e-mail: hang.liu@uibk.ac.at

The K_2O-CaO-SiO_2 system is critically influential in several industrial sectors involving glasses, ceramics, pyrometallurgical processes, energy production, and biomass power. It is of particular interest due to the presence of potassium calcium silicates in the ashes from biomass combustion, modified electric arc furnace slag as well as fertilizers produced from the residues of oil-shale industry or from steelmaking slags. Understanding their high-temperature behaviour can i) contribute to avoid negative effects in the production process due to slagging, fouling or sintering and ii) facilitate the reutilization of residual materials.

In recent years, numerous potassium calcium silicates have been successively identified. $K_2Ca_2Si_2O_7$ and $K_2Ca_6Si_4O_{15}$, notable for their comparatively high melting points, are key contributors to slagging within the system (Santoso et al. 2020). They have been reported to remain in the solid state at temperatures reaching up to 1200 °C. $K_2Ca_3Si_3O_{10}$, located adjacent to $K_2Ca_2Si_2O_7$ within the phase diagram, has been reported to occur under ambient pressure at temperatures of 900 °C, but does not prevail as a primary phase (Schmidmair et al. 2015). While the crystal structures of these potassium calcium silicates have been deciphered, no information is available concerning the question how the complex solid-state reactions in this system proceed and if intermediate / metastable phases are involved.

In the present study, the reaction pathways during the formation of the aforementioned three compounds from silica and carbonate educts were reconstructed through a combination of in-situ powder X-ray diffraction, DTA/TG, and isothermal annealing experiments. Our current observations suggest that K_2CO_3 absorbs water and CO_2 from the air to form $KHCO_3$ at room temperature and reverts through a dehydration process when heated to around 120 °C. Potassium carbonate in the educts tends to combine with $CaCO_3$ to form $K_2Ca(CO_3)_2$ before the formation of the silicates, and undergoes a polymorphic transition from Bütschliite to Fairchildite at ~500 °C. Upon complete decarbonation (~730-800 °C), in all starting mixtures corresponding to the target compositions $K_2Ca_2Si_2O_7$ (E_{122}), $K_2Ca_6Si_4O_{15}$ (E_{164}), and $K_2Ca_3Si_3O_{10}$ (E_{133}) the same two crystalline silicate phases could be identified equivocally: $K_2Ca_2Si_2O_7$ and Ca_2SiO_4. $K_2Ca_6Si_4O_{15}$ begins to form at ~890 °C, originating from the combination of Ca_2SiO_4 and probably potassium silicate. The temperature range between 920 and 1070 °C can be considered the dominant range for $K_2Ca_2Si_2O_7$, where the previously formed $K_2Ca_6Si_4O_{15}$ further reacts with potassium silicate to form $K_2Ca_2Si_2O_7$, and Ca_2SiO_4 undergoes complete resorption. Starting at 1070 °C, $K_2Ca_6Si_4O_{15}$ is the main phase. However, after further heating to 1150 °C, $K_2Ca_6Si_4O_{15}$ almost fully reacts into Ca_2SiO_4 which exhibits a notable potassium solubility. Above ~1150 °C, no crystalline phases were present for mixture E_{133}. In particular, $K_2Ca_3Si_3O_{10}$ is not observable in any stage of the heating process of the three educts.

Schmidmair D, Kahlenberg V, Perfler L, Tribus M, Hildebrandt J, Többens DM (2015)1: On the ambient pressure polymorph of $K_2Ca_3Si_3O_{10}$ - An unusual mixed-anion silicate and its structural and spectroscopic characterization. - J Solid State Chem 228, 90-98

Santoso I, Taskinen P, Jokilaakso A, Paek M-K, Lindberg D (2020): Phase equilibria and liquid phase behavior of the K_2O-CaO-SiO_2 system for entrained flow biomass gasification. - Fuel 265, 116894

H_2O degassing experiments of the lower Laacher See Phonolite – on the way to eruption

P. Marks[1], M. Nowak[1]

[1]*Eberhard Karls University Tübingen, Germany*
e-mail: patricia.marks@uni-tuebingen.de

The Laacher See volcano is one of the youngest volcanoes in Germany with its last eruption 13,006 ± 9 years BP (Reinig et al. 2021). About 6.3 km³ of phonolitic magma was explosively erupted by phreatomagmatic and plinian eruptions in less than 10 days (Wörner and Schmincke 1984). The eruption behavior of such volcanic systems is determined by the phase separation mechanism of H_2O fluid from the supersaturated hydrous silicate melt, caused by the pressure decrease of the magma. The number of fluid vesicles per unit volume of silicate melt (*VND*) is a standard parameter used to quantify the efficiency of fluid-melt separation and thus the acceleration of magma ascent. Two important homogeneous vesicle formation mechanisms are established in the investigation and evaluation of the degassing behavior of silicate melt systems. According to the classical nucleation theory, the *VND* increases strongly with decompression rate (Toramaru 2006) and is therefore a proper parameter for quantifying ascent rate. Recently and specifically for phonolitic melts, the process of spinodal decomposition has been demonstrated, which manifests in the independence of *VND* from the decompression rate (Allabar and Nowak 2018).

To characterize the degassing behavior of the lower Laacher See composition, systematic decompression experiments were conducted in the internally heated pressure vessel. The melts were hydrated with 5.7 or 5.0 wt% H_2O at 200 MPa and 1523 K for 96 h and then continuously decompressed at 1323 K with 0.064 – 1.7 MPa/s to final pressures between 110 MPa and 30 MPa. By reaching the final pressure, the samples were rapidly quenched to room temperature to preserve the vesicle textures and the residual H_2O contents in the melts and to minimize vesicle shrinkage until the glass transition temperature was reached. The *VND*s and the spatial distribution of the vesicles, as well as the H_2O contents in the decompressed melts were analyzed with quantitative image analysis, transmission light microscopy, and FTIR-spectroscopy.

Upon reaching sufficient supersaturation pressure of >100 MPa, all samples exhibit homogeneously dispersed vesicles in the sample center (Fig. 1). Vesicle sizes range from 2 to 13 µm in diameter. Preliminary results indicate that *VND* is independent of decompression rate at all decompression rates. Irrespective of the decompression rate, high log*VND*s of 4.1 to 5.6 mm^{-3} are observed. Further decompression of the degassed melts leads to the formation of coalescence, resulting in a significantly reduced *VND* of the melts.

These observations are consistent with that of Allabar and Nowak (2018), who determined a log*VND* of ~5.2 mm^{-3} for hydrous phonolitic melt of the AD79 Vesuvius white pumice composition. From this, a trend emerges that at least for hydrated phonolitic melt, spinodal decomposition plays a crucial role in the degassing behavior of the melt and thus in the explosive eruption behavior of the volcanic systems.

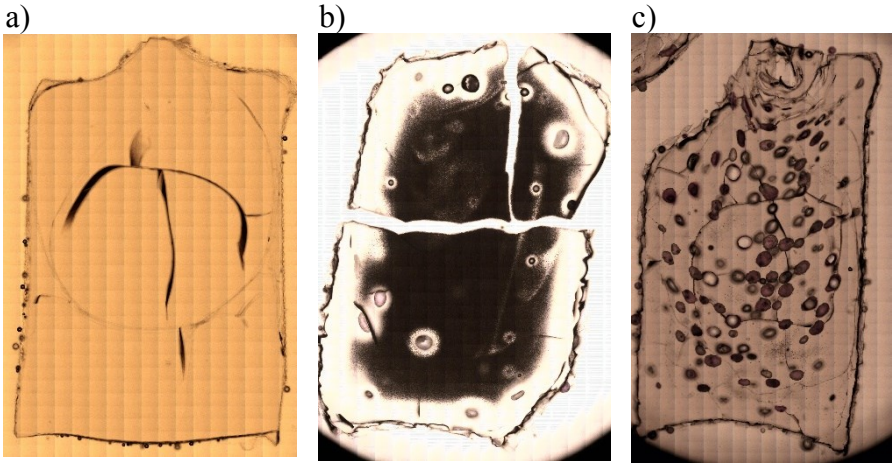

Figure 1. The three degassing steps of an ascending melt. a) No vesicle formation was initiated yet. b) Spontaneous phase separation was triggered by the extreme supersaturation of the melt. c) Further decompression leads to coalescence of the growing vesicles.

Allabar A, Nowak M (2018): Message in a bottle: Spontaneous phase separation of hydrous Vesuvius melt even at low decompression rates. - EPSL, 501, 192-201

Reinig F, Wacker L, Jöris O, Oppenheimer C, Guidobaldi G, Nlevergelt D, Adolphi F, Cherubini P, Engels S, Esper J, Land A, Lane C, Pfanz H, Remmele S, Sigl M, Sookdeo A, Büntgen U (2021): Precise date for the Laacher See eruption synchronizes the Younger Dryas. – Nature, 595, 66-69

Toramaru A (2006): BND (bubble number density) decompression rate meter for explosive volcanic eruptions. - J. Volcanol. Geotherm. Res.154, 303-316

Wörner G, Schmincke H-U (1984): Petrogenesis of the Zoned Laacher See Tephra. - J. Petrol., 25, 805-835

Thermal expansion of SiO_2 polymorphs keatite, RUB-11 and silica-sodalite

B. Marler[1], I. Grosskreuz[1]

[1]Department. of Geology, Minerlogy, and Geophysics, Ruhr University Bochum, Germany
e-mail: bernd.marler@rub.de

With very few exceptions, dense silica polymorphs like α-quartz or β-cristobalite exhibit a positive volume thermal expansion while microporous silica polymorphs (= guest free silica zeolites) like siliceous faujasite or siliceous chabasite show negative expansion (Lightfoot et al. 2001).

Here, we present the analysis of the thermal expansion coefficients of three silica polymorphs, which have, so far, not been investigated.

Keatite (tetragonal, $\rho = 2.50$ gcm^{-1}) is a rare, metastable SiO_2 polymorph possessing a dense silica framework, synthetic keatite is known since 1954 (Keat et al. 1954) and has more recently been discovered as a mineral (Hill et al. 2013).

The all-silica form of sodalite (cubic above 412 K, $\rho = 1.67$ gcm^{-1}) has the same microporous framework comprising cage-like voids (Werthmann et al. 2000) as the sodalite mineral, $Na_8Cl_2[Si_6Al_6O_{24}]$.

RUB-11 (monoclinic, $\rho = 2.11$ gcm^{-1}) can be regarded as an Interlayer Expanded Zeolite of the natural layer silicate magadiite, $Na_2[Si_{14}O_{28}(OH)_2]\cdot 8H_2O$, however, with additional SiO_4 tetrahedra interconnec-ting the silicate layers instead of intercalated sodium and water. RUB-11 possesses a silica framework with channel-like pores (Grosskreuz et al. 2023).

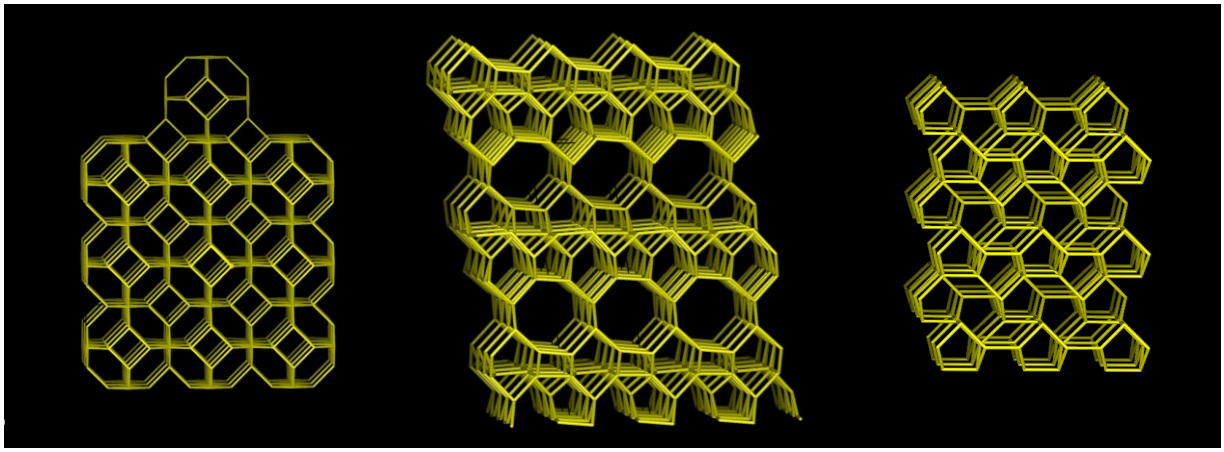

Figure 1. The framework structures of cubic silica sodalite (left), RUB-11 (middle), and keatite (right).

Experimental data: Keatite was synthesized heating a silicate gel prepared from $Si(OC_2H_5)_4$, $LiNO_3$, $Cr(NO_3)_3$ and water at 830 K. Trioxane-silica-sodalite and RUB-11 were hydrothermally synthesized from reaction mixtures of SiO_2/Trioxane/H_2O and SiO_2/ethylen-diamine/H_2O/Xe, respectively. Trioxane-silica-sodalite was subsequently heated to remove all organic material from the cage-like pores producing pure silica-sodalite.

Powder XRD data (CuKα_1) of all samples, kept in glass capillaries, were collected in Debye-Scherrer geometry. Silicon or quartz powder served as an internal standard. The samples were heated in steps of 50 K (silica-sodalite), 100 K (RUB-11) and 110 K (keatite) up to 729, 898 or 713K. Rietveld refinements revealed the lattice parameteres and unit cell volumes.

The guest-free silica sodalite is trigonal at room temperature and transforms into a cubic symmetry at 412 K (Werthmann et al. 2000). The cubic silica sodalite exhibits isotropic (negative) expansion while RUB-11 and keatite show a pronounced anisotropic behaviour with negative and positive expansion in different directions. Linear expansion coefficients are
Silica-sodalite (454 – 729 K): $\alpha[100] = -3.7 \cdot 10^{-6}$
RUB-11 (298 – 898 K): $\alpha[100] = -10.2 \cdot 10^{-6}$, $\alpha[010] = +10.1 \cdot 10^{-6}$, $\alpha[001] = -2.1 \cdot 10^{-6}$
Keatite (293 – 713 K): $\alpha[100] = -6.1 \cdot 10^{-6}$, $\alpha[001] = +15.0 \cdot 10^{-6}$
Corresponding expansion coefficients of the volumes $\alpha(V)$ are:
cubic silica sodalite = $-11.2 \cdot 10^{-6}$; RUB-11 = $-6.4 \cdot 10^{-6}$ and keatite = $+2.9 \cdot 10^{-6}$

When listing microporous and dense silica polymorphs with densities ranging from 1.3 to 2.9 gcm^{-1} it appears that materials with intermediate densities (about 2.0 gcm^{-1}) have particular small (positive or negative) expansion coefficients (see Table 1). Considering this fact, it seems not impossible to discover or specifically synthesize a silica polymorph with nearly zero expansion. Since SiO_2 polymorphs are chemically, mechanically and thermally very stable when exposed to most chemicals, pressure and/or high temperature such a material might be useful for many purposes.

Table 1. Selection of SiO_2 polymorphs of intermediate density

SiO_2 polymorph	Density [gcm^{-1}]	Volume thermal expansion coefficient [ppm/K], (temperature range)	Reference
MFI-type zeolite	18.4	–7.6 (373-673 K)	Bhange et al. 2007
RWR-type zeolite	19.2	+3.7 (298–773 K)	Koike et al. 2023
High density zeolite RUB-11	21.1	–6.4 (298–898 K)	This study
High density zeolite RUB-5	22.0	–7.5 (293–743 K)	Marler et al. 2020
Silica glass	22.0	+0.5 (273-873 K)	Heraeus 2023
High density zeolite RWZ-1	22.1	–3.9 (298–773 K)	Koike et al. 2023

Bhange DS, Ramaswamy V (2007): High temperature thermal expansion behavior of silicalite-1 molecular sieve: in situ HTXRD study. - Micropor Mesopor Mater 103, 235–242

Grosskreuz I, Krysiak Y, Gies H, Mugnaioli E, Marler B (2023): Synthesis and real structure of RUB-11, a novel high-density silica zeolite based on magadiite layers. - Submitted.

Heareus: Properties of fused silica (accessed April 27th 2023) - https://www.heraeus.com/en/hca/fused_silica_quartz_knowledge_base_1/properties_1/properties_hca. html#tabs-608478-5

Hill TR, Konish H, Huifang X (2013): Natural occurrence of keatite precipitates in UHP clinopyroxene from the Kokchetav Massif: A TEM investigation. - Am Mineral 98, 187-196

Koike M, Grosskreuz I, Asakura Y, Miyawaki R, Gies H, Wada H, Shimojima A, Marler B, Kuroda K. (2023): Bridging the gap between zeolites and dense silica polymorphs: Formation of all-silica zeolite with high framework density from natural layered silicate magadiite. - Submitted to Angew Chem

Keat PP (1954): A new crystalline silica. - Science 120, 328-330

Lightfoot P, Woodcock DA, Maple MJ, Villaescusa LA, Wright PA (2001): The widespread occurrence of negative thermal expansion in Zeolites. - J Mater Chem 11, 212-216

Marler B, Krysiak Y, Kolb U, Grafweg C, Gies H (2020): Two new members of the Silica-X family of materials: RUB-5, a silica zeolite with a very high framework density and RUB-6, a hydrous layer silicate, Micropor. - Mesopor Mater 296, 109981

Werthmann U, Marler B, Gies H (2000): Gastmolekülfreier Silica-Sodalith: Eine neue SiO_2-Modifikation, Z Kristallogr Supplement Issue, 17, 188

Structural changes in *Ln*-monazites under swift heavy ion irradiation

J. Marquardt[1], T. Lender[2], L. Bayarjargal[1], E. Haussühl[1], C. Trautmann[3], L. Peters[2], B. Winkler[1]

[1]Institute of Geoscience, Johann Wolfgang Goethe-University Frankfurt am Main
[2]Institute of Crystallography, RWTH Aachen
[3]GSI Helmholtz Centre for Heavy Ion Research, Darmstadt
e-mail: marquardt@kristall.uni-frankfurt.de

The safe disposal of nuclear waste is one of the intergenerational issues which needs to be solved. A potential route to effectively immobilize radionuclides could be realized by their incorporation into crystalline solid phases in future radioactive waste repositories. In particular, the immobilization of specific waste streams containing minor actinides (Np, Am, Cm) or plutonium in crystalline solid phases may be advantageous compared to glass matrices, which may be less resistant to leaching and disintegration (Donald et al. 1997; Ewing 1999; Lumpkin et al. 2006). Due to their radiation stability and chemical and structural flexibility, monazite-type compounds are considered suitable matrix materials (Schlenz et al., 2013).

To better understand structural changes due to radiation damage, synthetic monazite single crystals with different chemical compositions (La, Nd, Pm, Sm)PO_4 were irradiated at the UNILAC beamline of GSI Helmholtz Centre Darmstadt using 1.7 GeV Au ions and fluences of up to 1e13 ions/cm^2. The irradiated single crystals were characterized by Raman spectroscopy, secondary electron microscopy and single crystal X-ray diffraction.

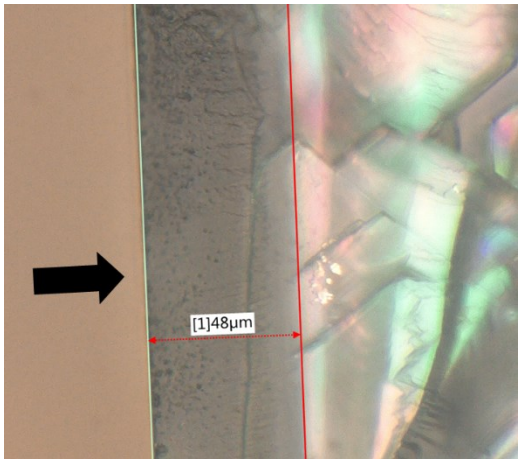

Figure 1. Cross section of a (Pr,Nd)PO_4 monazite crystal, prepared parallel to the direction of the irradiation indicated by the black arrow

The irradiation of monazite with 1.7 GeV Au ions results in an embrittlement of the crystals and the formation of a glassy surface layer of about ~48 µm thickness (Fig. 1), which correlates well with the projected range of ~44 µm according to SRIM-2013 calculations (Ziegler et al. 2010). The irradiation results in a significant broadening of all Raman modes up to the complete disappearance of the symmetric stretching mode ν_1 and further changes in the lattice dynamics. X-ray diffraction experiments revealed the amorphization of the surface layer.

Donald IW, Metcalfe BL, Taylor RNJ (1997): The immobilization of high level radioactive wastes using ceramics and glasses. - J Mater Sci 32, 5851-5887

Ewing RC (1999): Nuclear waste forms for actinides. - PNAS 96, 3432-3439

Lumpkin GR (2006): Ceramic waste forms for actinides. - Elements 2, 365-372

Schlenz H, Heuser J, Neumann A, Schmitz S, Bosbach D. (2013): Monazite as a suitable actinide waste form. - Z Kristallogr – Cryst Mater 228, 113-123

Ziegler JF, Ziegler MD, Biersack JP (2010): SRIM - The stopping and range of ions in matter. - Nucl Instrum Methods Phys Res B 268, 1818-1823

J.M & B.W. acknowledge the German Federal Ministry of Education and Research (BMBF) for financial support in the project No. 02NUK060E. T.L. & L.P. acknowledge support by BMBF under project number 02NUK060B.

High-pressure gneiss with pseudomorphs after jadeite from the Variscan Erzgebirge in Saxony

H.-J. Massonne[1]

[1]*School of Earth Sciences, China University of Geosciences, Wuhan, P.R. China*
e-mail: h-j.massonne@mineralogie.uni-stuttgart.de

The Erzgebirge in Saxony is known for occurrences of various ultrahigh-pressure (UHP) rocks (Massonne, 2001, 2003), but gneiss, the major rock type there, was rarely addressed in scientific studies (e.g., Willner et al. 1997). A paragneiss (sample E98-36), rich in quartz and white mica, was sampled very close to an eclogite body of the Gneiss-Eclogite Unit (GEU) c. 5 km north of the Saidenbach reservoir where UHP rocks were found.

Millimetre-sized garnet grains in this gneiss can be zoned with a relatively Ca-poor core (XCa = Ca/(Ca+Fe^{2+}+Mg+Mg) around 0.04, XMg = 0.16, XMn = 0.005) surrounded by a mantle with XCa = 0.07-0.09, XMg = 0.13-0.18, and XMn = 0.01. The contact between these two garnet generations is sharp. Large oriented white mica flakes are phengite with Si contents around 3.42 per formula unit (pfu) in the core and slightly decreasing Si contents towards the rim. A new generation of potassic white mica with lower Si contents formed at the rim of these flakes. A peculiar feature of the studied paragneiss is the occurrence of mm-sized clusters of small albite grains with thin potassic white mica flakes in between. The Si contents of these flakes is between 3.23 and 3.31 pfu and, thus, similar to those of the rim generation of large flakes. The observed elongated clusters, being oriented in the same direction as the large mica flakes, are interpreted as former jadeite grains, which decomposed during exhumation of the rock under infiltration of K-bearing hydrous fluids.

Thermodynamic modelling with PERPLE_X (Connolly, 2005: version 6.6.6) was applied to decipher the metamorphic evolution of the paragneiss. According to the calculated pressure-temperature (P-T) pseudosection contoured with various isopleths for garnet and potassic white mica, an early metamorphic stage (Ca-poor garnet core) occurred at P-T conditions of 0.9±0.1 GPa and 635±25 °C (Fig. 1). The conditions of the high-pressure (HP) stage (garnet mantle) were difficult to determine precisely because compositions of the early garnet mantle and phengite can coexist over a wider P-T range. Thus, a temperature increase from 580-600 °C to 660 °C can be accompanied by a slight pressure decrease from 1.8 to 1.7 GPa, but also by a clear one from ca. 2.4 to 1.7 GPa. This not well determinable portion of the P-T path is compatible with the presence of jadeite and absence of primary biotite. Further decompression without deformation resulted in the formation of pseudomorphs after jadeite. The obtained conditions of 660 °C at 1.7 GPa are similar to those of 715 °C at 1.8 GPa determined for the adjacent eclogite (Massonne 2011).

In-situ U-Th-Pb dating of monazite with the electron microprobe (e.g., Rahimi & Massonne, 2018) yielded an average age of 338.4 ± 2.3 (2σ) Ma (40 of 44 monazite analyses). This age was assigned to the HP event according to previous studies of rocks from the GEU (e.g., Hallas et al. 2021). A small monazite grain enclosed in garnet yielded an age of 386.4 ± 10.5 (2σ) Ma, which was related to the garnet core-forming event (Fig. 1).

Based on the here presented data and those gathered from the literature, the following conclusions are drawn: (1) An Early Carboniferous continent-continent collisional scenario was responsible for the HP event in the GEU. Evidence for metamorphism at UHP is lacking in metasediments and metagranitoids. Diamondiferous rocks in the Erzgebirge in Saxony are crystallization products of melts, which ascended from great Earth's depths and intruded the

Early Carboniferous HP rocks. (2) These HP rocks of the GEU, including eclogites, originally experienced Late Devonian medium-pressure, medium-temperature metamorphism and were constituents of a medium to lower portion of the downgoing plate in the Early Carboniferous collisional scenario. (3) Jadeite should characterize medium-temperature metasediments and metagranitoids that had experienced lithostatic pressure in excess of 1.6 GPa. This study demonstrates that jadeite can be recognized in corresponding HP rocks even after complete decomposition. This means that previously suggested UHP terranes worldwide, lacking relics and pseudomorphs of jadeite and coesite, have never experienced UHP.

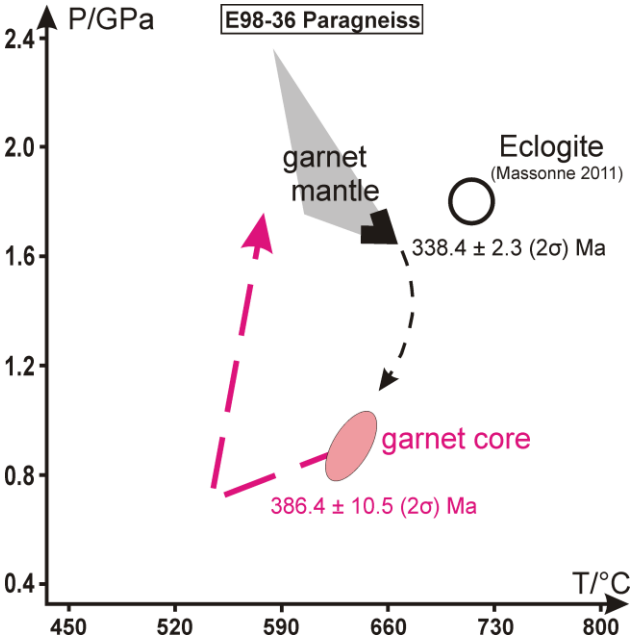

Figure 1. P-T evolution of paragneiss E98-36 developed by thermodynamic modelling. The broken paths were estimated. The given ages resulted from monazite dating using the electron microprobe. The open circle refers to P-T conditions derived by Massonne (2011) for eclogite adjacent to E98-36.

Connolly JAD (2005): Computation of phase equilibria by linear programming: a tool for geodynamic modeling and its application to subduction zone decarbonation. - Earth Planet Sci Lett 236, 524-541

Hallas P, Pfänder J A, Kroner U, Sperner B (2021): Microtectonic control of $^{40}Ar/^{39}Ar$ white mica age distributions in metamorphic rocks (Erzgebirge, N-Bohemian Massif): Constraints from combined step heating and multiple single grain total fusion experiments. - Geochim Cosmochim Acta 314, 178-208

Massonne H-J (2001): First find of coesite in the ultrahigh-pressure metamorphic region of the Central Erzgebirge, Germany. - Eur J Mineral 13, 565-570

Massonne H-J (2003): A comparison of the evolution of diamondiferous quartz-rich rocks from the Saxonian Erzgebirge and the Kokchetav Massif: are so-called diamondiferous gneisses magmatic rocks? - Earth Planet Sci Lett 216, 347-364

Massonne H-J (2011): Pre-conference field trip: Erzgebirge (Ore Mountains), Germany and Czech Republic; German part of the Saxonian Erzgebirge. - Geolines 23, 29-59

Massonne H-J (2023): A new type of saidenbachite with pseudomorphs after coesite phenocrysts from the north-western Bohemian Massif, Germany. - Terra Nova in press, https://doi.org/10.1111/ter.12659

Rahimi G, Massonne H-J (2018): Pressure-temperature-time evolution of a Variscan garnet-bearing micaschist from the northern Fichtelgebirge, NW Bohemian Massif in central Europe. - Lithos 316-317, 366-384

Willner A P, Rötzler K, Maresch WV (1997): Pressure-temperature and fluid evolution of quartzo-feldspathic metamorphic rocks with a relic high-pressure, granulite-facies history from the Central Erzgebirge (Saxony, Germany). - J Petrol 38, 307-336

The effects of anion and cation substitution on the crystal structure of Cu-based quaternary chalcogenides

D. Matzdorff[1,2], M. Avdeev[3], D. Sheptiakov[4], G. Gurieva[1], S. Schorr[1,2]

[1]Helmholtz-Zentrum Berlin für Materialien und Energie, Hahn-Meitner-Platz 1, 14109 Berlin, Germany
[2]Institut für Geologische Wissenschaften, FU Berlin, Malteserstraße 74-100, 12249 Berlin, Germany
[3]Australia's Nuclear Science and Technology Organisation, Sydney, Australia
[4]Paul Scherrer Institute, Villigen PSI, Switzerland
e-mail: david.matzdorff@helmholtz-berlin.de

The research of quaternary Cu-based chalcogenide semiconductors has caught a large interest for photovoltaic applications, as these materials consist of non-toxic and earth abundant elements. While being environmentally friendly and low cost and stable under environmental conditions, materials like Cu_2MnSnS_4 or Cu_2MnGeS_4 are very promising candidates for use as top cell absorbers in tandem solar cells, because they can cover a wide bandgap range of 1.52-1.72 eV (Beraich et al. 2020; Ramasamy et al. 2018). Compounds like $Cu_2MnSnSe_4$ could even be considered for the application in single junction solar cell with a band gap energy of 1.21 eV (Gurieva et al. 2022). This study presents new insight into the structural transformation mechanisms within the $Cu_2Mn(Ge,Sn)(S,Se)_4$ solid solution series via neutron powder diffraction.

Since Cu^+ and Ge^{4+} are isoelectronic cations and Mn^{2+} is electronic similar to Cu^+ and Ge^{4+}, they cannot be differentiated in a structural analysis based on X-ray powder diffraction data alone. However, their neutron scattering lengths are considerably different, that is why we apply neutron diffraction to analyze the crystal structure of $Cu_2Mn(Ge,Sn)(S,Se)_4$ mixed crystals. Moreover, the basis of our investigations is a careful determination of the chemical composition of the mixed crystals by WDX spectroscopy.

The endmembers of the $Cu_2Mn(Ge,Sn)(S,Se)_4$ solid solution series crystallize in different structure types: Cu_2MnSnS_4 and $Cu_2MnSnSe_4$ crystallize in the tetragonal stannite-type structure (space group $I\bar{4}2m$), whereas Cu_2MnGeS_4 and $Cu_2MnGeSe_4$ adopt the orthorhombic wurtz-stannite structure (space group $Pmn2_1$). Thus, within the solid solution series with mixed cations a structural transition from the tetragonal to the orthorhombic crystal structure can be expected.

For the presented study the compounds were synthesized by solid state reaction of pure elements in evacuated silica tubes at temperatures of 730 °C (Se-only compounds), 740-780 °C (mixed anion compounds) and 800 °C (S-only compounds). The chemical composition and homogeneity of the synthesized polycrystalline powder materials were investigated by WDX spectroscopy using an electron microprobe system. It was revealed that the synthesized powders contained the desired phase as a chemically single, homogeneous quaternary phase with slight shifts in the stoichiometric composition as well known in this type of materials (Schorr et al. 2020). LeBail refinement of the powder X-ray diffraction data was used to determine the lattice parameters of the mixed crystals. The cation distribution in the unit cell was defined by applying the average neutron scattering length analysis method (Schorr 2011) which is based on the site occupancy factors determined by Rietveld refinement of the neutron diffraction data. The derived cation distribution model is the basis to conclude on the crystal structure and structural disorder as well as to elucidate the mechanism of structural phase transition.

It will be shown that Sn-rich mixed crystals adopt the stannite type structure, whereas Ge-rich mixed crystals of the mixed cation solid solution series adopt the wurtz-stannite type structure. Within the intermediate range, two chemically identical but structurally different quaternary phases coexist, adopting the tetragonal and the orthorhombic structure respectively. It will also be shown that the respective anions influence the concentration of intrinsic point defects differently and independent to the off-stoichiometric composition.

The results of the chemical composition study in combination with structural characterization and optical bandgap evaluation from diffuse reflectance of $Cu_2Mn(Ge,Sn)(S,Se)_4$ mixed crystals will be presented. These investigations enabled us not only to determine the type and concentration of intrinsic point defects, but to show as well the structure type transformation from the stannite- to the wurtz-stannite-type structure.

Beraich et al. (2020): Facile synthesis of the wurtz stannite (orthorhombic) Cu2MnGeS4 thin film via spray ultrasonic method: Structural, Raman, optical and electronic study. - J All Comp 845, 156216

Gurieva G, Niedenzu S, Siminel N, Franz A, Schorr S (2022): The kesterite–stannite structural transition as a way to avoid Cu/Zn disorder in kesterites: the exemplary case of the Cu2(Zn,Mn)SnSe4. - Faraday Discussions 239, 51-69

Ramasamy et al. (2018): Nanocrystals of CuMSnS4 (M = In or Ga) for solar energy conversion applications. - Chemical Communications 54, 11757

Schorr (2011): The crystal structure of kesterite type compounds: A neutron and X-ray diffraction study. - Sol. Energy Mat Solar Cells 95, 1482-1488

Schorr et al. (2020): Point defects, compositional fluctuations, and secondary phases in non-stoichiometric kesterites. - J Phys Energy 2, 012002

The authors gratefully acknowledge the Australia's Nuclear Science and Technology Organisation (ANSTO) for providing us beamtime (proposal number 13403) at the ECHIDNA end station and the Paul Scherrer Institute and the Swiss Spallation Neutron Source (SINQ) for providing us beamtime (proposal number 20202094) at the HRPT diffractometer.

Trace element geochemistry and isotopic data of sulphides in Alpine-type Pb-Zn deposits in the Eastern and Southern Alps

F. Melcher[1], V. Bertrandsson Erlandsson[1], V. Gartner[1], E. Henjes-Kunst[1], P. Onuk[1], J. Raith[1], G. Rantitsch[1], F. Henjes-Kunst[2], B. Potočnik Krajnc[3], A. Šoster[3]

[1]Department of Applied Geosciences and Geophysics, Montanuniversität Leoben, Austria
[2]Federal Institute of Geosciences and Natural Resources (BGR), Hannover, Germany
[3]Faculty of Natural Sciences and Engineering, University of Ljubljana, Slovenia
e-mail: F.Melcher@unileoben.ac.at

More than 500 occurrences of Pb-Zn ores are documented in Mesozoic carbonate sequences of the Eastern and Southern Alps. They are invariably hosted by shallow lagoonal and reef carbonates of Middle and Upper Triassic (Anisian and Carnian) age and are collectively termed "Alpine-type" (APT) deposits. The district has a long mining history starting in Roman times and terminating in the early 1990ies when the last operations closed at Bleiberg (Austria), Cave del Predil/Raibl (Italy), and Mežica/Mies (Slovenia) (Schroll 2008). The Bleiberg deposit was closed in 1993 after more than 700 years of mining. It is regarded as a world-class deposit (Leach et al. 2005) and represents the type locality of APT Pb-Zn deposits. The historical total metal production from APT deposits exceeded 6 x 10^6 tons (Mt) Zn and Pb from a resource exceeding 110 Mt (Cerny 1989; Cerny & Schroll 1995; Leach et al. 2003; Spangenberg & Herlec, 2006). Renewed interest in base metals, and especially in their by-products such as Ge, Ga, In and Cd, has initiated modern exploration activities in some of the mining districts. Germanium and Cd have been recovered from ores in the past; about 200 tons Ge, mostly from Bleiberg and Raibl, were produced from APT deposits.

Although the deposits occur in a wide region, they share common features such as a simple mineralogical composition, complex ore textures, light sulphur isotopic compositions, Late Palaeozoic Pb model ages, and trace element compositions in sphalerite, galena and pyrite. Ore textures are complex and often equivocal. They include rare examples indicating syngenetic to early diagenetic origin, besides abundant epigenetic textures such as crosscutting veins and breccia ores. However, biogenic textures and relict bacteria colonies are present (Kucha et al. 2010). Therefore, some mineralization must have precipitated at shallow level at low temperature.

Sphalerite is low in Fe (commonly 0.01-0.5 %), Mn, Co, Ga and In, but commonly contains elevated Cd, Ge, As, Tl and Pb concentrations. Median concentrations of Ge determined by LA-ICP-MS are 846 ppm in the Fladung deposit, 229 ppm at Bleiberg and 222 sppm at Raibl where the highest contents of As and Tl have been determined. Sphalerite chemistry indicates that temperatures of formation range from 60 to 140 °C. This is lower than suggested by previous fluid inclusion data, but in line with results of thermal modelling. Metamorphosed sphalerite (>450 °C) in the Brenner and Stangalm Mesozoic reveals metal exchange to higher Fe and Mn, and lower Ga, Ge, As and Tl concentrations. Galena is Ag-poor, although Ag concentrations both in sphalerite and galena increase towards the north of the Austroalpine nappe system. Pyrite- and marcasite-rich ores display an As-Tl-(Hg) association, and are low in Co and Ni. Pyrite is stable to higher temperatures, keeping its original low-temperature trace element compositions.

The sulphur isotope composition of sulphides in APT deposits varies over a wide range and is often bimodally distributed, attaining a maximum at highly negative values ($\delta^{34}S \leq$-20 ‰) explained by bacteriogenic sulphate reduction, and a second maximum at $\delta^{34}S$ = -10 to 0 ‰ explained by thermogenic sulphate reduction from a second source (Schroll & Rantitsch 2005). APT ores in general show lead isotopic compositions above the crustal lead growth curves. The variable enrichment in ^{207}Pb and ^{208}Pb originated from an isotopically enriched continental source (Köppel 1997). Local differences in the bedrock geology and/or its variable common Pb composition are responsible for the Pb isotopic variability of the individual APT deposits. A metal source from the Paleozoic basement and Triassic sedimentary rocks is most likely.

Rb-Sr isochrons of sphalerite from the Bleiberg deposit indicate two phases of ore deposition: a first one at about 229 Ma and a second at about 207-201 Ma. Initial $^{87}Sr/^{86}Sr$ of the early (229 Ma) sphalerite agrees with Carnian seawater composition. The Carnian Rb-Sr isochron age corresponds to U-Pb ages of calcite associated to ore minerals of the (Southalpine) Gorno deposit (Giorno et al. 2022). The younger (≈205 Ma) age reflects fluid flow within the carbonate sequence, probably due to fracturing of the platform during initial rifting of the Penninic Ocean. This process is probably related to ongoing tectonic instability following sedimentation of the Upper Hauptdolomit with formation of deep basins, where hydrocarbon source rocks were deposited. In a wider context of central and southern Europe, mineralizing processes during the Mesozoic have been explained as a response to the Pangaea breakup (Burisch et al. 2022). The oldest hydrothermal processes in the circum-Mediterranean are related to the initial rift axes. Mineralization spans a range from 230 to 160 Ma with a maximum at 230-200 Ma.

Burisch M, Markl G, Gutzmer J (2022): Breakup with benefits - hydrothermal mineral systems related to the disintegration of a supercontinent. - Earth Planet Sci Let 580, 117373

Cerny I (1989): Die karbonatgebundenen Blei-Zink-Lagerstätten des alpinen und außeralpinen Mesozoikums. Die Bedeutung ihrer Geologie, Stratigraphie und Faziesgebundenheit für Prospektion und Bewertung. - Arch Lagerstforsch Geol Bundesanst 11, 5-125

Cerny I, Schroll E (1995): Heimische Vorräte an Spezialmetallen (Ga, In, Tl, Ge, Se, Te und Cd) in Blei-Zink- und anderen Erzen. - Arch Lagerstforsch Geol Bundesanst 18, 5-33

Giorno M, Barale L, Bertok C, Frenzel M, Looser N, Guillong M, Bernasconi SM, Martire L (2022): Sulphide-associated hydrothermal dolomite and calcite reveal a shallow burial depth for Alpine-type Zn-(Pb) deposits. – Geology 50, 853-858

Köppel V (1997): 3.5. Bleiisotope. – Arch Lagerstforsch Geol Bundesanst 19, 485-495

Kucha H, Schroll E, Raith JG, Halas S (2010): Microbial sphalerite formation in carbonate-hosted Zn-Pb ores, Bleiberg, Austria: Micro- to nanotextural and sulphur isotope evidence. – Econ Geol 105, 1005-1023

Leach DL, Bechstädt TH, Boni M, Zeeh S (2003): Triassic-hosted MVT Pb-Zn ores of Poland, Slovakia and Italy. - In: Kelly JG et al. (eds.): Europe´s major base metal deposits. Irish Ass Econ Geol, 169-213

Leach DL, Sangster DF, Kelley KD, Large RR, Garven G, Allen CR, Gutzmer J, Walters S (2005): Sediment-hosted Pb-Zn deposits: A global perspective. - Econ Geol 100th Anniv Vol, 561-607

Schroll E (2008): Die Blei-Zink-Lagerstätte Bleiberg. Die Geschichte ihrer Erforschung. - Carinthia II 62, 287 pp

Schroll E, Rantitsch G (2005): Sulphur isotope patterns from the Bleiberg deposit (Eastern Alps) and their implications for genetically affiliated lead-zinc deposits. - Mineral Petrol 84, 1-18

Spangenberg JE, Herlec U (2006): Hydrocarbon biomarkers in the Topla-Mežica zinc-lead deposits, Northern Karavanke/Drau Range, Slovenia: paleoenvironment at the site of ore formation. - Econ Geol 101, 997-1021

Corundum-rich rocks in the Tauern Window, Austria

F. Melcher[1], M. Feichter[1], H. Mali[1], H. Grill[2], B. Huet[3]

[1]Department of Applied Geosciences and Geophysics, Montanuniversität Leoben, Austria,
[2]Birkenweg, Neumarkt, Austria
[3]Geosphere Austria, Vienna, Austria
e-mail: F.Melcher@unileoben.ac.at

In the search for the origin of a 60 kg block of a dark grey corundum-rich rock that was found in the river bed of the Obersulzbach Valley near Hopffeldboden, Venediger Alps (Salzburg, Austria; Melcher et al. 2022), boulders of similar material were discovered underneath a cliff in the region named Bettlerscharte. In this area, Variscan granite gneisses of the Central Gneiss Supersuite are intercalated with metavolcanics (amphibolite, chlorite schist) and metasedimentary rocks (micaschist, graphitic phyllite, quartzite) attributed to the Habach Group. Corundum-bearing rocks with or without sulphide mineralization are associated with a diverse suite of metasedimentary and metavolcanic rocks that outcrop in the cliff northwest of the Bettlerscharte. Rocks comprise white, partly kyanite-bearing quartzite, garnet-bearing chloritoid-chlorite-muscovite schist, amphibolite, and epidote schist with massive bands of magnetite. The quartzites show strong foliation and disseminated sulphide mineralization comprising mainly pyrite, but in places also abundant molybdenite. The assemblage resembles the one described as type locality of the Habach Formation (Steyrer 1983).

Similar to the specimen found in the Obersulzbach valley investigated earlier (Melcher et al. 2022), microscopic examination of the corundum-bearing rocks reveals abundant magnetite, ilmenohematite, and variable pyrite in a very fine-grained non-foliated matrix, in which rare white mica flakes and aggregates are visible. The fine matrix consists mainly of anhedral corundum of 30-50 μm grain size intergrown with green-blue pleochroic Fe-rich chloritoid (#Mg = 15-27) and less abundant light green chlorite with #Mg ranging from 40-60. White mica aggregates consist of intergrown margarite and paragonite and are often surrounded by large chloritoid crystals. Apatite is present throughout the rock, although grain size and abundance vary. Accessory phases include diaspore, epidote/allanite, zircon, and monazite. Oxide minerals mainly consist of magnetite and ilmenohematite. Uraninite and Nb-rich rutile (4-6 wt% Nb_2O_5) are subordinate. Sulphides postdate the oxide-silicate assemblage and mainly consist of pyrite and chalcopyrite, with rare molybdenite. The corundum-rich assemblage is associated with rocks carrying relict garnet replaced by chloritoid, chlorite and white mica. These rocks also carry abundant magnetite, ilmenohematite and pyrite.

Chemical analysis of corundum-rich rocks by wavelength-dispersive X-ray fluorescence spectroscopy on fused discs reveals high contents of Al_2O_3 (36-55 wt%) and Fe_2O_3 (22-35 wt%), low SiO_2 (3.8-22 wt.%), CaO (0.7-2.6 wt.%), MgO (0.7-2.1 wt.%), K_2O (<1.8 wt.%) and Na_2O (<1.2 wt.%). Sulphur contents in some samples reach up to 10 wt.%. TiO_2 (2.2-4.2 wt.%) and P_2O_5 (0.7-1.2 wt.%) are severely enriched compared to typical crustal rocks. Among the trace elements, high contents of Zr (356-848 ppm), V (321-559 ppm), Nb (39-89 ppm), Cu (156-1550 ppm) and Ga (49-106 ppm) are noteworthy, along with low Cr, Ni, Y and REE.

Chemical composition and mineralogy both strongly argue in favour of a bauxitic origin of the samples, resembling Si-depleted, Fe-rich bauxite. Compared to other metabauxites, the P content is extraordinarily high. Apart from S, Fe, Cu and P, levels of minor and trace elements are within the ranges expected for bauxite. Trace element concentrations, especially low Ni-Cr contents favour an origin from acidic precursor rocks.

The association with both, rocks typical of the Habach Formation (amphibolite) and quartzitic metasediments is regarded as an indication for a situation where pre-Permian rocks have been weathered producing local bauxitic rocks associated with less Si-depleted, clay-rich material. These paleosoils have been covered by impure sandstone, probably in the Lower Triassic. Weathering horizons in similar stratigraphic and tectonic positions have been described from other areas within the Tauern Window (Barrientos & Selverstone 1987; Franz et al. 2021).

Preliminary metamorphic P-T conditions have been determined for the metabauxite using pseudosections calculated with the Theriak-Domino software package (de Capitani & Petrakakis 2010). The targeted sample is the one investigated in Melcher et al. (2022). The observed oxide-silicate assemblage with corundum, chloritoid, chlorite, margarite, paragonite, rutile, hematite, ilmenite and magnetite points to peak conditions at 500 ± 30 °C and 8.5 ± 1.5 kbar. In this range, the model predicts stability of corundum, chloritoid, chlorite, margarite, paragonite and rutile together with a complex topology between the fields containing one or two of the three Fe-Ti oxides hematite, ilmenite and magnetite. This explains the observed complex reaction features between those.

Barrientos X, Selverstone J (1987): Metamorphosed soils as stratigraphic indicators in deformed terranes: An example from the Eastern Alps. – Geology 15, 841-844

de Capitani C, Petrakakis K (2010): The computation of equilibrium assemblage diagrams with Theriak/Domino software. - Amer Mineral 95, 1006-1016

Franz G, Kutzschbach M, Berryman EJ, Meixner A, Loges A, Schultze D. (2021): Geochemistry and paleogeographic implications of Permo-Triassic metasedimentary cover from the Tauern Window (Eastern Alps). - Eur J Mineral 33, 401-423

Melcher F, Feichter M, Mali H, Grill H (2022): Ein ungewöhnliches Korundgestein im Tauernfenster: Metabauxite in der Habach-Gruppe? – Mitt Österr Mineral Ges 168, 89-99

Steyrer HP (1983): Die Habachformation der Typlokalität zwischen äußerem Habachtal und Untersulzbachtal (Pinzgau/Salzburg). – Mitt Österr Geol Ges 76, 69-100

Rohstoffe für den Green Deal: woher nehmen?

F. Melcher

Lehrstuhl für Geologie und Lagerstättenlehre, Montanuniversität Leoben, Österreich
Frank.Melcher@unileoben.ac.at

Die Europäische Union hat mit dem European Green Deal das ehrgeizigste Transformationsprogramm ihrer Geschichte initiiert. Die Reduktion der Treibhausgasemissionen sowie der Ausbau des Anteils erneuerbarer Energien werden gewaltige Mengen an mineralischen und metallischen Rohstoffen verbrauchen. Viele dieser Rohstoffe werden in der Union als kritisch klassifiziert und müssen daher zum überwiegenden Teil importiert werden. Hier ist vor allem die dominierende wertschöpfungsübergreifende Rolle Chinas in der Versorgung mit Rohstoffen und Zwischenprodukten zu nennen.

Trotz der Innovationen in Recyclingtechnologien und den Bemühungen zur Umsetzung einer Kreislaufwirtschaft werden primäre mineralische Rohstoffe weiterhin und sogar verstärkt genutzt werden müssen, um die Schlüsseltechnologien (Windkraft, Solarenergie, Batterien) und ihre Infrastruktur (Leitungen, Fundamente) zu versorgen. Es werden zusätzliche Mengen an strukturellen Materialien (Baurohstoffe, Stahl, Kupfer) und technologie-spezifischen Materialien benötigt. Letztere, beispielsweise Lithium, Kobalt, Seltene Erden, Indium und Germanium müssen derzeit zu nahezu 100% importiert werden.

Die Abhängigkeit der europäischen Industrie bezüglich der Rohstoffe für die Energiewende ist unumstritten und seit Jahren bekannt. Trotz intensiver Diskussion auf nationaler und europäischer Ebene hat sich die Situation für den Bergbau in Europa seit 30 Jahren nicht signifikant verbessert.

Der Vortrag wird besonders die Möglichkeiten der Versorgung mit mineralischen Rohstoffen aus europäischen Quellen beleuchten. Hier sind Potenziale für Lithium, Graphit, Seltene Erden und Kobalt, aber auch Baurohstoffe zu nennen. Die Eigenverantwortung der europäischen Länder impliziert, dass die Gewinnung zusätzlicher Rohstoffmengen genehmigt und geduldet werden muss, um größeren Schaden an Umwelt und Klima zu vermeiden. Erweiterungsverfahren oder Neuerschließungen sind jedoch mit erheblichen Problemen konfrontiert. Vielfältige konkurrierende Nutzungen müssen bedacht werden, und schließlich können Eingaben und Politik jedes Projekt kippen. Dies ist aus Sicht der Nachhaltigkeit der Versorgung mit den notwendigen Rohstoffen für die Energiewende nicht vereinbar. Somit ist der Ausbau der erneuerbaren Energien eine Herausforderung, die es an vielen Fronten zu meistern gilt.

On preventing Sn-loss in experimental studies

J. A.-S. Michaud[1], F. Holtz[1], T. Fusswinkel[2]

[1]Institute of Mineralogy, Leibniz University, Callinstraße 3, 30167 Hannover, Germany
[2] Institute of Applied Mineralogy and Economic Geology, RWTH Aachen University
Wüllnerstraße 2, 52062 Aachen, Germany
e-mail: j.michaud@mineralogie.uni-hannover.de

Tin (Sn) transport and concentration are essentially controlled by a combination of melt- and fluid-driven processes and its cycle within the crust strongly depends on its partitioning. Given the complexity of natural systems, it is rather hard to evaluate the effect of individual parameters (e.g., pressure (P), temperature (T), proportion and composition of involved phases or redox conditions) on Sn behaviour.

As an alternative, natural processes can be simulated experimentally under a range of conditions relevant to natural systems. However, in experiments conducted at elevated P-T, samples containers are made of noble-metal capsules (e.g., Au, Pt, Au-Pd) and Sn alloys with all these materials especially under reducing conditions and when an aqueous phase is present. This often results in capsule failure and/or to problems for the accurate determination of Sn partitioning between phases due to partial Sn loss during the experiment. Several experimental studies have focused on Sn behaviour (e.g., Keppler & Wyllie 1991; Schmidt et al. 2020; Michaud et al. 2021; Pichavant 2022) but to our knowledge none of the methods proposed so far were completely satisfactory when it comes to preventing Sn loss and determining partition coefficients accurately and reproducibly.

Inspired from Lerchbaumer & Audétat (2012) and Derrey et al. (2017), we propose a new capsule setup (Fig.1) which has been tested on the example of Sn partitioning experiments between a strongly peraluminous melt and an aqueous phase. In order to avoid interactions with the noble-metal capsule and minimise Sn loss, 15 mg of glass powder containing *ca*. 600 ppm Sn, 25µl of 8wt% NaCl fluid and a pre-cracked quartz cylinder are inserted in an inner silica capsule consisting of two fitting tubes. Silica gel or quartz powder is added to insure sealing of the silica tubes during heating.

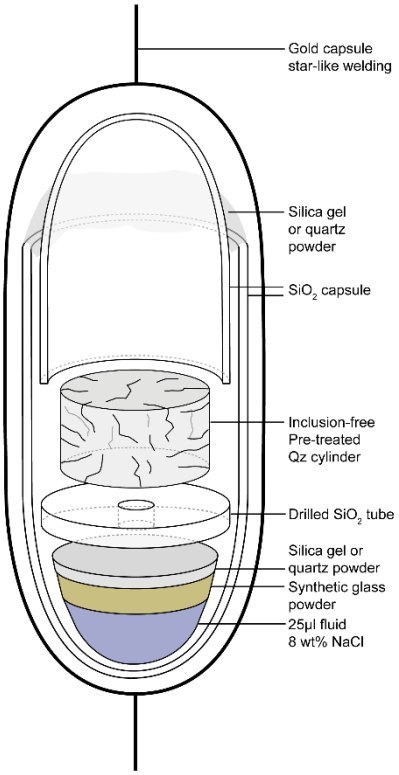

Fig.1: Capsule setup designed to prevent Sn-loss during HT-HP experiments.

Several experiments were run at 800°C, 150 MPa, under boiling conditions (i.e., phase separation resulting in coexisting brine and vapour-rich fluid inclusions), for 24 and 48h and under oxidising (QFM+3; fO_2 is 3 log units higher than fO_2 buffered by Quartz-Fayalite-Magnetite buffer) and reducing conditions (QFM -0.5).

Boiling assemblages were found in all samples, with brine and vapour-rich inclusions entrapped in quartz cylinders having generally a size in the range of 10 to >25 µm. Under reducing conditions, quenched glasses contain numerous albite crystals and few cassiterites. Under oxidising conditions, the glass is rather homogeneous and cassiterite has only been found within what was formerly a silica drilled tube separating the quartz cylinder from the rest (see Fig. 1).

Tin concentrations were measured in quenched glasses and brine and vapour-rich inclusions with electron microprobe and LA-ICP-MS. Under oxidising conditions, Sn concentrations are rather homogeneous in the quenched glass (i.e., ~ 200-250 ppm) and a bit more scattered in brine inclusions (i.e., 100-640 ppm; median 347 ppm) but all lower than the Sn concentration in the starting glass. Under reducing conditions, Sn concentrations in glass are more scattered in the 24h run (i.e., median 2631 ± 1464 ppm) than in the 48h one (i.e., median 1752 ± 699 ppm). This heterogeneity is probably related to the high crystallinity observed in these glasses. Concentrations in brine inclusions are rather clustered for both duration (i.e., median 107 ± 38 ppm and 84 ± 50 ppm for the 24 and 48h runs, respectively). Concentrations in vapour-rich inclusions could only be measured in the 48h run and are very low (i.e., median 0.6 ± 6 ppm).

Overall, Sn shows a contrasted behaviour depending on redox conditions, being preferentially partitioned to the fluid under oxidising and to the melt under reducing conditions. This result is supported by the presence of cassiterite crystallizing from the fluid at oxidizing conditions and of cassiterite crystallizing from the melt at reducing conditions. Our dataset and mass balance calculations indicate that the use of a silica capsule inserted in noble metal capsules is rather successful in preventing important Sn-loss during experiments.

Derrey IT, Albretch M, Dupliy E, Botcharnikov RE, Horn I, Junge M, Weyer S, Holtz F (2017): Experimental tests on achieving equilibrium in synthetic fluid inclusions: Results for scheelite, molybdenite, and gold solubility at 800 °C and 200 Mpa. - Amer Miner 102, 275-283

Keppler H, Wyllie PJ (1991): Partitioning of Cu, Sn, Mo, W, U and Th between melt and aqueous fluid in the systems haplogranite-H_2O-HCl and haplogranite-H_2O-HF. - Contr Miner Petrol 109, 139-150

Lerchbaumer L, Audétat A (2012): The quartz capsule - a new method to avoid alloying problems with noble-metal capsules in hydrothermal experiments. - Eur J Miner 24, 683-693

Michaud JA-S, Pichavant M, Villaros A (2021): Rare elements enrichment in crustal peraluminous magmas: insights from partial melting experiments. - Contr Miner Petrol 176, 96

Pichavant M (2022): Experimental crystallisation of the Beauvoir granites as a model for the evolution of Variscan rare metal magmas. - J Petrol 63, 1-28

Schmidt C, Romer R, Wohlgemuth-Ueberwasser CC, Appelt O (2020): Partitioning of Sn and W between granitic melt and aqueous fluid. - Ore Geol Rev 117, 103263

Atomistic processes in actinolite and tremolite at elevated temperatures

B. Mihailova[1], C. Rösche[1], N. Petrova[2], T. Malcherek[1], J. Schlüter[3]

[1]FB Erdsystemwissenschaften, Universität Hamburg, Grindelallee 48, 20146 Hamburg, Germany
[2]Institute of Mineralogy and Crystallography "Acad. Ivan Kostov", Bulgarian Academy of Sciences, Acad. Georgi Bonchev Str. 107, 1113 Sofia, Bulgaria
3Mineralogisches Museum, Leibniz-Institut zur Analyse des Biodiversitätswandels, Grindelallee 48, 20146 Hamburg, Germany
e-mail: boriana.mihailova@uni-hamburg.de

Elucidating the atomistic mechanism of high-temperature transformations of iron-containing amphiboles ($AB_2C_5T_8O_{22}W_2$, with $C_5 = M(1)_2M(2)_2M(3)$) may have important implications in several fields, including metamorphic petrology, geophysics, and environmental sciences. Here the effect of octahedrally coordinated Fe^{2+} on the temperature-driven dehydrogenation/dehydroxylation in Mg-rich amphiboles is analysed by a comparative study of tremolite and actinolite via *in situ* high-temperature Raman spectroscopy, thermogravimetric/mass-spectrometry analyses, and X-ray diffraction (Rösche et al. 2022).

We show that similar to Fe-rich amphiboles (Mihailova et al. 2021, 2022, Bernardini et al. 2023) thermally activated delocalized e^- and H^+ are also formed in Fe-bearing magnesian amphiboles, but at much higher temperatures than in ferrous (e.g. grunerite) and mixed-valence iron-rich amphiboles (e.g. riebeckite). The delocalized electrons in actinolite couple with polar FeO_6 phonons to form polarons. However, the polaronic dipoles in actinolite are not mutually aligned as in the case of Fe-rich amphiboles, because iron cations are present in the actinolite structure as isolated octahedra or dimers of octahedra, while the majority of MO_6 octahedra in the strips are occupied by Mg. The final product of the thermally-induced decomposition of both actinolite and tremolite is a single phase of monoclinic pyroxene with an intermediate chemical composition between diopside and clinoenstatite, having vacancies at the octahedral sites and, for actinolite, also Fe^{3+}. Cristobalite occurs only as a minor phase in amounts less than 1% and ~5% for tremolite and actinolite, respectively. The dehydroxylation of tremolite causes immediate collapse of the silicate double chain into SiO_4 single chains, which is followed up by a rearrangement of the amphibole B-type and C-type cations into pyroxene octahedral sheets. The actinolite-to-pyroxene breakdown is preceded by a state of "oxo-actinolite" in which all Fe^{2+} are exchanged to Fe^{3+}, all $^W(OH)^-$ groups next to Fe-containing $M(1)M(1)M(3)$ configurations are exchanged to $^WO^{2-}$, and all H^+, including those from *W*-site anions next to MgMgMg triads, are delocalized, but still in the bulk of the crystal grain.

Bernardini S, Della Ventura G, Schlüter J, Mihailova B (2023): Thermally activated electron hopping in Fe-rich amphiboles: implications for the high-conductivity anomalies in subduction zones. - Geochem 83, 125942

Mihailova B, Della Ventura G, Waeselmann N, Xu W, Schlüter J, Galdenzi F, Marcelli A, Redhammer GJ, Boiocchi M, Oberti R (2021): Atomistic insight into lithospheric conductivity revealed by phonon-electron excitations in hydrous iron-bearing silicates. - Commun Mater 2, 57

Mihailova B, Della Ventura G, Waeselmann N, Bernardini S, Xu Wei, Marcelli A (2022): Polarons in rock-forming minerals: physical implications. - Condens Matter 7, 68

Rösche C, Waeselmann N, Petrova N, Malcherek T, Schlüter J, Mihailova B (2022): Oxidation processes and thermal stability of actinolite. - Phys Chem Mineral 49, 47

Zemannite, $Mg(H_2O)_6[Zn^{2+}Fe^{3+}(TeO_3)_3]_2 \cdot nH_2O$, $n \leq 3$: Trigonal symmetry enables a fully ordered host-guest structure

R. Miletich[1], H.S. Effenberger[1], M. Ende[1]

Institut für Mineralogie und Kristallographie, Universität Wien
ronald.miletich-pawliczek@univie.ac.at

The microporous crystal structure of zemannite was originally described in space group $P6_3/m$ (Matzat 1967; Mandarino et al. 1967; Miletich 1995), later revised to $P6_3$ (Cametti et al. 2017; Missen et al. 2019). Most recently the diffraction pattern of a single-crystal sample was re-investigated using a high- sensitivity Dectris Pilatus pixel detector (Effenberger et al. 2023). Unexpectedly, several uneven low-order 00*l* reflections showed unequivocally verifiable weak intensities clearly violating the 6_3 screw-axis reflection conditions. These observations promoted detailed X-ray crystallographic investigated to be resumed.

The crystal-structure type of zemannite is characterised by a honey-comb like $[Zn^{2+}Fe^{3+}(TeO_3)_3]^{1-}$ framework building channels along [001]. It consists of M_2O_9 dimers formed by two face-sharing MO_6 octahedra, $M = (Zn^{2+},Fe^{3+})$ with $Zn^{2+}:Fe^{3+} \sim 1:1$. These dimers are linked by $(Te^{4+}O_3)^{2-}$ figures and form the channel walls. The channels are filled by the extra-framework constituents, i.e. 0.5 $[Mg(H_2O)_6]^{2+}$ cations per formula unit in addition to up to 1.5 interstitial H_2O molecules. So far, none of the space-group symmetries $P6_3/m$ or $P6_3$ was compatible with a fully ordered atomic arrangement. In space group $P6_3/m$ there is one $M = (Zn^{2+}Fe^{3+})$ position, thus an order of the *M* atoms is impossible. However, the ionic radii of the two *M* cations differ suggesting a tentative order and, furthermore, $Fe^{3+}{}_2O_9$ dimers besides $Zn^{2+}{}_2O_9$ dimers are not likely. Ordering of the extra-framework atoms is impossible within the given symmetry constraints for both space groups mentioned above. In the acentric space group the *M* position splits into two sites, *M*1 and *M*2; an order between Zn^{2+} and Fe^{3+} might be possible but could not be proofed so far (Cametti et al. 2017).

For this work X-ray diffraction data were collected at 298 ± 0.5 K, 200 ± 1 K, and 100 ± 3 K ($2\theta_{max} = 101.4°$, MoKα radiation). Careful inspections of the entire images did not show any evidence for satellite reflections in the surrounding of the Bragg-peak positions. Furthermore, there is no hint neither for diffuse scattering nor for the appearance of superstructure reflections. Thus, an incommensurately modulated atomic arrangement or disorder phenomena in neighbouring channels are not likely.

A series of comparative refinement models were performed in the space groups $P6_3/m$ and its subgroups $P6_3$, $P\bar{6}$, and $P3$. Order of the Fe and Zn atoms in the frame work is possible in all subgroups of $P6_3/m$. Due to mirror planes parallel to (0001), space group $P\bar{6}$ allows Fe_2O_9 or Zn_2O_9 dimers, which contradicts the results of *ab initio* calculations (Cametti et al. 2017). A fully ordered atomic arrangement of the one-dimensional extra-framework atoms is possible in $P3$ only (Fig. 1). Refinements confirm the earlier postulated theoretical structure model with $[Mg(H_2O)_6]^{2+}$ octahedra alternating with interstitial H_2O molecules along [001] (Miletich, 1995). The interaction between these structural units as well as the bonding between the host and guest atoms is achieved solely by hydrogen bonds. The final refinements in space group $P3$ yield R1 ~ 0.025 for the entire data sets.

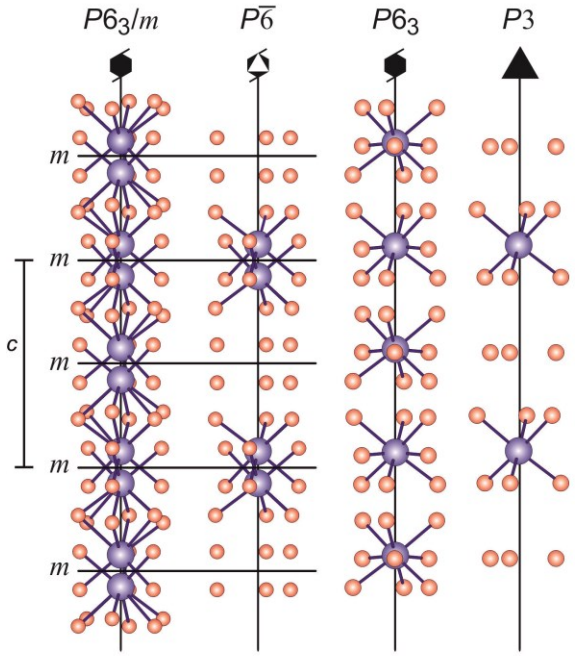

Figure 1. The extra-framework atoms and their distribution (full site multiplicity in the respective space group is shown). Mg and O atom position are shown as blue and red spheres, respectively. In *P*3 full order is achieved without the necessity of partial site occupations.

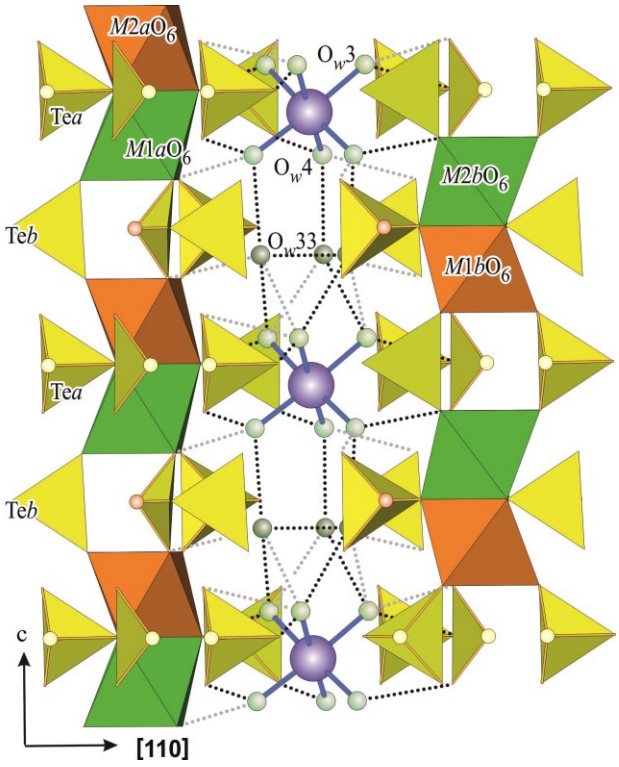

Figure 2. Detail of the atomic arrangement (space-group symmetry *P*3): the host structure consists of M_2O_9 dimers and TeO_3 groups. $M^{2+}O_6$ octahedra with M = ($\underline{Zn^{2+}}$, Fe^{3+}) are shown in green and M = ($\underline{Fe^{3+}}$, Zn^{2+}) in brown shades. – The channel is filled by $\underline{Mg}^{[6]}$ atoms (blue) and H_2O molecules (O atoms in shades of green). Short and long O-H···O hydrogen bridges are indicated as dotted black and grey lines.

In accordance with the observed violation of the 6_3 screw axis, it is evident from crystal-structure refinements and crystal chemical considerations, that the atomic arrangement of zemannite is best described in space group *P*3. Zn^{2+} and Fe^{3+} ions are not fully ordered in the individual MO_6 octahedra but show a predominant occupation that explains the violation of the 6_3 screw axis. It is to be mentioned that neighbouring M_2O_9 dimers are differently orientated with Zn^{2+} respectively Fe^{3+} centred octahedra pointing upwards and downwards, respectively (Fig. 2). In contrast, symmetry $P6_3$ cause a parallel orientation of all dimers.

Cametti G, Churakov S, Armbruster T (2017): Reinvestigation of the zemannite structure and its dehydration behavior: a single-crystal X-ray and atomistic simulation study. - Eur J Mineral 29, 53-61

Mandarino JA, Matzat E, Williams SJ (1967): Zemannite, a zinc tellurite from Moctezuma, Sonora, Mexico. - Canad Mineral 14, 387-390

Matzat, E (1967): Die Kristallstruktur eines unbenannten zeolithartigen Telluritminerals {(Zn,Fe)$_2$[TeO$_3$]$_3$} NaxH$_{2-x}$·yH2O. Tschermaks Mineral Petrogr Mitt 12, 108-117

Miletich R (1995): Crystal chemistry of the microporous tellurite minerals zemannite and kinichilite, $Mg_{0.5}[Me^{2+}Fe^{3+}(TeO_3)_3]\cdot 4.5H_2O$, ($Me^{2+}$ = Zn, Mn). - Eur J Mineral 7, 509-523

Missen OP, Mills SJ, Spratt J, Birch WD, Brugger J (2019): Crystal chemistry of zemannite-type structures: I. A re-examination of zemannite from Moctezuma, Mexico. - Eur J Mineral 31, 519-527

LA-ICPMS U-Pb dating of garnet from the Adula nappe, Central Alps

L.J. Millonig[1], J. Pleuger[2], T. John[2], A. Gerdes[1]

[1]FIERCE, Goethe University Frankfurt am Main
[2]Freie Universität Berlin
e-mail: l.millonig@em.uni-frankfurt.de

The Adula nappe is located in the Lepontine Alps, Switzerland and Italy, and comprises crustal gneisses, metasediments and mica schists, as well as mafic and ultramafic units including eclogites, amphibolites and peridotites. Rocks from the Adula nappe show a gradual increase in pressure and temperature from north to south and record a high-pressure (HP) event followed low-pressure (LP)/high–temperature (HT) conditions, with the intensity of the overprint also increasing to the south. HP metamorphism and subsequent LP-HT overprint are considered to result from a single P–T evolution. However, geochronological data from the Adula nappe yielded partially inconsistent results and the timing and extent of HP metamorphism in the Adula nappe remains somewhat ambiguous. While eclogites from the southern part of the nappe yielded ages between 42 and 34 Ma (garnet Lu–Hf and Sm–Nd; zircon U–Pb), eclogites in the northeastern part of the nappe yielded only Palaeozoic ages of ~330-340 Ma (U–Pb zircon) and ~324 Ma (Lu–Hf garnet) for the HP stage. Eclogites from the central part of the Adula nappe gave both Alpine (~37-39 Ma) and Variscan (336 Ma) garnet Lu-Hf ages and zircon U-Pb ages (~31-33 and ~370 Ma). P–T conditions recorded by the Adula nappe are attributed to Variscan-Alpine polymetamorphism and a polyphase Alpine deformation history, which obscured the mineral equilibria developed during each high-grade metamorphic event. Polymetamorphism of the Adula nappe is reflected in compositionally and chronologically distinct garnet domains and generations. However, published ages from polymetamorphic garnet from the Adula nappe represent approximate maximum or minimum ages, because the mixing of different garnet age domains during hand picking cannot be ruled out when using conventional dating techniques. We therefore applied in-situ garnet U–Pb dating by LA-ICP-MS to spatially resolve different garnet growth zones, as revealed by major and trace element mapping.

Our preliminary results indicate that Variscan metamorphism in the northeastern Adula nappe also occurred at ~370 Ma, whereas lithologies from the central and southern Adula nappe yielded garnet U-Pb dates of ~40-35 Ma. Moreover, some samples from the central Adula nappe yielded single well-defined Alpine garnet growth ages, whereas others indicate ill-defined pre-Alpine garnet growth events. Such samples will be further investigated in greater detail to resolve the two growth events.

In-situ monitoring of ATP hydrolysis as a function of p-T-Mg^{2+}: new insights into metabolic kinetics

C. Moeller[1], C. Schmidt[2], D. Testemale[3], F. Guyot[4], M. Kokh[1,5], M. Wilke[1]

[1]Institut für Geowissenschaften, Universität Potsdam, Germany
[2]Helmholtz-Zentrum Potsdam, Deutsches GeoForschungsZentrum GFZ, Germany
[3]Univ. Grenoble Alpes, CNRS, Institut Néel, Grenoble, France.
[4]IMPMC Muséum National d'Histoire Naturelle, Paris, France
[5]Institut für Mineralogie, Westfälische-Wilhelms-Universität, Münster, Germany
e-mail: chmoeller@uni-potsdam.de

The thriving exploration of geologically extreme environments has led to the discovery of new habitats of extremophiles. Fascinating biological communities were discovered at hot springs, in deep oceanic sediments, and hydrothermal vents. Biological-geological interaction enables life up to 120 °C and 300 MPa. Experimental studies, albeit controversial, expanded this T-P-range (Sharma et al. 2002, Takai et al. 2008). Stability of vital molecules like ATP can serve as proxies to determine physicochemical boundary conditions for life (Bains et al. 2015)

The exergonic enzymatic hydrolysis of adenosine triphosphate (ATP) to adenosine diphosphate (ADP) is a key reaction in all metabolic systems. It is counteracted by the abiotic hydrolysis of ATP; therefore, the rate constant and the related half-life can be used as a proxy for bioavailability. The abiotic hydrolysis is kinetically enhanced at elevated temperatures and low pH values (Leibrock et al. 1995; Moeller et al. 2022). The dependence on pressure of the rate constant of the hydrolysis can be best described by a power low and shows only a vanishingly low effect up to 500 MPa. Addition of Mg^{2+} and Ca^{2+} decelerate the hydrolysis; in contrast to Cu (II) and Co (III) complexes, which lead to an acceleration (Buisson and Sigel 1974, Suzuki et al. 1978).

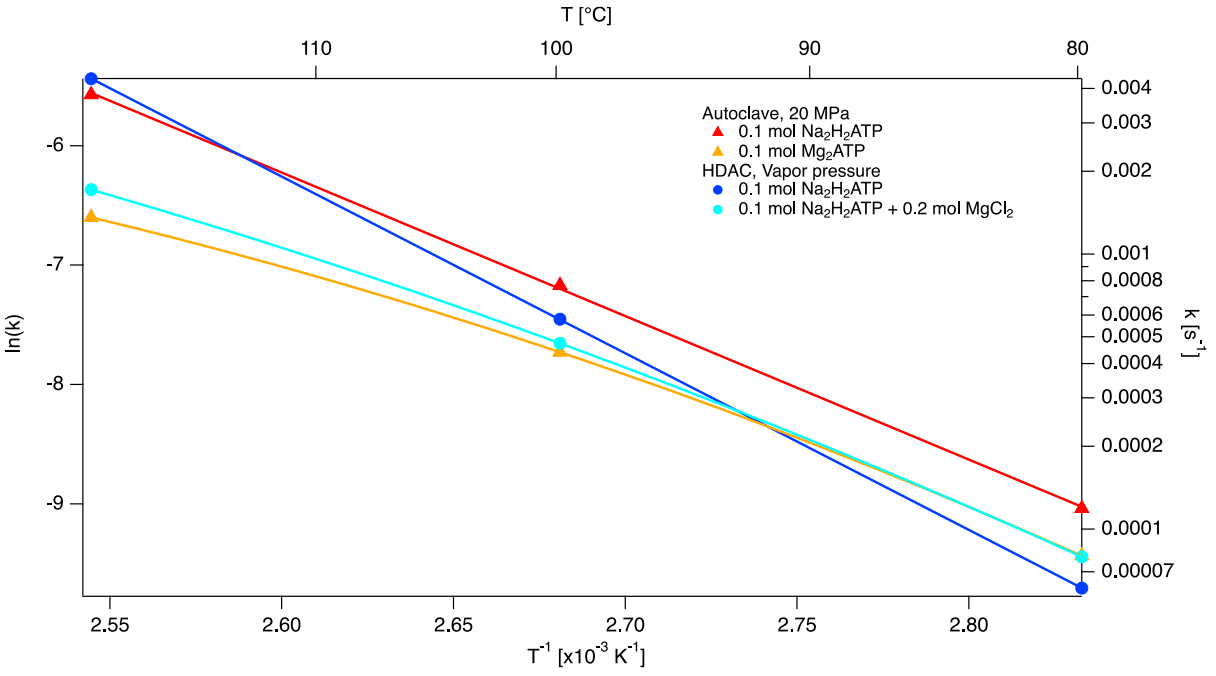

Figure 1: Arrhenius graph of the hydrolysis rate constants of ATP.

In biological systems, ATP is commonly found in a complexed form with Mg^{2+}. Earlier, experimental studies were performed on monovalent analogs of ATP like Na_2H_2ATP as commercial Mg_2ATP salts are rare and expensive. Effects of Mg^{2+} were simulated by addition of magnesium salts (e.g., in Leibrock et al. 1995). A novel in-situ protocol based on the combination of optical high-pressure cells and Raman spectrometry allowed us to determine the hydrolysis rate constants on small sample volumes without any artifacts due to quenching. The investigated temperature range was from 80 – 120 °C for sample solutions of Na_2H_2ATP + $MgCl_2$ and of Mg_2ATP. Our preliminary results verify a decrease of the hydrolysis rate constant by 30% at 80 °C. In contrast to studies on Na_2H_2ATP systems, our initial data suggest a significant deviation from the Arrhenius relation in the investigated T-interval (Fig. 1). This very new insight on the kinetic stability of Mg_2ATP suggests that the reaction mechanism changes at high temperature in the presence of magnesium. In terms of bioavailability, Mg^{2+} almost doubles the half-life of ATP at 120 °C which is 20% higher than previously assumed.

Sharma A, Scot JH, Cody GD, Fogel ML (2002): Microbial Activity at Gigapascal Pressures. - Science 295, 5539, 1514-1516

Takai K, Nakamura K, Toki T, Horikoshi K (2008): Cell proliferation at 122°C and isotopically heavy CH_4 production by a hyperthermophilic methanogen under high-pressure cultivation. - PNAS 10949-10954

Bains W, Xiao Y, Yu C (2015): Prediction of the maximum temperature for life based on the stability of metabolites to decomposition in water. - Life 5, 1054-1100

Leibrock E, Bayer P, Lüdemann HD (1995): Nonenzymatic hydrolysis of adenosinetriphosphate (ATP) at high temperatures and high pressures. - Biophys Chem 54, 175-180

Moelle C, Schmidt C, Guyot F, Wilke M (2022): Hydrolysis rate constants of ATP determined in situ at. - Biophys Chem 290

Buisson DH, Sigel H (1974): Significance of binary and ternary copper(II) complexes for the promotion and protection of adenosine 5′-di- and triphosphate toward hydrolysis. – Biochim Biophys Acta (BBA) - General Subjects 343, 45-63

Suzuki S, Higashiyama T, Nakahara A (1978): Nonenzymatic hydrolysis reactions of adenosine 5′-triphosphate and its related compounds—III: Catalytic aspects of some cobalt(III) complexes in ATP-hydrolysis. - Bioinorg Chem 8, 277-289

Mineralogical characteristics of agates and their host rocks in Chihuahua, Mexico

M. Mrozik[1,2], J. Götze[2]

[1] *Geowissenschaftliche Sammlungen, TU Bergakademie Freiberg, Brennhausgasse 14, 09599 Freiberg*
[2]*Institute of Mineralogy, TU Bergakademie Freiberg, Brennhausgasse 14, 09599 Freiberg*
e-mail: Maximilian.mrozik@geosamm.tu-freiberg.de

Agates from the state of Chihuahua in Mexico are known worldwide among collectors and jewelry dealers because of their color variety and high quality. The single deposits are limited to different areas which are distributed in the whole federal state of Chihuahua. The agates of the different localities partly differ in their basic coloring as well as in their general appearance and the abundance of pseudomorphs. Despite the wide distribution and individual locality-typical characteristics, most of the best-known deposits can be assigned to the same volcanic unit, the so-called Rancho el Agate Andesite. This is an approximately 300 m thick unit of intermediate lava flows, which all have a strongly vesicular texture (Keller et al. 1982). The host rocks for most of the presently mined agate deposits in the main production area of the Sierra del Gallego can be classified almost exclusively as quartz-free latite (Mrozik et al. 2023). The intermediate chemism of the rocks can be explained by a mixing of magmas with different SiO_2 contents.

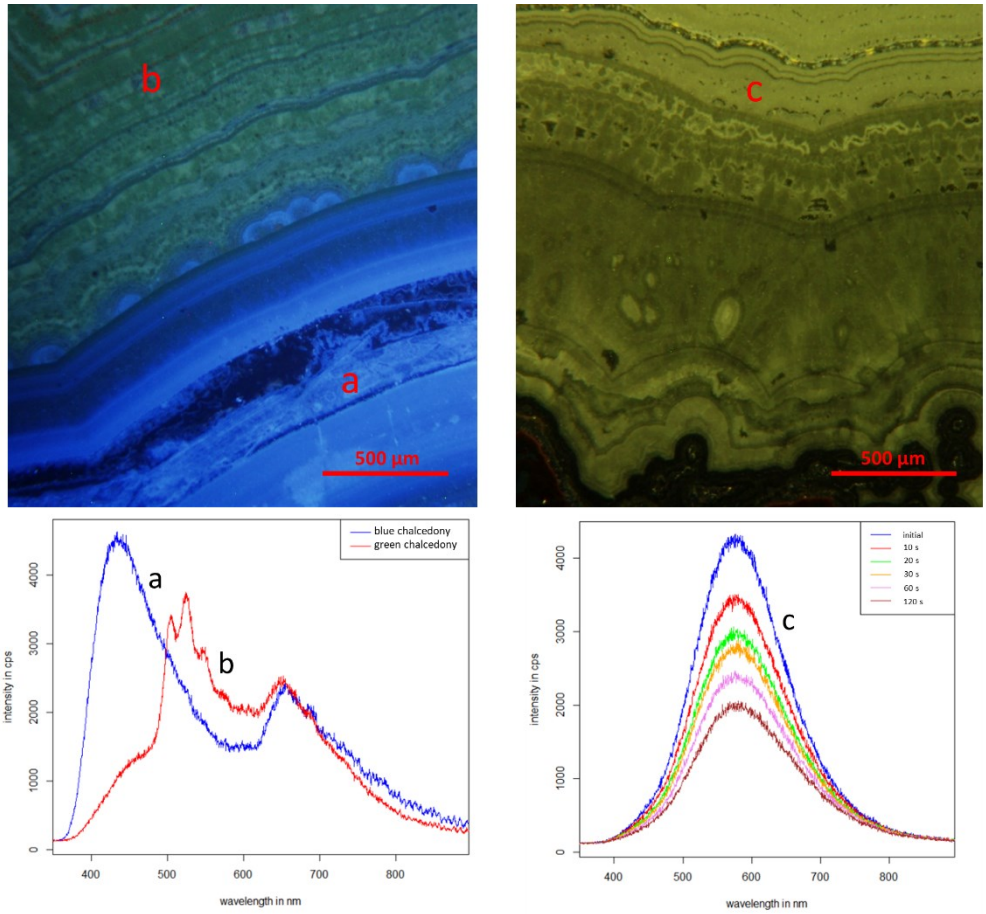

Figure 1. CL-micrographs with the associated CL-spectra. The CL-colors and spectra reveal different structural defects as well as the incorporation of trace elements and compounds like for example the uranyl-ion within the green luminescent parts of the chalcedony. (Figure from Mrozik et al. 2023)

Different reasons for the coloration of the agates could be determined by various spectroscopic methods as well as with trace element analyses and microscopic studies. While different structural defects can be detected in many areas of the mineralization (Fig. 1) the coloration of most of the bands in the agates is caused by inclusions, for example hematite and goethite. The different colors are not exclusively caused by the mineral phase but also by the particle size as well as the distribution of the coloring components within the matrix of the chalcedony. Some of these inclusions were incorporated within the agates during the initial crystallization of the chalcedony, others were later fixed within the matrix by secondary infiltration (Fig. 2) (Mrozik et al. 2023).

A mixture of near-surface weathering solutions with deep hydrothermal fluids from the Tertiary volcanism has led to the formation of the agates. The enrichment of differently mobile elements which were fixed during the formation of the agates in the structure of the chalcedony itself as well as in the paragenetic inclusions indicate the involvement of hydrothermal fluids. Due to the very different contents of under weathering conditions rather immobile elements like zirconium and chromium as well as almost exclusively hydrothermally accumulated elements like antimony and zinc a variable influence of deep hydrothermal fluids in the different agate occurrences can be assumed. Thus, the local differences in the agate formation are not caused by a basically different formation process but by a various influence of the respective fluids as well as slightly different local geochemical conditions. In the current studies different generations of chalcedony could be determined within the mineral formations (Fig. 2) which indicates that many of the agates were not formed by a single geochemical process but underwent a multiphase formation with partly different fluids under slightly differentiated conditions. (Mrozik et al. 2023)

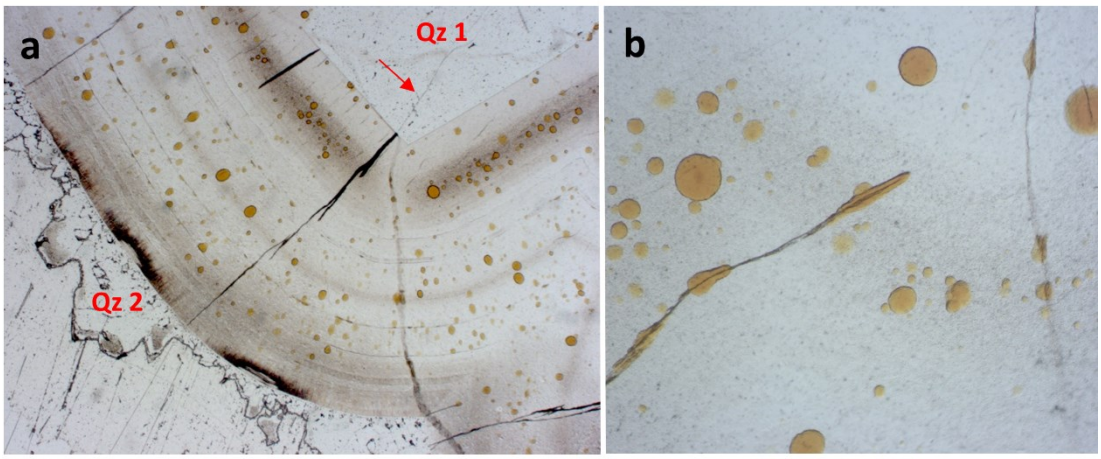

Figure 2. (a) The micrograph shows different generations of the SiO_2-mineralization with at least two generations of macrocrystalline quartz (Qz 1, Qz 2). The red arrow marks a secondary crack which can be followed within the first generation but ends at the second generation of quartz. (b) The micrograph shows a detailed view of the same agate which shows the distribution of different inclusions within the chalcedony matrix. Note that some of the inclusions are arranged along secondary cracks, which assigns a later formation of some of the coloring particles by infiltration. (Figure from Mrozik et al. 2023)

Mrozik M, Götze J, Pan Y, Möckel R (2023): Mineralogy, Geochemistry and Genesis of Agates from Chi-huahua, Northern Mexico. - Minerals 13, 687, https://doi.org/10.3390/min13050687

Keller PC, Bockoven NT, McDowell FW (1982): Tertiary volcanic history of the Sierra del Gallego area, Chihuahua, Mexico. - Geol Soc Amer Bull 93, 303-314

Special exhibition
Wonder world agate - fascination between legend and science

M. Mrozik[1], J. Götze[2], A. Massanek[1], M. Gäbelein[1]

[1] Geowissenschaftliche Sammlungen, TU Bergakademie Freiberg, Brennhausgasse 14, 09599 Freiberg
[2]Institute of Mineralogy, TU Bergakademie Freiberg, Brennhausgasse 14, 09599 Freiberg
e-mail: Maximilian.mrozik@geosamm.tu-freiberg.de

Due to their variety of colours and shapes, agates belong to the most fascinating mineral formations of nature and have played an important role as jewellery and gemstones since ancient times. The name "agate" appears in literature as early as 350 B.C. (Theophrast) and was probably derived from deposits on the river Achates (now Drillo) in Sicily.

Agate deposits and agate processing are recorded worldwide in both historical and currently mined regions. Of particular interest are the almost inexhaustible deposits of agate in the province of Rio Grande do Sul in Brazil, which have been supplying the world markets with raw agates for centuries. In China there is a centuries-old tradition of agate processing as a stone-carving art (Fig. 1). In the city of Fuxin in the province of Liaoning, also known as the "world city of agate", 60,000 people currently work in the agate industry. In Saxony, the systematic search for agate and "precious stones" was promoted early on by Elector August (1553 - 1586) and later especially by the Saxonian King "August the Strong". Therefore, systematic collections and descriptions already exist from this time. The region around Idar-Oberstein is also famous in history as a supplier and processing centre for high-quality agates.

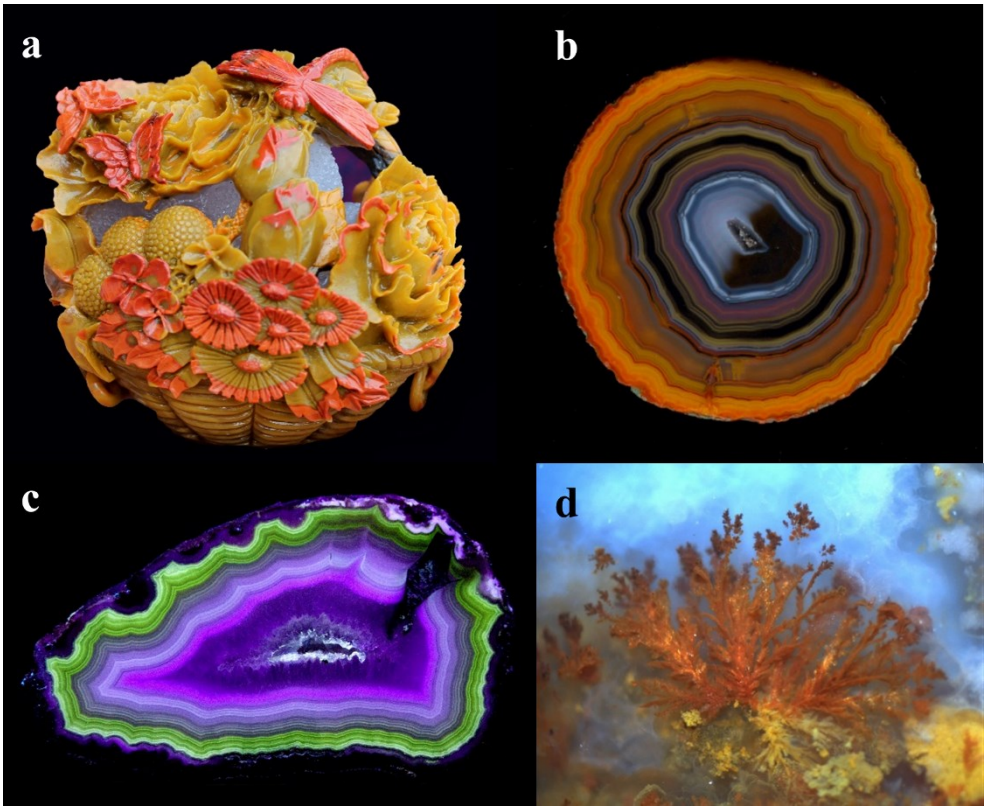

Figure 1. Different photographs and micrographs of agate samples. (a) stone carving art made from an agate from Xuanhua, China; (b) polished agate sample from Xuanhua, China; (c) luminescence colours under UV-light (254 nm) of an agate from Rancho Coyamito, Chihuahua, Mexico; (c) micrograph of an “Orpheus”-agate from Kardzhali, Bulgaria.

Besides their impressive aesthetics, agates also provide many clues for scientific research. This is mainly due to the fact that the formation of agate cannot be observed directly and also that until today no successful agate syntheses exist on a laboratory scale. One of the most discussed questions of the agate problem is probably the "secret" of agate formation, which has led to many speculations in the past and present. But the micro-world of agates also provides exciting insights into the complex processes of nature.

The exhibition gives an insight into the fascinating world of agates. With Wonder World Agate for the first time a combined special exhibition is housed in the three different collections in the city of Freiberg, which together form the largest mineralogical collection complex worldwide. The main part of the exhibition (Fig. 2), which presents impressive specimens from the most important agate deposits of the world, is displayed in the terra mineralia. You can find the different showcases arranged according to the different continents and most important agate deposits. Additionally, there are some thematic display cases (e.g. different types of agates, special agates or pictures in agates) as well as interactive elements explaining for example luminescence effects in agates or different microstructures. The whole exhibition is accompanied by numerous knowledge boards and art-like pictures of microstructures in agates to explain some exciting questions regarding the formation and properties of agates.

The Mineralogical Collection of Germany hosts agate samples from whole Germany. This part of the special exhibition shows the great variety and importance of German agate deposits.

The third part is housed in the Wernerbau framed by the historic mineralogical collection of the TU Bergakademie Freiberg. This exhibition part displays agates from some special localities in Saxony and shows the relation between primary and secondary agate deposits in one of the mineral richest states of Germany.

Figure 2. Some impressions of the actual special exhibition Wonder World Agate.

Minerals in a greenhouse environment: a cross-disciplinary exhibition

S.P. Mueller[1]

[1]Mineralogical Museum, University of Marburg, Germany
e-mail: s.mueller@geo.uni-marburg.de

During the winter months of 2023, the Mineralogical Museum Marburg was 'on tour' in the greenhouses of the Botanical Garden of the University of Marburg. In a collaborative, cross-disciplinary effort, we highlighted links between mineralogy and botany in a variety of display cases, in reference to the respective topical focus of the houses: e.g., which ore minerals are needed to build a smartphone, and how does their mining affect tropical rainforests? How do ferns turn into coal (and ultimately into diamonds)? Which minerals are typical for the Australian outback? How (and where) is amber formed?

The exhibition was open on a total of 9 Sundays during the winter months (a peroid the greenhouses are normally closed to the public) and attracted a large number of visitors to the botanical garden during this time. In particular, the interdisciplinary linking of what at first glance appear to be very different disciplines within natural sciences was positively highlighted in many of the visitors' feedbacks.

Thermoelastic properties of radiation-damaged zircon

M. Münchhalfen[1], J. Schreuer[1]

[1]Ruhr-Universität Bochum, Institut für Geologie, Mineralogie und Geophysik, Universitätsstraße 150, Bochum, 44801, Germany
e-mail: marie.muenchhalfen@rub.de

Radioactive decay of unstable isotopes causes damage to zircon, which significantly reduces its elastic stiffnesses (e.g., Özkan, 1976). These damages can be partially healed by temperature treatment of the zircon crystal. In order to study in situ the recrystallization of radiation-damaged zircon, thermoelastic properties, and thermal expansion data were collected between 100 K and 1600 K utilizing resonant ultrasound spectroscopy, dilatometry, and high-temperature powder x-ray diffraction. The investigated samples of natural gem-quality zircon belong to the damage stage I introduced by Holland & Gottfried (1955), i.e., the damage in the crystal structure is mainly dominated by the accumulation of isolated point defects.

While non-metamict zircon samples display a linear decrease in elastic stiffnesses, the partial radiation-damaged zircon samples undergo strong irreversible effects detected in all utilized methods. The increase of elastic stiffnesses starts at about 700 K, while the thermal expansion decreases (Fig. 1). The severity of this effect becomes more pronounced with an increasing initial state of damage and thus can be related to the healing of defects induced by radioactive decay. A second effect sets in at about 1100 K, likely related to a transition from static to dynamic behavior. This supports the idea that reducing radiation damage is a multi-stage process, including point defect healing and recrystallization of an amorphous fraction.

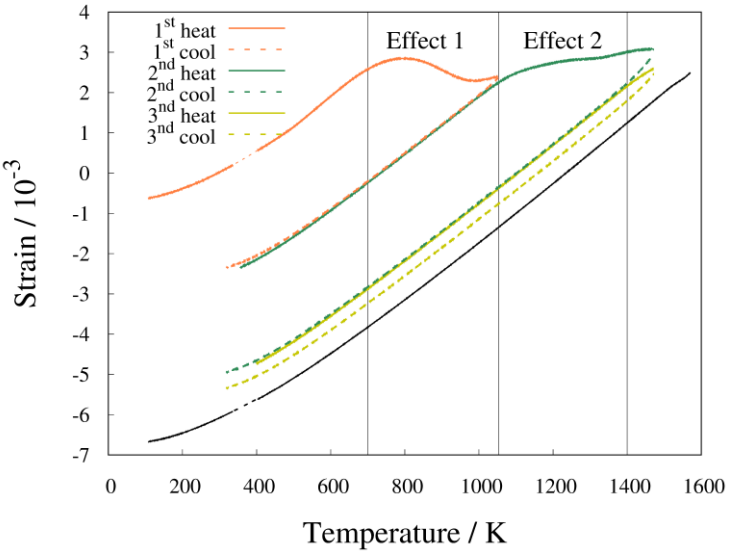

Figure 1. Different effects observed in thermal strain of radiation damaged zircon compared to non-metamict zircon (black line).

Özkan H (1976): Effect of nuclear radiation on the elastic moduli of zircon. - J Appl Phys 47, 4772-4779
Holland H, Gottfried D (1955): The effect of nuclear radiation on the structure of zircon. - Acta Cryst 8, 291-300

Rates, mechanisms and microstructures of transport-controlled reaction front propagation

T. Müller[1], S. Piazolo[2]

[1]*Geoscience Centre Göttingen, Georg-August-University, Germany*
[2]*School of Earth and Environment, The University of Leeds, United Kingdom*
e-mail: thomas.mueller@geo.uni-geottingen.de

Fluid-mediated mineral reactions are governing the redistribution of elements and isotopes in the geosphere. Incomplete elemental redistribution is preserved in the rock record in the form of geochemical reaction fronts. Key features of such systems are reaction induced creation/destruction of porosity increasing/decreasing permeability and further focussing of fluid into/away from the zone of reaction; hence this results in a positive or negative feedback between reaction, fluid ingress and further reaction. To the same end, sluggish element mobility can lead to variations in fluid chemistry within the propagating reaction front controlling the stable mineral assemblage and its chemical/isotopic composition. Recent studies provided conclusive evidence for the presence of transport-controlled reaction fronts in mineral reactions such as the replacement of calcite single crystals by Mg-carbonates (Jonas et al. 2015; 2017). Here, we present a follow-up investigation providing detailed chemical and microstructural data as well as a model for the kinetically controlled evolution of the reaction rim.

The replacement reactions of single calcite cubes (2 mm) were carried out experimentally in batch reactor vessel at 200 °C using a 1 M $MgCl_2$ fluid and a water-to-rock-ratio of 10 for run durations of 2-30 days. Solid reaction products have been characterized using an FEG-SEM including EBSD and chemical variations have been measured using an electron microprobe.

Experimental results reveal the time-dependent formation of a layered, multiphase reaction rim by dissolution-precipitation forming Mg-carbonate phases of different composition and variable porosity. The initial reaction rim is formed of small, rhombic almost pure magnesite crystals which become more Ca-rich as the reaction progresses. Subsequently, a sharp interface marks the change to the precipitation of high magnesium calcite (HMC) instead of magnesite, albeit the HMC precipitates with a constant X_{Mg} of 0.4. With increasing run durations, the reaction does not progress but grains in the existing reaction rim exhibit grain coarsening and elimination of (interconnected) porosity. This grain growth is accompanied by a chemical adjustment starting from the former magnesite-HMC interface initiating two new reaction fronts adjusting the magnesite composition, i.e., replacing Ca by Mg and the recrystallization of HMC by a VHMC phase with X_{Mg} of 0.5 representing a dolomite stoichiometry. EBSD analysis reveal that the recrystallization of the inner part of the reaction rim is accompanied by the formation of subgrain boundaries and rotation of c-axis during grain coarsening.

This study highlights the importance to quantitatively understand the link between reaction progress, fluid composition, fluid transport and the evolution of fluid pathways to describe and model reaction front propagation in reactive transport models.

Jonas L, Müller T, Dohmen R, Baumgartner L, Putlitz B (2015): Transport-controlled hydrothermal replacement of calcite by Mg-carbonates. - Geol 43, 779-782, doi: https://doi.org/10.1130/G36934.1

Jonas L, Müller T, Dohmen R, Immenhauser A, Putlitz B (2017): Hydrothermal replacement of biogenic and abiogenic aragonite by Mg-carbonates: Relation between textural control on effective element fluxes and resulting carbonate phase. - Geochim Cosmochim Acta 196, 289-306, doi: https://doi.org/10.1016/j.gca.2016.09.034

Gem spinel in the Imperial Crown of the Holy Roman Empire: Evidence for very early gemstone heating?

L. Nasdala[1], T. Lamers[2], H.A. Gilg[3], C. Chanmuang N.[1], M. Griesser[2], F. Kirchweger[2], A. Erlacher[1], M. Böhmler[4], G. Giester[1]

[1]Institut für Mineralogie und Kristallographie, Universität Wien, 1090 Vienna, Austria
[2]Kunsthistorisches Museum Wien, 1010 Vienna, Austria
[3]School of Engineering and Design, Technische Universität München, 80333 Munich, Germany
[4]WITec Wissenschaftliche Instrumente und Technologie GmbH, 89081 Ulm, Germany
e-mail: chutimun.chanmuang@univie.ac.at

The Imperial Crown of the Holy Roman Empire, part of the Imperial Regalia, is the key exhibit in Vienna's Imperial Treasury. It is currently investigated within the three-year interdisciplinary project 'Crown' (www.projekt-reichskrone.at) led by Kunsthistorisches Museum Vienna. The research aims, among others, at issues regarding the Imperial Crown's materials, manufacturing technology and time, as well as its state of preservation. During the first measurement campaign in Spring 2022, we had the task to determine conclusively – and, if possible, to characterise further – all 172 (inorganic) gemstones in the crown, whereas studies of the pearls were planned for the second measurement campaign (2023).

Figure 1. The front plate of the Imperial Crown of the Holy Roman Empire (size 11.2 cm × 14.9 cm) contains two spinels, a pink stone (#A3) in the upper row, left side, and a large red stone (#A25) in the centre of the third row. Photo © KHM-Museumsverband (Christian Mendez); reproduced with permission.

Non-destructive spectroscopic analyses were done on site, using a fibre-coupled WITec confocal Raman probe system equipped with an alpha300 controller. Photoluminescence (PL) and Raman spectra were excited with a 457 nm diode laser (0.05–8.5 mW measured behind the objective). An Olympus 20× objective (free working distance 25 mm) was used.

Besides 71 blue sapphires, 50 garnets, 20 emeralds, 13 amethysts, four chalcedonies and 11 glass imitates, there are three spinels in the Imperial Crown, two in the front plate (Fig. 1) and one in the central cross (Nasdala et al. 2023). The analytical identification of spinel in the

Imperial Crown is of art-historical interest. So far the first appearance of gem spinel in European jewellery was known for the thirteenth century (e.g., Ogden 2021) whereas the central, large spinel in the front plate (#A25) seems to be original; that is, set into the Imperial Crown about 1000 years ago already. This stone hence represents one of the very earliest uses of spinel in jewellery. Furthermore, the stone has two drill holes that indicate an even older use.

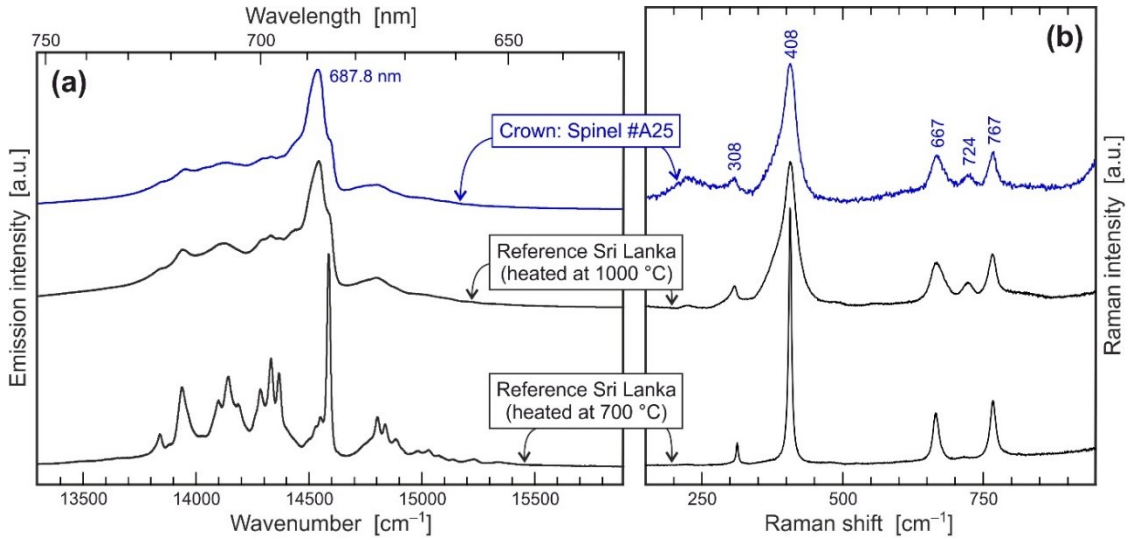

Figure 2. PL spectrum (a) and Raman spectrum (b) of spinel #A25 (blue graphs), shown in comparison with reference spectra (black graphs) obtained from a gem-quality spinel from Sri Lanka that was heat-treated in air.

The central spinel in the front plate (stone #A25) turned out to be of particular scientific interest, as it did not yield PL and Raman spectra that are typical of $MgAl_2O_4$ with (close to) normal occupation of cation sites. Instead, the PL spectrum (Fig. 2a) is characterised by loss of fine structure. Such spectra are obtained from natural Mg-Al spinel only after being heat-treated (Widmer et al. 2015; Liu et al. 2022). Similarly, heat-treatment results in significant broadening and asymmetry of Raman bands (Fig. 2b). These spectroscopic phenomena are assigned to heating-induced cation disorder; that is, increase of partial inversion of the cation occupation, according to $^{[4]}Mg\ ^{[6]}Al_2\ O_4 \rightarrow\ ^{[4]}(Mg_{1-x}Al_x)\ ^{[6]}(Al_{2-x}Mg_x)\ O_4$ (with $x > 0.2$) (Widmer et al., 2015; Ma et al., 2022). The spectra obtained from spinel #A25 hence give strong indication that this stone was heated to close to 1000 °C. This is supported also by the presence of a multitude of healed fractures, 'lily pad' inclusions, and melted sulphides at the surface.

Heating of red 'yāqūt' to enhance colour and transparency is known back to the ninth century (e.g., Troupeau 1998). 'Yāqūt' (an Arabian term) has generally be assumed to refer to gem corundum, but the possibility cannot be eliminated that it – and hence also the early heating – may have included spinel as well. Our spectroscopic results indicate that, as early as about 1000 years ago, spinel #A25 may have been subjected to heat-treatment.

Liu Y, Qi L, Schwarz D, Zhou Z (2022): Color mechanism and spectroscopic thermal variation of pink spinel reportedly from Kuh-i-Lal, Tajikistan. - Gems Gemol 58, 338-353

Ma Y, Bao X, Sui Z, Zhao X, Liu X (2022): Quantifying Mg–Al cation distribution in $MgAl_2O_4$-spinel using Raman spectroscopy: An experimental calibration. - Solid Earth Sci 7, 60-71

Nasdala L, Lamers T, Gilg HA, Chanmuang N C, Griesser M, Kirchweger F, Erlacher A, Böhmler M, Giester G (2023): The Imperial Crown of the Holy Roman Empire, part I: Photoluminescence and Raman spectroscopic study of the gemstones. - J Gemmol 38(5), 448

Ogden JM (2021): Gem knowledge in the thirteenth century: The St Albans jewels. - J Gemmol 37(8), 816

Troupeau G (1998): Le premier traité arabe de minéralogie: Le livre de Yūḥannā Ibn Māsawayh sur les pierres précieuses. - Ann Islamologiques 32(6), 219

Widmer R, Malsy A-K, Armbruster T (2015): Effects of heat treatment on red gemstone spinel: Single-crystal X-ray, Raman, and photoluminescence study. - Phys Chem Miner 42(4), 251

Determination of the electronic polarizabilities of bromine in bromates, perbromates, and bromides

S. Nezamabadi[1], P. Fuzon[2], F. Kraus[2], R.D. Shannon[3], I. Spieß[1], R.X. Fischer[1]
[1] FB 5 Geowissenschaften, Universität Bremen, Klagenfurter Straße, D-28359 Bremen, Germany
[2]FB Chemie, Philipps-Universität Marburg, Hans-Meerwein-Str. 4, D-35032 Marburg, Germany
[3]Geological Sciences/ CIRES, University of Colorado, Boulder, Colorado 80309, USA
e-mail: rfischer@uni-bremen.de

Empirical electronic polarizabilities of Br^{5+}, Br^{7+}, and Br^{-} were determined to predict refractive indices of bromates, perbromates, and bromides, respectively, at λ= 589.3 nm. Polarizabilities of the bromine ions were derived from the total electronic polarizabilities of compounds containing Br calculated from the mean refractive indices using the Anderson-Eggleton relationship (Anderson, 1975; Eggleton, 1991; Shannon and Fischer, 2016). Refractive indices (RI) of bromates and bromides are taken from literature data and from measurements on potassium bromate ($KBrO_3$) and potassium bromide (KBr), respectively. Because of the lack of literature data on perbromates, we have done RI measurements on sodium perbromate monohydrate ($NaBrO_4 \cdot H_2O$).

Structure analyses were performed using single-crystal X-ray diffraction data of $KBrO_3$, KBr, and $NaBrO_4 \cdot H_2O$. Refractive indices were determined using the immersion method with a micro-refractometer spindle stage at λ= 589.3 nm as described by Medenbach (1985), yielding n_e = 1.538 and n_o = 1.677 (<n> =1.6307) for optically uniaxial $KBrO_3$ (Figure 1), and n_x = 1.470, n_y = 1.491, n_z = 1.492 (<n> = 1.4843) for an optically biaxial $NaBrO_4 \cdot H_2O$ crystal (Figure 2).

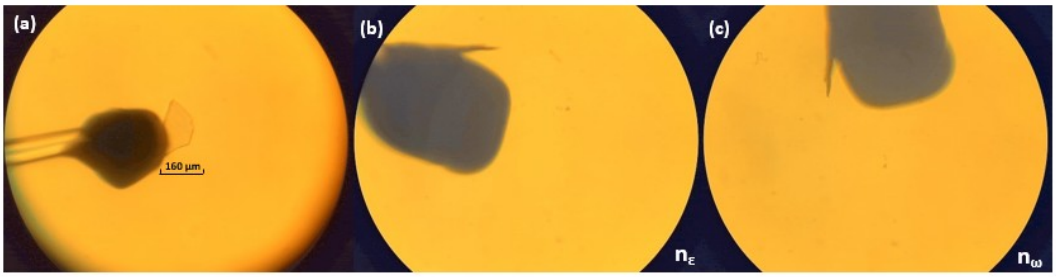

Figure 1: (a) $KBrO_3$ crystal mounted on the spindle stage of the polarization microscope. (b) orientation of the crystal to determine n_e = 1.538. (c) orientation of the crystal to determine n_o = 1.677. Due to the equality of the refractive indices of the sample and the immersion oil, the sample is not visible in (b) and (c).

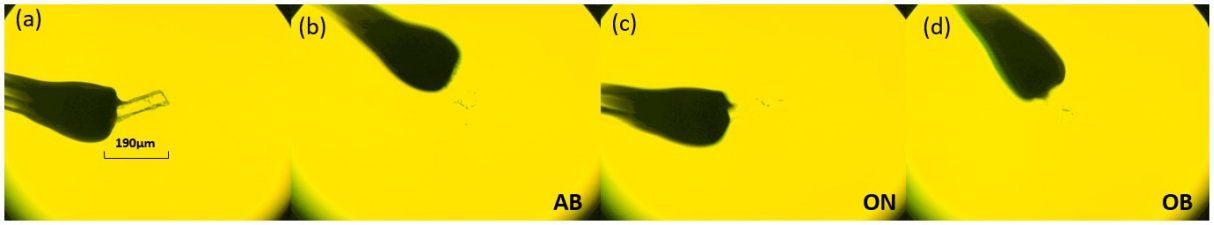

Figure 2: (a) $NaBrO_4 \cdot H_2O$ crystal mounted on the spindle stage of the polarization microscope. (b) orientation of the crystal to determine n_x = 1.470. (c) orientation of the crystal to determine n_y= 1.677. (d) orientation of the crystal to determine n_z= 1.492. Since the refractive index of the sample matches that of the oil, the sample is not visible in (b), (c), and (d).

Analyzing 18 compounds with established refractive indices containing Br^{5+}, along with data from this study, the polarizability of $^{[3]}Br^{5+}$ was determined by calculating the difference between the total polarizabilities of the respective compounds and the sum of polarizabilities of their ions omitting Br with values for the ions taken from Shannon and Fischer (2016). The individual electronic polarizability of $^{[3]}Br^{5+}$ was found to be 2.20 ± 0.34 [Å^3].

The determination of the refractive indices of $NaBrO_4 \cdot H_2O$ with four-coordinated Br^{7+} yielded an electronic polarizability value of 1.086 [Å^3] for Br^{7+}. Using this value now enables the prediction of refractive indices of perbromates with polarizability values from Shannon & Fischer (2016) as listed inFehler: Verweis nicht gefunden Table 1.

Table 1: Predicted mean refractive indices of compounds containing tetrahedrally coordinated Br^{7+}. Crystal data are from the ICSD database. V_m is the molar volume of the compound, α_{tot} is the total electronic polarizability of the compound and <*n*> is the mean refractive index.

Compound	Space group	V_m [Å^3]	α_{tot} [Å^3]	<*n*> (± 0.025)
$KBrO_4$	*P n m a*	98.98	8.949	1.541
$CsBrO_4$	*I* 4_1/*a m d*	122.5475	10.680	1.522
$NH_4(BrO_4)$	*P n m a*	107.73	9.785	1.544
$LiBrO_4 \cdot H_2O$	*C* 1 2/*c* 1	100.4775	9.349	1.557
$LiBrO_4 \cdot 3H_2O$	*P* 6_3 *m c*	147.565	12.630	1.513
$Ba(BrO_4)_2 \cdot 3H_2O$	*P* 6_3/*m*	237.185	22.955	1.580
$Ca(BrO_4)_2 \cdot 4H_2O$	$P\bar{1}$	266.25	23.190	1.522
$Co(BrO_4)_2 \cdot 6H_2O$	$P\bar{3}$ *m* 1	305.34	26.543	1.521
$Ni(BrO_4)_2 \cdot 6H_2O$	$P\bar{3}$	291.18	26.467	1.544

For the anion Br^- the two parameters α^o and N_o were determined describing the anion polarizability α^- of Br^- according to $\alpha^- = \alpha^o \cdot 10^{-No/V}$ with $V = V_{an}^{1.2}$ where V_{an} is the anion volume (see Shannon & Fischer, 2016).

Anderson OL (1975): Optical properties of rock-forming minerals derived from atomic properties. - Fortschr Miner 52, 611–629

Eggleton RA (1991): Gladstone-Dale constants for the major elements in silicates: Coordination number, polarizability, and the Lorentz-Lorentz relation. - Canad Miner 29, 525–532

Medenbach O (1985): A new microrefractometer spindle-stage and its application. - Fortschr Miner 63, 111-133

Shannon RD, Fischer RX (2016): Empirical electronic polarizabilities of ions for the prediction and interpretation of refractive indices: oxides and oxysalts. - Amer Mineral 101, 2288–2300

Mirdita ophiolites, Albania: Refertilization of spinel-plagioclase-peridotites in the shallow Mantle Lithosphere

T. Ntaflos[1], P. Koutsovitis[2], K. Onuzi[3], C. Hauzenberger[4]

[1]Department of Lithospheric Research, University of Vienna, Josef-Holaubek-Platz 2, 1090 Vienna, Austria
[2]Department of Geology, University of Patras, Greece
[3]Instituti i Gjeoshkencave,Rr. "Don Bosko", Nr.60, Tirane, Albania
[4]Department of Earth Sciences – NAWI Graz Geocenter, University Graz Universitaetsplatz 2, Austria
e-mail: theodoros.ntaflos@unive.ac.at

The Albanian ophiolites are located between the Dinarides (N. Macedonia and Serbia) in the east and the Hellenides in the west. The Mirdita Ophiolites in Albania are divided into two units namely the western ophiolitic unit with MORB geochemical affinity and the eastern ophiolitic unit with SSZ affinity. The western unit consists of the Krabbi, Puka, Comsique and Skenderbeu massifs where intrusives and dykes are present as well. All massifs represent upper mantle, variably serpentinized spinel and plagioclase peridotites.

The Krabbi massif with a diameter of 30 km is a piece of upper mantle ultramafic body consisting of spinel-plagioclase lherzolites and harzburgites with bulk-rock Mg# ranging from 89.5 to 91.8 and Ca/Al ratio varying from 1.13, that is slightly higher than the Primitive Mantle ratio of 1.1, to 1.26 indicating an excess of Ca in the studied samples. Minor and trace elements trends such as Ni, V and Yb versus Mg# are very similar to those of the orogenic peridotites. The chondrite normalized REE abundances have convex upward patterns where the majority of the samples show that the Yb_N is slightly higher compared to La_N suggesting moderate metasomatic events affecting the LREE.

Besides the rock forming mineral olivine, orthopyroxene, clinopyroxene and spinel there are also disseminated plagioclases and kaersutites. Strongly tectonized samples show secondary protogranular and porphyroclastic textures. Rounded spinel occurs mainly as inclusion in olivine and orthopyroxene whereas holly-leaf shaped spinel is interstitial.

The plagioclase neither coexists nor surrounds spinel, which precludes any subsolidus transition from spinel- to plagioclase-peridotite stability field. However, the clinopyroxene, as can be inferred from their negative Eu-anomaly in the chondrite normalized REE patterns, appears to be in equilibrium with coexisting plagioclase. Apparently, the plagioclase-rich residual melt affected the peridotites in the spinel-peridotite field but crystallized and equilibrated with clinopyroxene at shallow depths.

A striking textural feature is the frequent replacement of olivine grains by orthopyroxene with simultaneous formation of Ti-rich diopside and Al-rich spinel, suggesting metasomatic infiltration of a melt with tholeiitic composition. This feature has been observed in the samples with Mg# = 89.5, Al_2O_3 = 4.3 wt% and CaO = 3.77 wt% similar to the composition of the Primitive Mantle.

The existence of fertile peridotites with similar to the Primitive Mantle composition suggests that the otherwise strongly depleted oceanic lithospheric mantle has been refertilized after metasomatic introduction of melts with tholeiitic composition.